Investigating the regulation of *PXDN* expression by the early growth response 1 (EGR1) transcription factor in the context of human fibrotic diseases

by

Thokozile Makhanya

(1064330)

Dissertation

Submitted in fulfilment of the requirements for the degree

Master of Science

in

Molecular and Cell Biology

in the Faculty of Science, University of the Witwatersrand, Johannesburg, South Africa

Supervisor: Professor Demetra Mavri-Damelin

August 2023

Declaration

I, Thokozile Makhanya (1064430), am a student registered for the degree of Master of Science (Dissertation) in the academic year 2023.

I hereby declare the following:

- I am aware that plagiarism (the use of someone else‘s work without their permission and/or without acknowledging the original source) is wrong.
- I confirm that the work submitted for assessment for the above degree is my own unaided work except where explicitly indicated otherwise and acknowledged.
- I have not submitted this work before for any other degree or examination at this or any other University.
- The information used in the thesis has not been obtained by me while employed by, working under the aegis of, any person or organisation other than the University.
- I have followed the required conventions in referencing the thoughts and ideas of others.
- I understand that the University of the Witwatersrand may take disciplinary action against me if there is a belief that this is not my own unaided work or that I have failed to acknowledge the source of the ideas or words in my writing.

Signed  31/08/2023

Abstract

Peroxidasin (PXDN) is a novel member of the peroxidase-cyclooxygenase family of haem-containing proteins that catalyze oxidative reactions. It consolidates the extracellular matrix (ECM) by using hydrogen peroxide (H_2O_2) as a substrate to generate hypohalous acid intermediates, which help catalyze the formation of sulfilimine bonds between collagen IV protomers. The aberrant expression of PXDN has been linked to the development of various diseases where the architecture of the ECM is compromised such as cardiovascular diseases, ocular diseases, cancer, and fibrosis. Fibrosis develops due to repetitive tissue injury which is followed by aberrant wound healing that causes the excessive deposition of ECM proteins such as collagen into the injured tissue. In turn, ECM crosslinking enzymes such as PXDN are upregulated, and the matrix becomes thick and heavily crosslinked. This study aims to elucidate whether early growth response 1 (EGR1), a zinc-finger transcription factor which regulates cell proliferation, differentiation, apoptosis, and a key pro-fibrotic protein, can drive *PXDN* expression. To address the aim, HEK293 cells were treated with TGF-β1, a master activator of fibrotic genes, and western blot and immunofluorescence microscopy were performed to detect EGR1 and PXDN and their cellular localization, respectively. Chromatin immunoprecipitation (ChIP) was performed to determine if EGR1 binds to the *PXDN* promoter and the luciferase reporter assay was employed to determine if the interaction resulted in an alteration in gene expression. Our western blot findings showed that for EGR1, there was a statistically insignificant increase in protein expression in response to the TGF-β1 treatment. PXDN expression could not be quantified due to the high background on the blots. Further analysis by immunofluorescence microscopy showed that EGR1 expression was increased and was localised to the nuclei in response to the TGF-β1 treatment. We also observed that PXDN was predominantly expressed extracellularly and showed a significant increase in protein expression with treatment. The bioinformatics analysis has identified two putative EGR1 binding sites in the *PXDN* promoter and ChIP-PCR showed that binding occurred at one of these sites. This site was cloned into the pGL4.10 vector to determine whether EGR1 drives *PXDN* expression. Due to unsuccessful transfection optimization, the luciferase assay could not be performed and therefore for future work this assay needs to be performed to verify if EGR1 can drive *PXDN* expression. In conclusion, we showed that PXDN is a TGF-β1-responsive gene and may be regulated by EGR1. Studying the interaction of EGR1 and PXDN may establish roles for PXDN in fibrosis and further consolidate PXDN as a possible anti-fibrotic therapeutic target.

Acknowledgements

This research project is the most exciting and challenging thing that I have ever done, and I was very blessed to have had support from various people and would like to relay my deepest gratitude to them. Firstly, I would like to thank my supervisor, Professor Demetra Mavri-Damelin for designing the project and working tirelessly with me to bring it to fruition. Due to the pandemic, we experienced massive delays, but her expertise and calmness saw me through this tumultuous period. With her guidance and input, I have grown as a researcher and learned a great deal about molecular biology and for this, I am eternally grateful. I would also like to thank I would like to thank Dr Deran Reddy from the Wits Microscopy and Microanalysis Unit (MMU) for the extensive training in using the Olympus BX63 Microscope and Dr Angela Botes from the school of Molecular and Cell Biology (MCB) for allowing me to use the Q-sonica in her lab.

I would like to give a big thanks to my colleagues at the Functional Genetics Research Laboratory, starting with Dr Tebogo Marutha for teaching me how to culture cells, use the different equipment we have in the lab and perform the various experiments that were part of this project. He did everything with the outmost kindness and patience, and I hope that I may radiate these qualities and be a pillar of support to other students as he was for me. I would also like to thank Lebogang Moshupya, Kayleen Jegels, Jemma Falkov, Mistral Sabastian, and Jamie Fernandez for their support and assistance around the lab, I learnt so much through interacting with them and value the friendships that we made. A special thanks to my family for their unwavering love and support, more especially my mother Nomasonto Makhanya for her prayers. Everything that I do is through drawing strength from them, and I hope this work inspires and makes them proud. I am incredibly grateful to my friends, Mathabatha Ntjie, Keketso Muchichwa and Xolisiwe Mhlathi, for their continuous encouragement throughout this journey.

Most importantly I would like to thank God for blessing me with the opportunity to do this degree and giving me the strength to see it through. Finally, I would like to thank the National Research Foundation (NRF) for the funding granted from the NRF Innovations Postgraduate Scholarship, without them this project would not have been possible.

"The future belongs to those who believe in the beauty of their dreams"

Eleanor Roosevelt

Table of contents

List of figures

List of tables

List of abbreviations

APS - Ammonium persulfate

Arg - Arginine

ASD - Anterior segment dysgenesis

BM - Basement membrane

bp - Base pairs

BSA - Bovine serum albumin

CDK - Cyclin-dependent kinase

ChIP - Chromatin immunoprecipitation

CKD - Chronic kidney disease

COX - Cyclooxygenase

DAPI - 4',6'-diamidino-2-phenylindole

DBD - DNA binding domain

DMEM - Dulbecco's Modified Eagle Medium

DNMT - DNA methyltransferase

dsDNA - Double-stranded DNA

DUOX - Dual oxidase

EBS - EGR binding site

ECM - Extracellular matrix

EDTA - Ethylenediaminetetraacetic acid

EGF - Epidermal growth factor

EGR1 - Early growth response 1

EMT - Epithelial-to-mesenchymal transition

EPO - Eosinophil peroxidase

ERK - Extracellular signal-regulated kinase

FBS - Foetal bovine serum

FEV - Forced expiratory volume

FGF - Fibroblast growth factor

FITC - Fluorescein isothiocyanate

gDNA - Genomic DNA

HEK293 - Human embryonic kidney cells 293

HGF - Hepatocyte growth factor

His - Histidine

HOBr - Hypobromous acid

HOCl - Hypochlorous acid

HRP - Horseradish peroxidase

HSC - Hepatic stellate cells

IEG - Immediate early gene

IFN-γ - Interferon gamma

IL - Interleukin

JNK - Jun kinase

KGF - Keratinocyte growth factor

LDL - Low-density lipoprotein

LOX - Lysl oxidases

LPO - Lactoperoxidase

LRRs - Leucine-rich repeats

MCS - Multiple cloning site

MMP - Matrix metalloproteinases

MPO - Myeloperoxidase

NAFLD - Non-alcoholic fatty liver disease

NASH - Non-alcoholic steatohepatitis

NLS - Nuclear localization signal

NOX - NADPH oxidases

NTC - No template control

NAC - No antibody control

NPC - No primary antibody control

PBS - Phosphate buffered saline

PCR - Polymerase chain reaction

PDGF - Platelet-derived growth factor

PMSF - Phenylmethanesulfonyl fluoride

PXDN - Peroxidasin

PXDNL - Peroxidase-like

POX - Peroxidase domain

RIF - Radiation-induced fibrosis

RIPA - Radioimmunoprecipitation assay

ROS - Reactive oxygen species

SDS - Sodium dodecyl sulfate

SDS-PAGE - Sodium dodecyl sulfate polyacrylamide gel electrophoresis

siRNA - Short interfering RNA

TAE - Tris-acetate EDTA

TBST - Tris-buffered saline with Tween-20

TCA - Trichloroacetic acid

TEMED - Tetramethylenediamine

TF	- Transcription factor
TGF-β	- Transforming growth factor-β
TLC	- Total lung capacity
TNF-α	- Tumour necrosis factor-α
TPO	- Thyroid peroxidase
Tris	- Tris(hydroxymethyl)aminomethane
TSS	- Transcription start site
VEGF	- Vascular endothelial growth factor
vWFC domain	- von Willebrand factor C
ZF	- Zinc finger

List of symbols

µg	- Microgram
µl	- Microlitre
℃	- Degrees Celsius
G	- Grams
kDa	- Kilodaltons
mA	- Milliamperes
mg	- Milligram
ml	- Millilitre
mM	- Millimolar
ng	- Nanogram
nm	- Nanometre
rpm	- Revolutions per minute

Introduction

1.1 PXDN

1.1.1 Classification

Peroxidasin (PXDN) is an animal haem peroxidase that catalyzes oxidative reactions needed in the formation of the extracellular matrix (ECM) (Nelson *et al.,* 1994). Peroxidases are a large family of oxidoreductases that utilize hydrogen peroxide (H_2O_2) to oxidize substrates. They are classified into two broad groups, the haem-free peroxidase-catalases and the haem-containing peroxidase-cyclooxygenase group (Zámocký *et al.,* 2010). The peroxidase-cyclooxygenase family is comprised of myeloperoxidase (MPO), lactoperoxidase (LPO), eosinophil peroxidase (EPO), thyroid peroxidase (TPO), cyclooxygenase (COX), PXDN and peroxidase-like (PXDNL) (Zámocký *et al.,* 2010; Péterfi *et al.,* 2014). MPO, LPO and EPO are involved in innate immune defences through their production of hypohalous acids, which destroy invading microorganisms (Davies *et al.,* 2008). TPO is involved in thyroid hormone synthesis and COX in the synthesis of prostaglandins (Ruf and Carayon, 2006; Rouzer and Marnett, 2009). In comparison to its other protein family members, PXDN has a unique function in consolidating the matrix (Bhave *et al.,* 2012). PXDNL on the other hand is also reported to be involved in ECM formation and promoting cell motility but does not seem to exhibit peroxidase function (Papageorgiou and Heymans, 2014).

1.1.2 Expression

PXDN is a unique haem-peroxidase expressed in vertebrates and invertebrates. In *Drosophila melanogaster*, PXDN is expressed by haemocytes during embryonic development where it functions in tissue formation and epidermal elongation by catalysing the formation of tyrosine bonds (Nelson *et al.,* 1994). It is also found in species such as *Caenorhabditis elegans, Chilo suppressalis* and Cnidaria and plays similar roles to that in the fruit fly by being involved in the developmental stages of the organisms (Tindall *et al.,* 2005; Gotenstein *et al.,* 2010; Fidler *et al.,* 2014; Ma *et al.,* 2020**).** The human PXDN is expressed in the early stages of development and is found in all tissues supported by the ECM basement membrane (BM) but most notably the eyes, the heart, and the kidneys (Horikoshi *et al.,* 1999; Péterfi *et al.,* 2009; Khan *et al.,* 2011). In these tissues, the protein is synthesized in the endoplasmic reticulum of fibroblasts, endothelial and epithelial cells, where it is subsequently secreted into extracellular spaces (Péterfi *et al.,* 2009; Lázár *et al.,* 2015). PXDN expression is induced by various stimuli, including cytokines such as TGF-β1 and oxidative stress, which occur during

processes such as cell migration and tissue injury (Péterfi *et al.,* 2009; Hanmer and Mavri-Damelin, 2018).

1.1.3 Structure

The human *PXDN* gene is found on the 2p25.3 telomeric region and has 23 exons, the longest transcript of which gives rise to a multidomain protein (Figure 1.1) (Weiler *et al.,* 1994; Cheng *et al.,* 2008). The domains consist of a peroxidase domain (POX) that is conserved in mammalian peroxidases (Zámocký and Obinger, 2010). This domain is the catalytic site of peroxidases and contains a covalently linked haem prosthetic group, which enhances the catalytic activity of these enzymes and protects them from the highly reactive oxidant byproducts that they generate (Zederbauer *et al.,* 2007). The haem is added during post-translational modifications and is covalently attached with ester bonds via acidic aspartate (Asp) and glutamate (Glu) residues. With the exception of MPO, which has an additional covalent sulfonium ion bond, all the other haem-containing peroxidases have two ester bonds (Zederbauer *et al.,* 2007). In PXDN, the ester bond is formed between Asp-826 and Glu-980 (Paumann-Page *et al.,* 2017). The iron in the porphyrin ring is linked to proximal and distal histidine (His) residues. The proximal His is linked to asparagine (Asp) and the distal one is attached to Glu and arginine (Arg). The His/Arg residues are responsible for the heterolytic cleavage of H_2O_2 whilst Glu binds the halide substrates (Soudi *et al.,* 2015).

In addition to the conserved POX domain, PXDN also contains non-catalytic domains which include leucine-rich repeats (LRRs), immunoglobulin (IgG) like domains and a C-terminal von Willebrand factor C (vWFC) domain (Figure 1.1) (Cheng *et al.,* 2008). These domains are characteristic of ECM proteins and suggest that PXDN is involved in protein-protein interactions in the matrix and cell adhesion (Cheng *et al.,* 2008; Lázár *et al.,* 2015). The PXDN protein is formed through the trimerization of monomers at their N-terminal ends via disulfide bonds occurring between cysteine (Cys)-696 and 1412 and together, these form a protein with a molecular weight of 165 kDa (Cheng *et al.,* 2008; Paumann-Page *et al.,* 2020). Another important component of the PXDN protein is the N-terminal secretion signal peptide, which is used to transport the protein from the endoplasmic reticulum of cells to the ECM where it crosslinks collagen IV (Péterfi *et al.,* 2009; Soudi *et al.,* 2012). PXDN also undergoes *N*-glycosylation on its asparagine (Asn) groups, and this contributes about 12 kDa to the overall 165 kDa molecular weight of the protein (Cheng *et al.,* 2008; Soudi *et al.,* 2015). The role of the glycan group has not been specifically described for PXDN; however,

this modification is generally reported to help with protein folding, stability, transport, secretion, and ECM organization (Varki, 2017; Schjoldager *et al.*, 2020).

Figure 1.1: The structure of the PXDN. PXDN contains multiple domains with the defining one being the haem-containing catalytic peroxidase domain (POX) which is conserved in the peroxidase protein family. The protein also has an N-terminal signal peptide (S), leucine-rich repeats (LRRs), immunoglobulin (IgG) like domains and a C-terminal von Willebrand factor C (vWFC) domain (Obtained from Ma *et al.*, 2020).

1.1.4 Functions

1.1.4.1 ECM consolidation

The most well-described role of PXDN is crosslinking collagen IV fibres found in the ECM BM with sulfilimine bonds (Bhave *et al.*, 2012). The BM is a specialised sheet-like structure that anchors epithelial cells, forms physical barriers between different cells and supplies them with growth factors (LeBleu *et al.*, 2007). The BM is primarily composed of collagen IV and it also contains laminin, perlecan, and nidogen and the modifying enzymes such as matrix metalloproteinases (MMPs), lysyl oxidase (LOX) and PXDN (Ramos-Lewis and Page-McCaw, 2019). Type IV collagen fibres are exclusively found in the BM and encoded for by the *COL4A1-COL4A6* genes. These genes encode for six homologous monomeric α-chains (α1-α6), which polymerize to form heterotrimeric protomers (Khoshnoodi *et al.*, 2008). On the N-terminus of the trimer is the collagenous 7S domain and on the C-terminus is the non-collagenous 1 (NC1) domain, with the collagen IV network assembled when protomers are joined end-to-end at these terminal domains. LOX forms disulfide bonds between four protomers at their 7S domains and this forms a dodecameric juncture. On the NC1 domains a hexamer is formed through the association of two protomers and this interaction is stabilized by sulfilimine bonds catalysed by PXDN (Bhave *et al.*, 2012; Añazco *et al.*, 2016; Brown *et al.*, 2017).

The assembly of the collagen IV network starts with the activation of PXDN through the proteolytic cleavage of its vWFC domain by proprotein convertase (PC) and this enhances the catalytic activity of PXDN (Colon and Bhave, 2016). Once PXDN is cleaved, it binds H_2O_2 in the catalytic site and starts to oxidize substrates. The H_2O_2 that is used by haem

peroxidases is primarily obtained from NADPH oxidases (NOX) and dual oxidases (DUOX) (Zhang *et al.,* 2012; Sirokmány and Geiszt, 2019). For crosslinking collagen IV, however, recent evidence shows that PXDN functions independently of NOX/DUOX-derived H_2O_2. Sirokmány *et al.* (2018) showed that in the absence of NOX/DUOX isoforms sulfilimine bonds were still formed in the BM of the aorta, kidneys, thyroid, and bladder of model mice. This finding is consistent with the widespread tissue expression of PXDN in comparison to NOX/DUOX enzymes and the other peroxidases. The researchers instead postulate that the potential source of the H_2O_2 used by PXDN is derived from the mitochondria.

PXDN functions by cleaving the peroxidic bond of bound H_2O_2 molecules and this allows it to oxidize the halides bromine, chloride and iodide and the pseudohalide thiocyanate into hypobromous acid (HOBr), hypochlorous acid (HOCl) hypoiodous acid (HOI) and hypothiocyanous acid (HOSCN) (Paumann-Page *et al.,* 2017). HOI and HOSCN have been shown to inhibit crosslinking and are therefore rarely generated by PXDN (McCall *et al.,* 2014). Between Cl^- and Br^- ions, PXDN preferentially halogenates Br^- as its bromosulfonium intermediate has a lower activation energy than the chlorosulfonium intermediate, making the reaction more thermodynamically favourable for the catalysis of the sulfilimine bond (McCall *et al.,* 2014). McCall *et al.* (2014) further describe Br^- as having a 50,000-fold greater efficiency at crosslinking collagen compared to Cl^- even at low plasma concentrations as it is a trace element in the body.

To crosslink collagen IV, PXDN first catalyses the peroxidase cycle and here the iron (Fe^{3+}) on the haem group reacts with H_2O_2 to form water and oxoiron intermediates. The oxorion molecules feed into the halogenation cycle and react with bromine (Br-) to form HOBr (Paumann-Page *et al.,* 2017). The HOBr then binds to the NC1 domain of collagen IV protomers and on the first protomer it reacts with the sulphur on methionine-93 (Met-93) to form a bromosulfonium intermediate. The intermediate then reacts with the nitrogen on hydroxylysine-211 (Hyl-211) of the other protomer and a sulfilimine bond (S=N) is formed (Figure 1.2). The sulfilimine bond creates NC1 hexamers and these, along with the N-terminal 7S bonds, form the collagen IV scaffold network which stabilizes the BM so it can support and anchor overlaying epithelial and endothelial cells, regulate cell polarity, proliferation, differentiation, and migration (LeBleu *et al.,* 2007; Bhave *et al.,* 2012; McCall *et al.,* 2014; Bhave *et al.,* 2017).

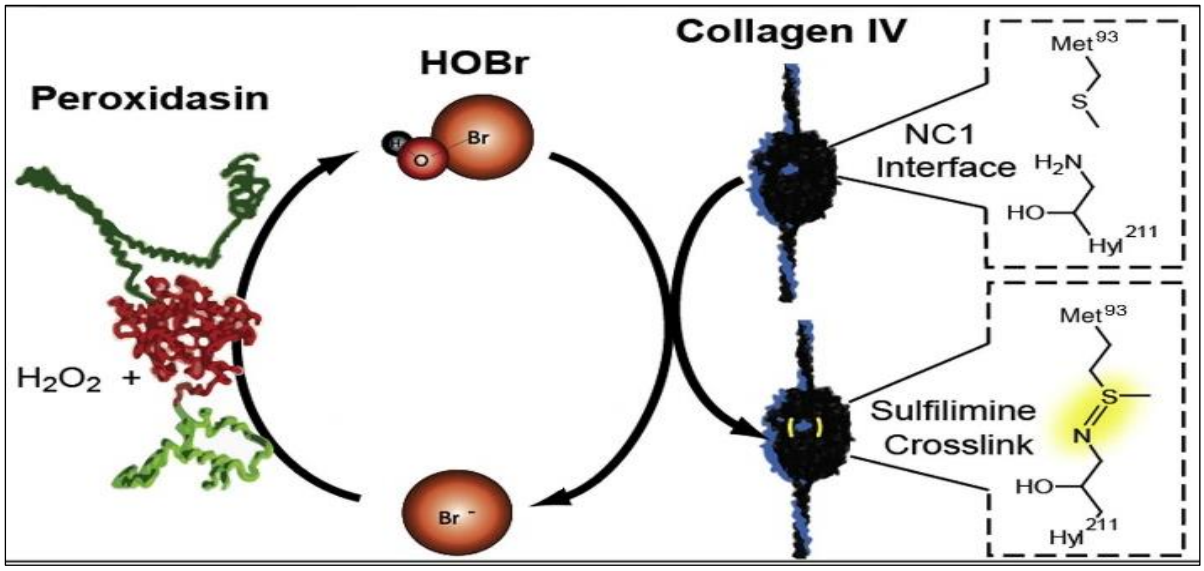

Figure 1. 2: The crosslinking of collagen IV protomers by PXDN. PXDN is found in the collagen IV scaffold of the basement membrane (BM) which underlies tissues. It catalyses the oxidation of bromine ion (Br^-) by H_2O_2 to form hypobromous acid (HOBr) which binds to the NC1 interface of collagen IV protomers and crosslinks neighbouring Met-93 and Hyl-211 residues to form a sulfilime bond (S=N) (Adapted from McCall *et al.,* 2014).

In addition to catalysing the formation of sulfilimine crosslinks, PXDN forms dityrosine bonds that stabilize the ECM (Cheng *et al.*, 2011; Bathish, *et al.*, 2020). In a recent study, it was further shown that the loss of PXDN not only compromised the collagen IV crosslinks but it affected the assembly of fibronectin and laminin networks (Lee *et al.*, 2020). PXDN is therefore an important protein needed for the assembly and stability of the ECM.

1.1.4.2 ECM-mediated cellular activities

PXDN is involved in various ECM-mediated cellular activities including cell attachment, proliferation, and migration. Tauber *et al.* (2010) investigated the attachment of cells under haem oxygenase 1 (HO-1) signalling and showed that BeWo choriocarcinoma cells expressing the protein were more adherent as compared to those deficient in HO-1. PXDN was shown to facilitate this process by aiding the cells to adhere to the ECM proteins laminins, fibronectin, and collagen I. PXDN has also been shown to facilitate the proliferation of various cells such as ovarian cells, vascular smooth muscle cells and lens and corneal cells (Shi *et al*., 2011; Yan *et al*., 2014; Zheng *et al*., 2018). Lee *et al*. (2020) also recently showed that PXDN plays a role in the proliferation of vascular endothelial cells. Here, the siRNA knockdown of PXDN transcript reduced the cells proliferation and adherence and caspace3/7 levels increased, resulting in the reduced viability of the cells.

Another important role of PXDN is mediating cell migration and it does this through epithelial-to-mesenchymal transition (EMT), an ECM remodelling process that allows cells to be motile as they lose their cell-cell and cell-matrix attachments (Kalluri and Weinberg, 2009). PXDN was shown to respond to transforming growth factor-β (TGF-β), a potent inducer of EMT and, under its signalling, PXDN levels decreased and this subsequently decreased cell attachment and increased their migration (Xu *et al.,* 2009; Sitole and Mavri-Damelin 2018). EMT also occurs under oxidative conditions and this is driven by the increased levels of reactive oxygen species (ROS), which are generated from cellular respiration and NOX (Schieber and Chandel, 2014; Jiang *et al.,* 2017). Hanmer and Mavri-Damelin (2018) showed that when cancerous cells are treated with H_2O_2, PXDN levels increase; the knockdown of *PXDN* during oxidative stress, however, led to a decrease in cell attachment, migration, and invasion.

1.1.4.3 Innate immunity

The haem-peroxidases MPO and LPO have well-described roles in host immunity and more recently PXDN has also been shown to participate in this protective function albeit to a lesser extent. Li *et al.* (2012) found that PXDN is secreted by endothelial cells into the plasma, and it can bind to bacteria at physiological pH. When *E. Coli* was incubated with PXDN, H_2O_2 and Cl^-, the bacteria died, but without the H_2O_2 and Cl^- chemical substrates, the enzyme was unable to kill the bacteria, indicating that its oxidation of Cl into HOCl is the key in its bactericidal activity (Li *et al.,* 2012). The study done by Shi *et al.* (2018) demonstrated that the bactericidal activity of PXDN is only directed towards gram-negative bacteria, which contain lipopolysaccharide (LPS) that activate the enzyme. In the study, PXDN was shown to bind to the bacteria at the LPS regions through the N-terminal LRR and IgG domains and was able to kill *Escherichia coli* and *Pseudomonas aeruginosa* in the presence of H_2O_2 and Cl^- (Shi *et al.,* 2018). The study further demonstrated that PXDN-deficient mice with gram-negative pneumonia had a substantially lower survival rate than the wild-types and eventually died. These findings therefore highlight that PXDN is involved in lung defences (Shi *et al*., 2018).

1.1.5 The pathophysiological roles of PXDN

1.1.5.1 Developmental structural deformities

PXDN plays a key role in consolidating the structural integrity of the BM and this is key in organogenesis as it provides cells with structural support, anchorage, establishes their apicobasal polarity and mediates their proliferation and migration (Jayadev and Sherwood,

2017). In invertebrates, the loss of PXDN results in structural deformities and early embryonic death. Mutations in the PXN gene of *Drosophila* result in the loss of collagen IV sulfilimine crosslinks, causing tearing in midgut visceral muscles and the larvae die at the third instar stage (Bhave *et al.,* 2012). *C. elegans* has two PXDN homologues, PXN-1 and PXN-2 and mutations in the former do not cause developmental defects but in the latter, mutants have been shown to have a disorganized BM which deleteriously affects muscle-epidermal attachment, epidermal elongation, egg laying and causes muscular dystrophy and early larval lethality (Gotenstein *et al.,* 2010). These PXDN mutations are synonymous with collagen IV mutations where it is reported that the muscle tissue of invertebrates detach from the epidermis as the BM is not tensile enough to support their contractions (Borchiellini *et al.,* 1996). This illustrates that collagen IV needs to be present and properly reinforced by PXDN for proper embryonic development.

1.1.5.2 Ocular diseases

PXDN mutations in vertebrates also cause pathophysiological conditions and in mice and humans, eye defects have been extensively described. Mice with a biallelic knockout of *PXDN* have decreased collagen IV sulfilimine crosslinks and this causes a range of ocular defects including severely reduced eye size, closed eyelids, cataracts, and abnormal eyeball formation which causes anophthalmia or microphthalmia (Kim *et al.,* 2019). Interestingly these *PXDN* mutation must be homozygous as heterozygous mice had similar phenotypes to wildtypes indicating that the *PXDN* gene is haplosufficient (Kim *et al.,* 2019). Anterior segment dysgenesis (ASD) is a pathology wherein the lens, cornea and iris develop abnormally. ASD is commonly associated with genes such as *PAX6, PITX2, FOXC1,* and *COL4A1* but recently *PXDN* has been identified as a novel contributing gene (Reis and Semina, 2011; Choi *et al.,* 2015). Homozygous nonsense mutations in mice were shown to result in the loss of the peroxidase and vWFC domains, and the *PXDN* knock-out mouse models developed ASD, microphthalmia, glaucoma and retinal dysgenesis (Yan *et al.,* 2014). Similarly, in humans, homozygous mutations have been shown to cause ASD, congenital cataracts, corneal opacity, glaucoma, anophthalmia and microphthalmia (Khan *et al.,* 2011; Choi *et al.,* 2015). These ocular anomalies are thought to occur due to the destabilization of the BM, which affects the structural support to the developing anterior chamber structure and in addition, there is an increased accumulation of free radicals in the eye and these damage ocular structures causing inflammation and leading to impaired eye development and function (Khan *et al.,* 2011).

1.1.5.3 Cardiovascular diseases

In humans, PXDN is expressed quite ubiquitously throughout the body but studies have shown that it is more abundant in the heart and vascular tissues, hence the gene was alternatively named vascular peroxidase 1 (VPO1) (Cheng *et al.,* 2008). VPO1 was shown to cause atherosclerosis through the oxidation of low-density-lipoproteins (LDL) and apolipoprotein E (ApoE) resulting in endothelial cell injury, lipid accumulation in the arteries which forms plaque thus initiating atherogenesis (Yang *et al.,* 2013). Plaque formation is also exacerbated during inflammation as the high expression of tumour necrosis factor α (TNF-α) and lipopolysaccharides (LPS) increase VPO1 levels, which in turn oxidizes LDL and recruits foam cells to the arteries and atherosclerosis progresses (Yang *et al.,* 2016). Another role of VPO1 in cardiovascular diseases is linked to mitigating oxidized LDL (ox-LDL)-induced apoptosis of endothelial cells. Increased intracellular levels of ox-LDL activate NOX2 and this increases ROS levels and then VPO1 and HOCl. These in turn increase p38 MAPK and caspase-3 resulting in endothelial cell death which contributes to thrombosis and atherosclerosis (Bai *et al.,* 2011).

1.1.5.4 Cancer

The earliest detection of PXDN in cancer was in melanoma cells where it was found to be highly expressed and it was consequentially termed melanoma-associated gene 50 (MG50) (Weiler *et al.,* 1994). Paumann-Page *et al.* (2021) recently corroborated these early findings by showing that the mRNA and protein levels of PXDN were highly expressed in invasive melanoma cells compared to the non-invasive subtype, therefore PXDN enhances their migration. Ovarian cancer cells also have high levels of *PXDN* expression and when the gene is silenced, this decreases the proliferation, migration, and invasion of cells and this was attributed to a perturbation in the PI3K/Akt pathway (Zheng and Liang, 2018). In breast cancer, the oncogenic effects of PXDN are similarly linked to the PI3K/Akt pathway and this was shown by Young *et al.* (2015) where they found that *PIK3CA* mutant cells had high expression levels of genes which included *PXDN, laminin, fibronectin, and thrombospondin 1* (*THBS1*). The knock-down of these genes decreased proliferation. PXDN also contributes to carcinogenesis via the moderation of H_2O_2, which is a potent ROS. This was illustrated in prostate cancer, where the protein is overexpressed and it reduces the intracellular levels of ROS thus inhibiting apoptosis from being triggered and tumours survive (Dougan *et al.,* 2019). In colon cancer however, PXDN increases ROS levels thus triggering p53-mediated

apoptosis and from this PXDN was termed p53-responsive gene 2 protein (PRG2) (Horikoshi *et al.,* 1999).

PXDN also contributes to the development of cancer by being aberrantly expressed with other proteins such as HO-1 which promotes tumour growth and survival. The proteins were shown to co-localize in invasive trophoblasts and the knockdown of HO-1 in the cells decreased their adhesion, migration, and invasion. When the *PXDN* was instead silenced, the cells similarly showed decreased adhesion to laminins and fibronectin and were less invasive. This, therefore, showed that PXDN mediates the oncogenic effects of HO-1 in the ECM (Tauber *et al.,* 2010). In bladder cancer, a hub of genes was identified using gene co-expression networks and *PXDN* was among them along with *COL1A1, COL1A2, COL5A1, COL8A1, COL11A1, MMP2* and *TGFβ1I1*, all of which were associated with poor prognosis (Di *et al.,* 2019). In glioblastomas, PXDN is also overexpressed and protein-protein interaction networks identified *COL4A1* and *COL5A1* as some of the genes associated with promoting tumour proliferation, migration, and survival (Shi *et al.,* 2022). In addition to aberrantly expressed proteins, PXDN is also co-expressed with the long non-coding RNAs (lncRNA) AC046143.1 and hepatocellular carcinoma up-regulated EZH2-associated long non-coding RNA (HEIH) which are known to promote tumour progression (Shi *et al.,* 2022). Interestingly PXDN has also been shown to activate cancer hallmarks including EMT, glycolysis, hypoxia, and inflammation (Shi *et al.,* 2022). In oral squamous cell carcinoma (OSCC), PXDN is highly expressed with concomitant increases in lactate and ATP, and this increases tumour metastasis and invasion (Kurihara-Shimomura *et al.,* 2020). Collectively, these studies show that PXDN has both pro- and anti-tumour effects on cancers by moderating ROS levels, ECM remodelling, being co-expressed with other oncogenes and driving key cancer phenotypes.

1.1.5.5 Fibrosis

The aberrant expression of PXDN is also linked to the development and progression of fibroproliferative diseases. PXDN, along with MPO and EPO, have been shown to cause fibrosis through the production of hypohalous acids. These highly reactive compounds can oxidize proteins and lipids that can cause inflammation, which triggers abnormal wound healing (Davies *et al.,* 2008). Fibrotic mouse models with unilateral ureteral obstruction (UUO) were shown to have high expressions of the PXDN, MPO and EPO with concomitant increases in renal inflammation and fibrosis. The knockout of these peroxidases identified PXDN and EPO as the proteins promoting fibrosis due to the synthesis of HOBr as there was

a markedly reduced collagen I deposition and α-smooth muscle actin (α-SMA) expression, in the renal tubules (Colon *et al.,* 2019). α-SMA is an important protein which gives fibroblasts a contractile phenotype thus enabling them to migrate into injured and fibrotic tissue sites (Shinde *et al.,* 2017). PXDN has been shown to participate in wound healing by modulating the architecture and stiffness of the matrix and it therefore plays a role in fibrosis where matrix stiffness is a hallmark (Thannickal *et al.,* 2014). Bhave *et al.* (2017) demonstrated the role of PXDN in matrix stiffness by knocking out its gene in mouse models and this significantly reduced the renal tubule collagen IV sulfilimine crosslinks along with the tubular BM stiffness.

Aberrant PXDN expression is also associated with the development of Goodpasture (GP) disease, which is an autoimmune disease wherein antibodies attack the α3 chain NC1 domains of collagen IV molecules in BM of the alveoli and glomerulus (Kalluri *et al.,* 1994). In a study done by McCall *et al.* (2018) anti-PXDN autoantibodies were found in 46% of the GP disease cohort. These patients had reduced HOBr synthesis and more severe inflammation in the of the vasculature. Inflammation is a key parameter in fibrogenesis and because in GP disease glomerulonephritis and pulmonary haemorrhaging occur, as they progress fibrosis would develop. Panjwani *et al.* (2003) report that in 80% of GP disease cases, patients will have abnormal chest radiography and interstitial fibrosis and the prognosis worsens with the detection of scarring and interstitial fibrosis.

PXDN has been shown to cause renal, cardiac, liver and fibrosis (Péterfi *et al.,* 2009; Liu *et al.,* 2019; Sojoodi *et al.,* 2022). Péterfi and colleagues were the first to demonstrate that the protein is expressed in the endoplasmic reticulum of human pulmonary and dermal fibroblasts, key pro-fibrotic cells found in the connective tissue which transdifferentiate into myofibroblasts during wound healing and secrete matrix proteins and exert contractile forces on the wound area to help with its closure (Péterfi, *et al.,* 2009). Furthermore, the study showed that PXDN mRNA expression increased in response to TGF-β1, a pro-fibrotic cytokine and it activated myofibroblasts as seen with an increase in α-SMA and in turn the cells secreted PXDN into the extracellular space of fibrotic kidneys of mice. Here PXDN colocalized with fibronectin and together these proteins enhance the stiffening of the renal BM (Péterfi, *et al.,* 2009). In the heart, VPO1 expression is upregulated following myocardial infarction-induced fibrosis. Here PXDN induces the differentiation, migration, and proliferation of cardiac fibroblasts through HOCl biosynthesis which activates the Smad2/3 and ERK1/2 pathways. The activated fibroblast in turn increases the expression of collagen I

and α-SMA and this promotes fibroplasia. Echocardiography analysis showed that siRNA knockdown of VPO1 improved cardiac function in the mouse models and they had a better survival rate (Liu *et al.,* 2019).

In liver fibrosis, PXDN is expressed and secreted into the fibrotic tissue by hepatic stellate cells (HSC), resident liver cells that can differentiate into myofibroblast (Puche *et al.,* 2013; Sojoodi *et al.,* 2022). PXDN is upregulated during liver fibrosis and this was detected in the liver biopsies of patients with cirrhosis and non-alcoholic fatty liver disease (NAFLD) and mouse models with carbon tetrachloride (CCl_4)-induced fibrosis. The analysis of the deficiency of PXDN ($PXDN^{-/-}$) in the CCl_4-injured mice resulted in reduced collagen I crosslinks and fibrolysis occurred due to the increase in MMP8 and MMP13 expression thus reducing the density of the fibrotic deposits. Furthermore, the loss of PXDN increased the recruitment of M2 macrophages $CD45^+F4$, $CD206^+$ and $CCR2^+$, which mitigate inflammation and promote normal tissue healing (Braga *et al.,* 2015; Sojoodi *et al.,* 2022). Overall, these changes improved liver function and regeneration as seen with decreased alanine transaminase (ALT) and aspartate transaminase (AST) (Sojoodi *et al.,* 2022). Overall, these studies illustrate that PXDN mediates tissue fibrosis by remodelling the ECM, regulating HOBr and HOCl levels, responding to TGF-β stimulation, regulating fibroblast differentiation and proliferation and macrophage recruitment. Thus, targeting the PXDN may ameliorate fibrosis.

1.1.6 The regulation of *PXDN* expression

The regulation of *PXDN* expression involves epigenetic mechanisms, transcriptional and mRNA transcript regulation. DNA methylation is the most described epigenetic modifications that occurs on the *PXDN* promoter, and similar to other genes the modification occurs in, it downregulates the expression of the *PXDN* gene (Moore *et al*., 2013; Zhou *et al.*, 2022). Interestingly folic acid, a molecule known to prevent oxidative damage in cells has been shown to be an inducer of *PXDN* methylation. This was illustrated in human umbilical vein endothelial cells (HUVECs) treated with ox-LDL and here folic acid stimulated the expression of DNA methyltransferases (DNMTs), and this resulted in the hypermethylation of the *PXDN* promoter thus preventing the accumulation of LDL in arteries which cause atherosclerosis. In the absence of folic acid however PXDN levels increased and atherosclerosis developed (Cui *et al*., 2018). This illustrates that PXDN expression can be regulated by the methylation of its promoter.

Transcriptional regulation is another key mechanism that regulates the expression of the *PXDN* gene and so far, two upstream regulators have been identified: Snai1 and nuclear factor erythroid 2–related factor 2 (Nrf2). The Snai1 TF is responsible for triggering EMT and it primarily does this by inhibiting the expression of E-cadherin and this allows cells to become mesenchymal (Nieto, 2002). EMT mainly occurs through the alteration of the ECM and since PXDN is responsible for its formation and reinforcement it is one the key genes whose expression is altered to enable EMT processes to occur. Under Snai1 regulation, *PXDN* expression has been shown to become downregulated and this facilitates the proliferation and migration of cells (Sitole and Mavri-Damelin, 2018). As previously described, PXDN responds to changes in ROS levels, and in a study by Hanmer and Mavri-Damelin (2018) they showed that Nrf2 activates its expression. This finding is very fitting as Nrf2 is a master regulator of the antioxidant response and is activated in response to increased levels of ROS to protect cells from oxidative damage (Itoh *et al.*, 1997).

The expression of *PXDN* can also be modified by targeting its mRNA for degradation. Briem *et al.* (2019) identified miR-203a as the miRNA mediating this process. Here they showed that the 3′-untranslated region (3′-UTR) of the *PXDN* promoter contains three miR-203a binding sites and miR-203a repressed its expression in the mesenchymal breast epithelial cell line D492M leading to their decreased proliferation. The expression of the PXDN protein can also be altered post-translationally. PXDNL, a PXDN homolog protein which is only expressed in the heart and lacks any peroxidase catalytic activity has been shown to alter PXDN expression. PXDNL forms a complex with PXDN and this inhibits the activity of PXDN (Péterfi and Geiszt, 2014). To further understand the role of PXDN in fibrosis, in this study we focused on the transcriptional regulation of PXDN under the early growth response 1 (EGR1) TF.

1.2 Tissue fibrosis

1.2.1 Pathogenesis

Fibrosis is the excessive deposition of ECM proteins in the connective tissue of organs (Krieg *et al.*, 2007). The disease may develop due to physical trauma, infections, chemical irritants, and autoimmune reactions (Wynn, 2008). Fibrosis can also be an end-stage of chronic diseases such as hypertrophic cardiomyopathy, chronic kidney disease (CKD), NAFLD and non-alcoholic steatohepatitis (NASH) and most recently coronavirus disease (COVID-19) has also been implicated (Brunt, 2004; Cho, 2010; Ho *et al.*, 2010; Ali and Ghonimy, 2021; Heyens *et al.*, 2021). These factors cause repetitive tissue injury which activates abnormal

wound healing thereby leading to fibrosis. Wound healing occurs through four phases starting with haemostasis, followed by inflammation, then proliferation and ending with the remodelling phase (Figure 1.4). In haemostasis, haemorrhaging is stopped via vasoconstriction as platelets and fibrins are activated and form a clot that causes blood coagulation (Armstrong and Golan, 2011; Palta *et al.*, 2014). In the inflammatory phase, macrophages, leucocytes and neutrophils are recruited and they secrete antimicrobial peptides and proinflammatory cytokines such as tumour necrosis α (TNF-α), interferon-gamma (IFN-γ) and interleukins (IL), and these trigger inflammation, which clears invading microbes and damaged cells (Borthwick *et al.*, 2013). Once the inflammatory phase is completed, activated immune cells undergo apoptosis, but in fibroplasia, this does not happen resulting in uncontrolled inflammation (Lee and Kalluri, 2010).

In the proliferative phase, the matrix is repaired and the damaged cells are replaced with new cells. TGF-β has been shown to be a strong driver of this phase (Meng *et al.*, 2016). Fibroblasts are activated to transdifferentiate into myofibroblasts, which secrete matrix proteins such as collagen into the extracellular space (Darby *et al.*, 2016). To enhance matrix repair, fibrocytes from the bone marrow and pericytes are also recruited to wound and secrete more proteins (Grieb *et al.*, 2011; Thomas *et al.*, 2017). Matrix crosslinking enzymes such as PXDN, LOX and transglutaminase 2 (TG2) are upregulated to facilitate the formation of the preliminary ECM granulation tissue so that cells can attach to form new tissue, but in fibroplasia, these enzymes excessively crosslink the matrix and it becomes stiff (Péterfi *et al.*, 2009; Cai *et al.*, 2017; Tatsukawa and Hitomi, 2021). Growth factors such as fibroblast growth factor (FGF), PDGF, EGF, VEGF and depending on the tissue type other site-specific ones such as HGF and keratinocyte growth factor (KGF) are expressed to stimulate cell growth and proliferation (Werner *et al.*, 2007; Demidova-Rice *et al.*, 2012; Li *et al.*, 2013). The resident cells of the affected tissue proliferate and migrate into the wound and adhere to the BM and reepithelialisation occurs followed by angiogenesis, which restores blood perfusion (Li *et al.*, 2003; Ben Amar and Wu, 2014).

In the remodelling phase, the wound is closed and this is facilitated by the contraction of myofibroblasts, which express high levels of α- SMA (Shin and Minn, 2004; Shinde *et al.*, 2017). The expression of MMPs is also upregulated and these degrade the excess amounts of ECM proteins secreted into the wound (Caley *et al.*, 2015). Apoptosis is then initiated to eliminate myofibroblasts along with any unviable cells (Guerin *et al.*, 2021). In fibrosis however, matrix proteolysis is reduced as TIMP are upregulated and myofibroblasts evade

apoptosis and senescence and as a result, the affected tissue thickens and scars (Arpino *et al.*, 2015; Hinz and Lagares., 2020). In the lungs, the clinical manifestation of fibrosis includes decreased total lung capacity (TLC), forced expiratory volume (FEV) and severe coughing and thromboembolisms and these cause dyspnoea (Nakamura and Suda, 2015). In the kidneys nephropathy occurs resulting in a decreased glomerular filtration rate, increased intratubular pressure and proteinuria (Kuusniemi *et al.*, 2005; Kaissling *et al.*, 2013). Liver fibrosis increases the portal hypertension, reduces clotting factor synthesis, there's a build-up of bile and patients may develop jaundice and ascites (Kobelska-Dubiel *et al.*, 2014). Fibrosis, therefore, alters the architecture of the ECM and this disrupts the normal physiological functioning of tissues and if left untreated it can cause organ failure and death.

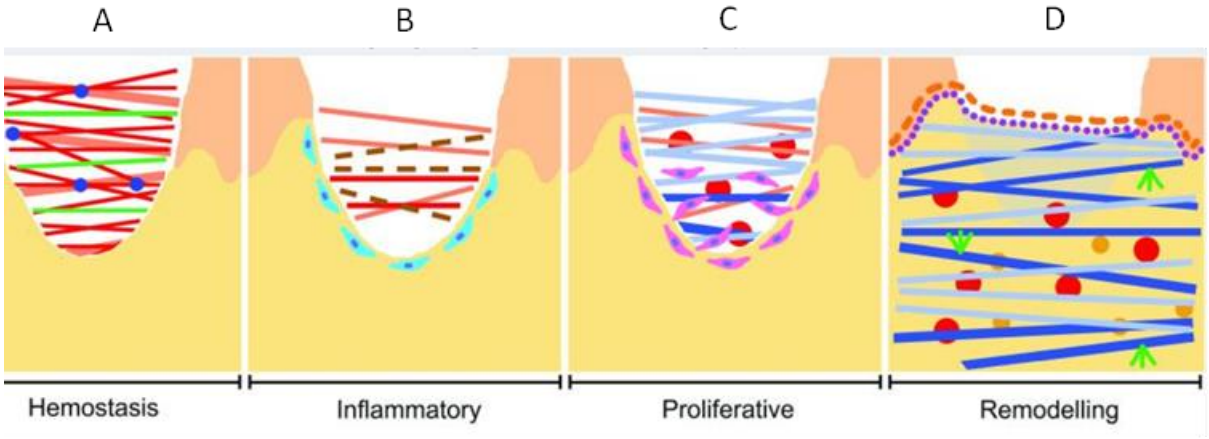

Figure 1.3: The phases of wound healing. A) Platelet and fibrin clots are formed to coagulate blood. B) The immune system is activated to prevent infections and clear damaged cells. C) Fibroblasts are recruited and they secrete proteins that repair the ECM which will anchor new cells and new vasculature is formed. D) The injured tissue is remodelled so that it closes and forms a scar (Adapted from Tracy *et al.*, 2016).

1.2.2 Type II EMT as a fibrosis pathway

EMT is a process in which epithelial cells undergo a series of mechanochemical transformations to attain a motile mesenchymal phenotype (Kalluri and Weinberg, 2009). EMT involves the ECM as it is the main structural scaffolding anchoring epithelial cells (Morrissey and Sherwood, 2015). In EMT, the ECM adhesion complexes including adheren junctions, tight junctions and desmosomes are degraded and this results in the loss of cell-cell and cell-ECM attachments and their apicobasal polarity and cells become increasingly motile (Lamouille *et al.*, 2014). During EMT, genes such as *N-cadherin, vimentin, fibronectin* and *MMPs* are upregulated and they increase the motility of cells and this is accompanied by the

downregulation of genes such as *E-cadherin* which facilitate the anchorage of cells to the ECM (Nisticò *et al.*, 2012; Liu *et al.*, 2015; Li *et al.*, 2017; Loh *et al.*, 2019). The changes in the expression levels of these gene can be regulated by EMT-inducing factors such as TGF-β1 and TFs such as Snai1, Slug, twist-related protein 1 (Twist1) and EGR1 and they promote the acquisition of a mesenchymal phenotype (Willis and Borok, 2007; Medici *et al*., 2008; Wang *et al*., 2016; Wang *et al*., 2023).

There are three types of EMT, type I is associated with embryo development and organogenesis, type II is associated with wound healing and fibrosis and type III EMT is involved in cell proliferation and causes cancer (Kalluri and Weinberg, 2009). Of interest in this project is type II EMT as it contributes to the development and progression of fibrosis. This EMT subtype mainly involves fibroblasts, cells that are predominantly found in connective tissues and responsible for the secretion of matrix proteins such as collages, fibronectin, elastin, and laminins (Kendall and Feghali-Bostwick, 2014). Following tissue injury fibroblasts cells are activated by signalling molecules such as TGF-β to undergo EMT to form myofibroblasts and in addition EMT can be induced on adipose cells, monocytes, and epithelial and endothelial cells to produce more myofibroblasts (Marconi *et al.*, 2021). Once formed, myofibroblasts can migrate to the injured tissue and facilitate tissue repair by secreting matrix proteins (Darby *et al.*, 2016). Myofibroblasts are also reported to generate contractile force in the injured sites and surrounding area, and this helps with the closure of the wound (Shin and Minn, 2004). During normal healing, myofibroblasts stop secreting matrix proteins once re-epithelialisation has occurred but with persistent tissue injury their activity is sustained in the proliferative phase of wound healing and in addition, they evade apoptosis and this results in tissue fibrosis (Hinz and Lagares, 2020).

1.2.3 TGF-β1 as a driver of fibrosis

TGF-β1 is a cytokine that stimulates cell growth, proliferation, differentiation, migration, and apoptosis (Zhang *et al.*, 2017). It belongs to the TGF-β family which is comprised of TGF-β1, TGF-β2 and TGF-β3. These three proteins have highly homologous structures, but their genes are found on different chromosomes with TGF-β1 on 19q13.1, TGF-β2 on 1q41 and TGF-β3 is on loci 14q24 (Fujii *et al.*, 1986; Barton *et al.*, 1988; Ten Dijke *et al.*, 1988). The TGF-β proteins interact with the same cell surface receptors and activate similar pathways, but TGF-β1 is the most abundant and characterised isomer and hence the term TGF-β tends to be associated with it (Kubiczkova *et al.*, 2012). TGF-β proteins are synthesized as inactive precursors associated with the latency-associated protein (LAP) and these form the small

latent complex (SLC) (Dubois *et al.,* 2001). The SLC associates with latent TGF-β binding protein (LTBP) to form a large latent complex (LLC) and it is secreted into the extracellular space. Once the appropriate stimuli are received by the cell, such as wound healing, TGF-β is released from the LLC and can bind to its protein kinase receptors (Walton *et al.,* 2010; Poniatowski *et al.,* 2015). The active TGF-β ligand then binds to its TβRI and TβRII receptors and they form a heterotetramer, which phosphorylates intracellular proteins (Huang and Chen, 2012). Two TGF-β pathways can be activated by the receptors, the conical and the nonconical pathways. In the conical pathway, SMAD proteins are phosphorylated leading to a signalling cascade that eventually activates downstream TFs which then activate the expression of TGF-β target genes (Zi *et al.,* 2012). In the non-conical pathway multiple pathways can be activated by the cytokine namely, MAPK (JNK/ERK/p38), PI3K/ATK/mTOR, RhoA/Rock/Cofllin, TREF/NF-κB, and Ras/RAF/ERK (Zhang, 2017).

During persistent tissue injury, TGF-β1 acts as a key mediator of fibroproliferation. The levels of the cytokine are upregulated as macrophages, leucocytes, fibroblasts, epithelial and endothelial cells continuously secrete it and in addition, its receptors are upregulated making cells more responsive to its effects (Nakerakanti and Trojanowska., 2012; Meng *et al.,* 2016). TGF-β1 aberrantly increases the expression of TNF-α and IL-4, IL-5, IL-13, and IL-21 (Richter *et al.,* 2015). Inflammation is also exasperated by the upregulation of ROS releasing proteins such as NOX4 and this promotes the development of fibrosis (Cucoranu *et al*., 2005). The pro-fibrotic roles of TGF-β1 are predominantly directed to fibroblasts as they secrete ECM proteins which augment fibrosis. TGF-β1 activates type II EMT by increasing the expression of N-cadherin, Snai1 and α-SMA and this allows fibroblasts to differentiate into myofibroblasts, which can migrate into the injured fibrotic sites (Willis and Borok, 2007). TGF-β1 also increases the numbers of myofibroblasts by aberrantly activating cyclin-dependent kinases (CDKs) to facilitate their progression through the cell cycle and these increased numbers cause physiological scarring (Yamamoto *et al.,* 2020). TGF-β1 also increases the survival of fibroblasts via upregulating the expression of anti-apoptotic genes such as BCL2, BCL-XL and X-linked inhibitor of apoptosis protein (XIAP) (Hinz and Lagares, 2020).

As myofibroblasts persist in the ECM, they secrete excess amounts of proteins such as collagens, fibronectin, laminins, glycoproteins, and proteoglycans and the matrix thickens and scars (Klingberg *et al.,* 2013). Matrix thickening is further exasperated as TGF-β1 suppresses the catalytic activity of matrix proteases such as MMPs and plasminogen activator

via activating their inhibitors TIMPs and plasminogen activator inhibitor-1 (PAI-1) and consequently, proteins accumulate in the ECM leading to tissue fibrosis (Samarakoon *et al.,* 2008; Arpino *et al.,* 2015). To stabilize the remodelled matrix which contains excess proteins, TGF-β upregulates the expression of matrix crosslinking enzymes such as LOX and PXDN and the matrix stiffens resulting in the loss of tissue elasticity (Péterfi *et al.,* 2009; Lu *et al.,* 2019). TGF-β1 also creates a fibrotic microenvironment that sustains fibroproliferation through upregulating the expression of growth factors such as VEGF, PDGF, CTGF, and EGF. These promote angiogenesis and the growth and proliferation of myofibroblasts and organ-specific cells, and these increase the deposition of proteins into the surrounding ECM and therefore fibrosis worsens (Ihn, 2002; Chen *et al.,* 2006; Pakyari *et al.,* 2013).

1.2.4 Pharmacological treatments of fibrosis

Fibrosis is a progressive, life-threatening disease that remodels the connective tissue of organs thus interfering with their normal physiological functioning (Wynn, 2008). Various drugs have been approved for the treatment of the disease whilst many others are undergoing pre-clinical and clinical trials. Infections and pro-inflammatory cytokines are major activators of an exaggerated immune response and targeting them has been shown to improve fibroproliferation. In cystic fibrosis, inhaled antibiotics such as tobramycin, aztreonam lysine and levofloxacin are used (Taccetti *et al.,* 2021). Anti-fibrotic drugs also target pro-inflammatory cytokines and in a three-year study conducted by Brown *et al.* (2011) conducted on patients with arthrofibrosis the inhibition of IL-1 with anakinra had reduced patient's knee pain and swelling and significantly improved their range of motion. TNF-α expression can be inhibited with infliximab, a monoclonal antibody that is used to treat patients with Crohn's disease (Poggioli *et al.,* 2007). When the drug was used on Crohn's disease patients with fibrotic strictures, the intestinal biopsies from patients who had responded to infliximab had decreased depositions of collagen and fibronectin and thinner mucosal linings compared to their non-responder counterparts (de Bruyn, *et al.,* 2018).

TGF-β1 plays a central role in the development of fibrosis and various drugs have been used to moderate its effects. Disterine (P144) functions by binding to the TGF-β1 receptors TβRI and TβRII and inhibits the phosphorylation of Smad2/3 and when the drug was administered to rabbits with radiation-induced fibrosis (RIF) the treated group had decreased muscle fibrosis, alopecia, and collagen deposits (Cruz-Morande *et al.,* 2022). Pirfenidone also targets TGF-β1 expression and in human lung fibroblasts, it was shown to cause a decrease in α-SMA expression and collagen I synthesis (Conte *et al.,* 2014). Rapamycin is another anti-

fibrotic drug and it blocks the TGF-β1 downstream gene mammalian target of rapamycin (mTOR) and has been used successfully in the treatment of kidney fibrosis and it was also shown to reduce the proliferation, metabolic rate, and collagen I synthesis of primary fibroblasts from biopsies of patients with laryngotracheal stenosis (Chen *et al.,* 2012; Namba *et al*., 2015). The profibrotic effects of TGF-β1 can also be mediated indirectly through targeting downstream TFs. In an idiopathic pulmonary fibrosis (IPF) study, Jayachandran *et al.* (2009) demonstrated that targeting Snai1/2 with siRNA in alveolar epithelial type II (ATII) cells treated with TGF-β1 decreased their migration and the expression of the EMT markers E-cadherin, occludin (OCCL) with a parallel increase in vimentin and α-SMA.

Tissue fibrosis develops due to the altered synthesis and degradation of ECM proteins. Reduced matrix turnover occurs due to the upregulated expression of TIMP proteins which inhibit MMP proteases (Benyon and Arthur, 2001). When HSCs were subjected to TIMP1-siRNA, researchers found that this reduced the proliferation of the cells and overall liver stiffness (Fowell *et al.,* 2011). In fibrogenesis, cells express high levels of B-cell lymphoma-2 (BCL2) proteins and this helps them evade apoptosis (Drakopanagiotakis *et al.,* 2008). Navitoclax (ABT-263) has been used to block the activity of BCL-2 protein and in a mouse model of dermal fibrosis this decreased myofibroblast survival (Lagares *et al.,* 2017). Similarly, in mice with radiation-induced pulmonary fibrosis, navitoclax activated the clearance of senescent pneumocytes and this reversed fibrosis in the animals (Pan *et al.,* 2017). Growth factors are major mitogens for fibroproliferation and are also targeted in anti-fibrotic therapies. Nintedanib competitively binds to the tyrosine kinase receptors of FGF, PDGF and VEGF and blocks their phosphorylation and thus fibroblast proliferation and migration and angiogenesis decreases (Wollin *et al.,* 2015). Excessive matrix crosslinking is another key feature of fibrosis which results in a stiff matrix. The livers of CCl_4 injured rats treated with the LOX inhibitor, β-aminopropionitrile have been shown to have reduced stiffness and myofibroblast activation (Georges *et al.,* 2007). It is evident that targeting key signalling molecules in the fibrotic process can deliver positive outcomes and as such, it is important to identify more contributing genes to expand treatment options.

1.3 EGR1

1.3.1 Classification

EGR1 is a zinc-finger (ZF) TF that regulates cell growth, differentiation, and apoptosis (Sukhatme *et al.,* 1988). The protein was discovered independently by different researchers and therefore it has several names including nerve growth factor-induced A

(NGFI-A) (Milbrandt, 1987), Krox24 (Lemaire *et al.,* 1988) and Zif268 (Christy and Nathans, 1989), but EGR1 (Sukhatme *et al.,* 1988) is the most commonly used term. EGR1 belongs to the immediate early gene (IEG) protein family that also includes EGR1, 2,3 and 4, the genes of which are separately encoded for on chromosomes 5q31, 10q31, 8p21 and 2p13, respectively (O'Donovan *et al.,* 1999; Go *et al.,* 2019). The EGR proteins share homologous domains, most notably the ZF DNA binding domain (DBD) and thus recognise similar transcription factor binding site (TFBS) sequences in target genes. The EGR isoforms do however perform slightly different cellular functions; EGR1 is involved in cell growth and differentiation; EGR2 in peripheral nerve myelination and immunity; EGR3 activates T cells and regulates the sympathetic nervous system, and EGR4 in involved with central nervous system function (Beckmann and Wilce, 1997).

1.3.2 Structure

EGR1 is a 57 kDa protein but based on its post-translational modifications this size can vary between 75-100 kDa (Sukhatme *et al.,* 1988; Cheng *et al.,* 2008). The protein is a monomer composed of three Cys_2His_2 (C_2H_2) type ZFs (Figure 1.3). Each ZF is made of two antiparallel β-sheets on the amino side and an α-helix and on the carboxy end. The two cysteine residues are situated on the β-sheets whilst the histidines are on the α-helix and altogether these tetrahedrally stabilize the central zinc iron (Zn^{2+}) that is necessary for DNA binding (Cao *et al.,* 1990; Pavletich and Pabo, 1991). The DBD of EGR1 is conserved within its protein family and all constituting TFs recognise and bind to the same 9 bp GC-rich site with the consensus sequence 5'-GCG(T/G)GGGCG-3' termed the EGR binding site (EBS) which is located in the promoter of their target genes (Christy and Nathans, 1989). Here, each ZF binds to a trinucleotide within the EBS sequence (Figure 1.3). The α-helices make contact with the major groove of DNA via hydrogen bonds and the β-sheets stabilize the interaction and allow the protein to transactivate genes (Pavletich and Pabo, 1991). The ZFs bind in an antiparallel manner on the EBS with ZF3 being on the 5' end, followed by ZF2 and then ZF3 (Figure 1.3) (Zandarashvili *et al.,* 2012). The other functional domains of EGR1 include strong and weak activation domains on either terminals and a repressor domain, and these allow the EGR1 to act as both a negative and positive gene regulator. Completing the structure of the EGR1 protein is a bipartite nuclear localization signal (NLS) which is directly

situated before the DBD and it is responsible for directing the protein to the nucleus once the appropriated stimulus is received by the cell (Gashler *et al.*, 1993).

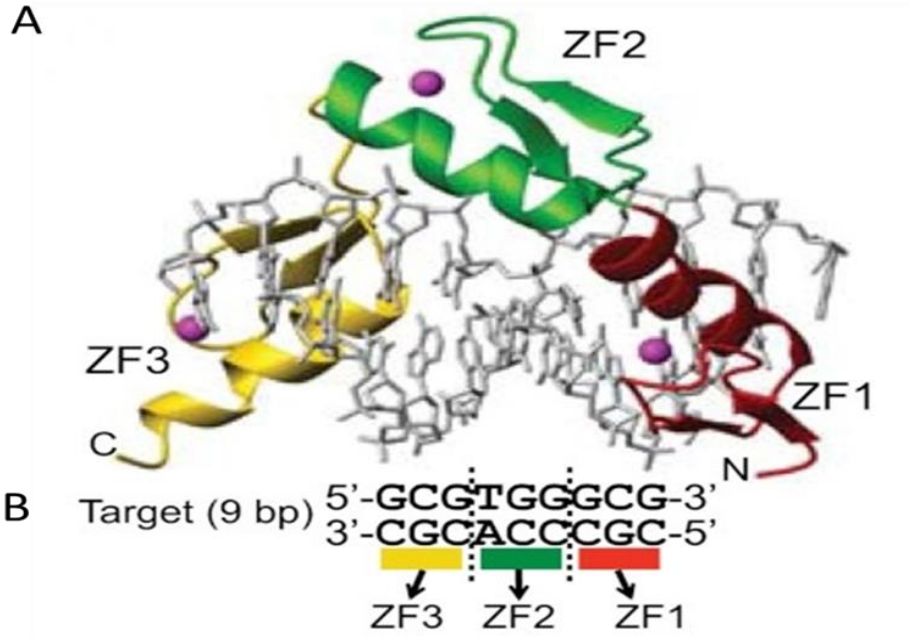

Figure 1.4: The structure of the EGR1 and its corresponding DNA binding site. A) EGR1 is composed of three zinc fingers (ZF1, ZF2 and Z3), which have an α-helix and two β-sheets. The α-helices fit into the major groove of the DNA and interact with the target DNA sequences and the β-sheets hold the protein in place during binding. B) The EGR binding site (EBS) is a 9 bp GC-rich sequence and the ZFs bind in an antiparallel direction starting with ZF3 followed by ZF2 and ZF1 (Adapted from Zandarashvili *et al.*, 2012).

1.3.3 *EGR1* expression

EGR1 is conserved in a host of different animal species such as zebrafish, mouse, chickens, cows, and humans (Close *et al.*, 2002; Sayasith *et al.*, 2006; Guo *et al.*, 2014; Løtvedt, *et al.*, 2017). The protein is expressed in various cells such as fibroblasts, mast cells, adipocytes, chondrocytes, and in endothelial and epithelial cells (Schwachtgen *et al.*, 1998. Li *et al.*, 2006; Bhattacharyya *et al.*, 2008; Rockel *et al.*, 2009; Zhang *et al.*, 2013). The expression of *EGR1* is induced by a broad range of biochemical and physiological stimuli such as growth factors, cytokines, hormones, oxidative stress, hypoxia, and tissue injury (Christy and Nathans, 1989; Gashler and Sukhatme., 1995; Tremblay and Drouin, 1999; Sperandio *et al.*, 2009; Bhattacharyya *et al.*, 2011; Qin *et al.*, 2022). These cues activate the expression of *EGR1* via the mitogen-activated protein kinase (MAPK) signalling pathway which activates the sequential phosphorylation between protein kinases, and this activates the expression of

target genes so they deliver the appropriate cellular responses (Keshet and Seger, 2010; more). There are three distinct MAPK pathways for EGR1 expression, and these depend on the stimulus received, if the stimulus is biochemical the extracellular signal-regulated kinase (ERK) pathway is activated and if it is extra or intracellular stress, then the JNK or p58 pathway is activated (Lim *et al.,* 1998; Guha *et al.,* 2001).

1.3.4 The transactivation of genes by EGR1

The transactivation of genes by EGR1 starts with its activation via phosphorylation. This is done by activation of both the protein kinase C (PKC) and tyrosine kinase pathways and these increase the transactivation activity of EGR1 (Huang *et al.,* 1998). Importantly, the activation of EGR1 is sustained by the downregulation of protein phosphatase inhibitors 1 and 2A and these maintain the phosphorylation modifications on the residues of EGR1 so that it can be able to transactive target genes (Cao *et al.,* 1992). Once activated, EGR1 undergoes nuclear translocation and here the importin protein 7 (Imp7) associates with the NLS of EGR1 and helps it move through the nuclear pores (Chen *et al.,* 2011). Once in the nucleus, EGR1 then binds as a monomer to the EBS and regulates the expression of genes (Christy and Nathans, 1989). EGR1 regulates the expression of a multitude of genes involved in cell growth, proliferation, and apoptosis. These include cell cycle genes such as *thymidine kinase* (Molnar *et al.,* 1994) and cyclin D proteins 1,2 and 3 (Wei *et al.,* 2017). Growth factors are also some of the EGR1-regulated genes and include the *epidermal growth factor* (*EGF*) (Arora *et al.,* 2008), *platelet-derived growth factor* (*PDGF*) (Khachigian *et al.,* 1997) and *vascular endothelial growth factor* (*VEGF*) (Shimoyamada *et al.,* 2010). ECM proteins are also some of the most prominent EGR1 target genes and include the various types of collagens such as *COL1A1, COL1A2 COL3A1, COL5A1, COL6A1* and *COL14A1* (Chen *et al.,* 2006; Havis and Duprez, 2020), *fibronectin* (Liu *et al.,* 2000) and *MMP9* (Shin *et al.,* 2010). EGR1 also regulates the apoptotic *p53* gene (Krones-Herzig *et al.,* 2005). Interestingly, EGR1 can also regulate the activity of other TFs such as *forkhead box protein C2* (*FOXC2*) (Zhang *et al.,* 2013). As an IEG, the half-life of EGR1 is very short therefore once it has performed its task, it is quickly targeted for ubiquitination and sumoylation by SUMO1 and Ubc9 ubiquitin and this results in its proteasome-mediated degradation (Manente *et al.,* 2011). EGR1 has also been shown to downregulate its own expression by recruiting its repressors NGFI-A-binding proteins 1 and 2 (NAB1 and NAB2) (Kumbrink *et al.,* 2005; Bhattacharyya *et al.,* 2009).

1.3.5 The pathophysiological roles EGR1

EGR1 is involved in cell growth and proliferation, and this makes it a key contributor to the development of various diseases, most notably cancer and fibrosis. EGR1 is overexpressed in human prostate cancers due to the loss of its co-repressor NAB2 (Abdulkadir *et al.,* 2001). The overexpression of EGR1 is further increased by the activity cyclin D1 and it then causes continuous growth of prostate cells (Xiao *et al.,* 2005). In prostate cancer, EGR1 also activates the androgen receptor (AR) and this sensitizes cells to testosterone thus promoting tumorigenesis (Yang *et al.,* 2003). EGR1 also acts as an oncogene that promotes metastasis and invasion, both key hallmarks of cancer, through the downregulation of E-cadherin, which is responsible for cell-cell adhesion in ECM adherens junctions (Pećina-Šlaus, 2003). Grotegut *et al.* (2006) demonstrated that in lung cancer cell lines, hepatocyte growth factor (HGF) activated EGR1 expression via the MAPK pathway and as well as Snai1, a regulator of EMT. They found that the *Snai1* promoter contained four EBSs, and once activated by EGR1, Snai1 then reduced the expression of E-cadherin leading cells to become metastatic and highly invasive. Similarly, Cheng *et al.* (2013) showed that under the stimulation of EGF, EGR1 was upregulated and increased *Snai2* (*Slug*) levels, which then reduced E-cadherin expression resulting in increased motility and invasion of ovarian cancer cells. EGR1 can act as a tumour suppressor and this is mediated via the transactivation of p53, which induces replicative senescence and activates apoptosis (Krones-Herzig *et al.*, 2003).

Fibrosis is characterized by an increased deposition of fibrous proteins and EGR1 has been shown to contribute to this under the TGF-β1 stimulation; EGR1 is rapidly induced in skin fibroblasts and binds to the *COL1A2* promoter leading to increased collagen 1A2 secretion (Chen *et al.,* 2006). A similar pattern has been reported in rheumatoid arthritis synovial fibroblasts where EGR1 upregulates the expression of type I and II collagen (Alexander *et al.,* 2002). EGR1 also activates the expression of tissue inhibitor of metalloproteinases (TIMP) and this reduces matrix turnover thus promoting fibrosis (Aicher *et al.,* 2003). In an animal-based study done by Wu *et al.* (2009) they used bleomycin-induced scleroderma mouse to investigate the expression patterns of EGR1 and the resulting phenotype. Here they found that EGR-null mice had reduced inflammation and fibrosis, but the wound healing was compromised whilst the EGR1-overexpressing counterparts had increased collagen levels and wound healing abilities. This study, therefore, illustrates that EGR1 has roles in wound healing and acts as a fibrotic factor. In myocardial fibrosis, the inhibition of EGR1 expression reverses fibrotic features in mouse models. When miR-150-5p is expressed, it targets the

EGR1 transcript reducing its levels and followed by the reduced expression of collagen I and III, key proteins that increase matrix stiffness (Shen *et al.*, 2019).

1.4 Study rationale

The cellular functions of PXDN are not fully understood however, studies done on its transcriptional regulation are bridging this gap as illustrated in the studies done by Sitole and Mavri-Damelin (2018) and Hanmer and Mavri-Damelin (2018). Herein they contributed to the elucidation of the functions of PXDN by linking it to Snai1 and Nrf2 and we now know that PXDN functions in EMT and antioxidant responses (Sitole and Mavri-Damelin 2018; Hanmer and Mavri-Damelin, 2018). Our project will employ a similar approach by investigating whether EGR1 regulates the expression of PXDN. By establishing a link between the two proteins we can establish roles for PXDN in cell growth, differentiation, proliferation, and apoptosis which are key processes that EGR1 is known to regulate. The investigation of the relationship between EGR1 and PXDN will additionally provide insights into their role in fibrosis as they are both overexpressed in the pathology and have been shown to respond to the TGF-β1 which promotes the development and progression of the disease. From this PXDN may be used as a novel prognostic and therapeutic marker for fibrotic diseases.

1.5 Aims and objectives

This research aimed to determine whether EGR1 regulates *PXDN*. The following objectives were performed.

1. Detect and quantify the protein expression of EGR1 and PXDN using western blot.
2. Identify the cellular localization of the expression of EGR1 and PXDN with immunofluorescence microscopy.
3. Identify whether EGR1 interacts with the *PXDN* promoter using chromatin immunoprecipitation (ChIP).
4. Determine if EGR1 activates or represses *PXDN* gene expression using the luciferase reporter assay.

2. Materials and methods

2.1 Reagents

Gibco® cell culture reagents were purchased from ThermoFisher Scientific (Waltham, Massachusetts, United States) and NEST® plasticware (Wuxi, Jiangsu, China) was used. Chemical reagents were purchased from Sigma-Merck (St. Louis, Missouri, United States). The names of other manufacturers will be listed next to the respective product. The recipes of regents that were prepared are detailed in Appendix A and the catalogue numbers are listed in Appendix B.

2.2 Cell culture

Human embryonic kidney 293 cells (HEK293) were a gift from Dr Clement Penny (Oncology Research lab, University of the Witwatersrand, Johannesburg). The cells were cultured in 100 mm round plates and maintained in Dulbecco's Modified Eagle Medium/Nutrient Mixture F-12 (DMEM/F-12) (1:1) supplemented with 10% Fetal Bovine Serum (FBS) and 1% of 10,000 U/ml penicillin-streptomycin and kept at 37 ℃, in a 5% carbon dioxide (CO_2) humidified incubator. Cells were sub-cultured when approximately 80% confluent. The media was discarded, and the cells were washed three times with cold 1X phosphate-buffered saline (PBS). Following this, 0.25% trypsin-EDTA and 1X PBS (1:3) were added to the plate to catalyse the dissociation of cell-cell and cell-surface adhesion molecules and the cells were incubated for 3 minutes at 37 ℃ to facilitate the enzymatic dissociation reaction. The trypsinization was deactivated with 2 ml fresh media and cells were further detached by gently pipetting up and down to obtain single cells. From the cell suspension 200 µl was resuspended into a new plate containing 8 ml fresh media and the cells were cultured for between 48-72 hours or until confluent and used for experiments. For extended storage cells were cryopreserved in glycerol freezing media and stored at -80 ℃. Once resuscitated, cells were sub-cultured twice before use in experiments.

2.2.1 Cell counts

Cell counts were performed for the immunofluorescence and the luciferase reporter assay experiments which need a specified number of cells to be plated. Counting was done using the 0.0025 mm^2 Neubauer haemocytometer (Paul Marienfeld, Lauda-Königshofen, Baden-Württemberg, Germany). The cells were washed and enzymatically dissociated from the plate as detailed in section 2.2. The cells were mixed with 0.2% trypan blue dye (1:1) then loaded on the haemocytometer. Cells were viewed on the Zeiss ID-02 Inverted Microscope (Oberkochen, Baden-Württemberg, Germany) and counting was done on the inner 5X5 grids

in both the upper and lower chambers. For immunofluorescence, $1x10^5$cells were seeded in a 6-well plate containing sterile 22X22 mm coverslips and for the uciferase assay $1x10^4$ cells/well were seeded in a black 96-well plate with a clear bottom.

2.2.3 Treatments

When the cells were around 80% confluent, they were serum starved for 12 hours and then treated with TGF-β1. For western blot 5 ng/ml was used for immunofluorescence and ChIP 10 ng/ml was used. The cells were treated for 6, 12 and 24 hours. Untreated cells were included to compare the differences that the cells displayed with and without the treatment.

2.3 Western blot

Western blot is a quantitative technique used to detect protein expression. The data obtained from western blotting is especially useful in comparing if protein expression levels change across multiple samples when cells are exposed to specific conditions or variables. We used the technique to determine if HEK293 cells endogenously express our proteins of interest (EGR1 and PXDN) and whether this expression level would change in response to TFG-β1 treatment. In addition to obtaining qualitative data, blotting would help us pick a time point to use downstream in the ChIP assay when EGR1 is highly expressed to increase its binding chances to EBSs in the chromatin.

2.3.1. Protein extraction

Cells were washed three times with cold 1X PBS and scraped from the culturing dish. A 1 ml suspension of cells in 1X PBS was transferred into a clean microcentrifuge tube. Whole protein was extracted from cells by pelleting them through centrifugation at 11 000 rpm, at 4 ℃ for 10 minutes then resuspending in 1X radioimmunoprecipitation assay (1X RIPA) containing 10 mM phenylmethylsulfonyl fluoride (PMSF) and 1mM leupeptin. The cells were lysed by vortexing the tubes and then spinning on the RM-Multi 1 Rotator Mixer (Starlab, Neuer Höltigbaum, Hamburg, Germany) for 1 hour at 4 ℃. The lysate was then centrifuged at 12 500 rpm, for 5 minutes at 4 ℃ to pellet the cell debris. The supernatant was then collected, and this was aliquoted into PCR tubes and stored at -80 ℃. Some was set aside for quantification using the Bramhall assay.

2.3.2 Bramhall assay

The Bramhall assay was performed to determine the concentration of the extracted protein. This assay is used for proteins extracted with high SDS-containing lysis buffers which are incompatible with other protein quantification assays such as the Bradford assay (Bramhall *et*

al., 1969; Bradford, 1976). A Whatman™ No.1 filter paper was incubated in distilled water for 20 minutes, then in 95% ethanol, 100% ethanol and finally in 100% acetone for 5 minutes each with gentle rocking at 15 rpm. The paper was dried under a fume hood and onto it, 1,3,6,12,16 and 20 µl of 1 mg/ml of bovine serum albumin (BSA) (Glentham Life Sciences, Leafield, Corsham, United Kingdom) weres blotted along with 2 µl of the extracted protein supernatant. Following this, the paper was again air dried, and the proteins were fixed to the filter paper by incubating in 7.5% trichloroacetic acid (TCA) for 45 minutes. The paper was then stained in Coomassie brilliant blue G250 for 1 hour. The excess coomassie was removed by incubating in the paper in the destain solution for 1 hour. The stained protein blots were individually cut from the filter paper and placed in 5 ml elution buffer and incubated for 2 hours in the dark to elute the proteins.

The tubes containing the eluted protein were mixed and 160 µl was pipetted in triplicates onto a 96-well plate. The absorbance was read at 595 nm using a Multiskan GO Microplate Spectrophotometer (ThermoFisher Scientific) and the elution buffer was used as a blank. Measurements obtained from the microplate reader software were exported to Microsoft Excel (Office 365**)** and calculations for the protein concentration were performed. The BSA concentration (µg/µl) and corresponding absorbance values were used to plot a standard curve. The equation of the line of best fit (y= mx+ c) was used to determine the concentration (µg/µl) of the extracted protein samples using their measured absorbance values. This concentration was then used to find the volume of protein to load on the polyacrylamide gel.

2.3.3 Discontinuous SDS-PAGE

Proteins were resolved on a discontinuous sodium dodecyl sulfate–polyacrylamide gel electrophoresis (SDS-PAGE) to separate the protein extracts by size. EGR1 is 80 kDa (Cao *et al.,* 1990) and PXDN is 165 kDa (Cheng *et al.,* 2008). The resolving gel for EGR1 was prepared to 12% and for PXDN an 8% gel was made. The differences in the resolving gel percentages are based on the sizes of the target protein as lower molecular weight proteins resolve better on higher percentage gels and higher molecular weight proteins resolve better on low percentage gels. In addition to the gel percentages, the running voltage and protein transfer conditions used were based on the size of each protein. These details, together with the antibodies used to probe for the proteins of interest are summarized in Table 2.1.

Table 2.1: SDS-PAGE percentages, antibody dilutions and transfer conditions for EGR1, PXDN and β-actin

	EGR1	**PXDN**	**β-actin**
SDS-PAGE percentage	12%	8%	12%
Protein loading amount	Initial amount- 40 µg Optimized amount- 20 µg	Initial amount- 150 µg then 100 µg Optimized amount- 80 µg	20 µg
SDS-PAGE running voltage	150 V	180 V	150 V
Primary antibody	EGR1 rabbit monoclonal antibody (Cell Signaling Technology: #4154)	PXDN mouse monoclonal antibody (Santa Cruz Biotechnology: sc-293408)	β-actin rabbit polyclonal antibody (Cell Signaling Technology: #4967)
Primary antibody dilution	1:1000	Initial dilution- 1:1000 Optimized dilution 1:2000	1:2000
Secondary antibody	Goat anti-rabbit HRP antibody (Cell Signaling Technology: #7074)	Horse anti-mouse IgG HRP (Cell Signaling Technology: #7076)	Goat anti-rabbit HRP antibody (Cell Signaling Technology: #7074)
Secondary antibody dilution	1:2000	Initial dilution- 1:2000 Optimized dilution- 1:1500	1:4000
Transfer time	2 hours	3 hours	2 hours
Tween-20 percentage in the 1X TBST wash buffer	0.1%	0.2%	0.1%

The resolving gels (pH 8.8) (Table 2.2) were prepared first and poured into the 1 mm gap between the short glass plate and spacer glass plate and a 0.1% SDS overlay was poured on top to ensure an even gel interface. The resolving gels were then left for about 20 minutes to polymerize, and the overlay was removed. Afterwards, the stacking gels (pH 6.8) (Table 2.2) were prepared and poured on top of the resolving gel and a comb was inserted to create wells in which to load the protein samples.

Table 2.2: Discontinuous SDS-PAGE recipes

	Resolving gel (10 ml)		**Stacking gel (5 ml)**
Reagent	8%	12%	5%
dH_2O	4.6 ml	3.3 ml	3.4 ml
29:1 Acrylamide/ bisacrylamide	2.7 ml	4.0 ml	830 µl
1 M Tris-HCl pH 6.8	-	-	630 µl
1.5 M Tris-HCl pH 8.8	2.5 ml	2.5 ml	-
10% SDS	100 µl	100 µl	50 µl
10% APS	100 µl	100 µl	50 µl
TEMED	6 µl	4 µl	4 µl

Once the gels had set, the extracted protein was thawed on ice and then mixed with a 4X protein loading buffer and the samples were linearized by boiling for 5 minutes and then loaded onto the gel. The PageRuler™ Plus Prestained Protein Ladder, 10-250 kDa (ThermoFisher Scientific) was used as the molecular weight marker. To control for equal protein loading between the samples on the EGR1 and PXDN gels, the same protein samples were used to run a parallel β-actin gel. The bands obtained from this gel would indicate whether proteins were loaded equivalently across the gel. The gels were electrophoresed in a Mini-PROTEAN® Tetra Cell tank (Bio-Rad, Hercules, California, United States) containing running buffer until the dye front fell off from the gel. Using the protein ladder as a guide, the gel was cut across the region where the protein of interest would have migrated. These gel fragments were prepared for the electrophoretic transfer of the protein bands. The remaining gel portions were stained in coomassie overnight with constant shaking at 100 rpm then destained the following day for 1 hour to check if there was protein on the gel and that it was properly separated into different sizes.

2.3.4 Wet electrophoretic transfer

The protein bands separated on the SDS-PAGE gel were transferred to 0.45 µm WesternBright ® nitrocellulose membranes (Advansta, San Jose, California, United States) using a wet electrophoretic transfer system. Briefly, the gel was assembled next to the nitrocellulose membrane, and these were then sandwiched on either side by two filter papers and a transfer sponge pre-soaked in the transfer buffer. The gel was placed facing the cathode side and the nitrocellulose facing the anode side of the Mini Trans-Blot® module (Bio-Rad). Electroblotting was performed in the Mini-PROTEAN® Tetra Cell tank (Bio-Rad) containing prechilled transfer buffer and an ice pack to prevent overheating at 300 mA at 4 ℃ for varying times (Table 2.1). Following the transfer, the gel was stained in coomassie overnight and then destained for 1 hour to confirm the successful transfer of proteins.

2.3.5 Immunodetection

The nitrocellulose membranes were washed once with cold 1X Tris-Buffered Saline with 0.1% Tween-20 **(**1X TBST) for 5 minutes at 180 rpm. For the PXDN blot washes, the Tween-20 percentage used for the washes was later increased from 0.1% to 0.2% to get rid background around the bands. The membrane was then blocked with 5% BSA diluted in the 1X TBST for 1 hour at room temperature (RT) to prevent the non-specific binding of antibodies. Thereafter the membranes were washed once with cold 1X TBST, and then incubated with primary antibodies (Table 2.1) diluted in 5% BSA overnight at 4 ℃. The following day, the membranes were washed five times in 1X TBST for 5 minutes each and then incubated with corresponding secondary horse radish peroxidase (HRP)-conjugated antibodies diluted in 5% BSA for 1 hour, at RT, in the dark. Excess secondary antibodies were removed by washing the membrane five times in cold 1X TBST then the membrane was taken into a dark room for band development.

2.3.6 Chemiluminescence detection

The nitrocellulose membranes were developed using the WesternBright™ ECL chemiluminescence HRP substrate (Advansta). The luminol enhancer solution was mixed with the peroxide solution (1:1) and poured evenly on top of the membrane. The membrane was dabbed onto a paper towel to remove the excess chemiluminescence reagent then placed in an X-ray film cassette and exposed to LucentBlue X-ray Films (Advansta). The films were then immersed in the developer washed off in water then placed in the fixer washed again in water then air dried.

2.3.7 Densitometry

Protein band intensities were quantified using the Image Studio light, Version 5.2. Calculations were performed in Microsoft Excel (365) and measurements were normalized using the β-actin loading control and represented as relative densitometry units (%).

2.4 Immunofluorescence microscopy

Immunofluorescent microscopy was done to detect changes in the expression levels of our target proteins following treatment and the cellular localization of the proteins at those respective time points. This, in parallel with western blotting, would guide the ChIP assay as the TF in question needs to be highly expressed and present in the nucleus so it can be crosslinked to its specific TFBS.

2.4.1 Sample preparation

Plates were removed from the incubator and the cells were washed once with cold 1X PBS. The cells were fixed to the coverslips with 3% formaldehyde for 10 minutes. Cells were then washed three times with 1X PBS and permeabilized with 0.1% Triton X-100 diluted in 1X PBS for 10 minutes. Permeabilization would make the cell membrane porous so that the antibodies would be able to pass through and access the intracellular target proteins. Once permeabilized, the cells were washed three times with 1X PBS to get rid of the excess detergent. To inhibit the non-specific binding of antibodies, the coverslips were blocked with 1% BSA and incubated at RT for one hour then washed once with the cold 1X PBS.

2.4.2 Indirect immunofluorescence

Primary antibodies were used to probe for EGR1 and PXDN in HEK293 cells. These were diluted in the 1% blocking buffer. The antibodies and the dilutions used are detailed in Table 2.3. The cells were then incubated overnight at 4 ℃. A no primary antibody control (NPC) was included to verify that the primary antibodies were only bound to their specific target protein. The following day, the cells were washed five times with cold 1X PBS and the corresponding fluorescein isothiocyanate (FITC) conjugated secondary antibodies diluted in the blocking buffer were added. The cells were incubated for 2 hours at RT in the dark. The cells were again washed five times with cold 1X PBS to remove excess secondary antibodies. A no antibody control (NAC) was included to normalize for autofluorescence. Lastly, 0.05 µg/ml of 4', 6-diamidino-2-phenylindole dihydrochloride (DAPI) was used to counterstain the nuclei. The coverslips were then removed from the 6-well plate and mounted onto microscope slides using the Fluoromount™ Aqueous Mounting Medium. The slides were left

to set for two hours at RT in the dark then stored in a dark microscope slide cassette holder at 4 ℃ until visualization the following day.

Table 2.1: Antibodies used for immunofluorescence microscopy.

Target protein	**Primary antibody**	**Primary antibody dilution**	**Secondary FITC-conjugated antibody**	**Secondary antibody dilution**
EGR1	EGR1 rabbit monoclonal antibody (Cell signaling Technology: #4154)	1:400	Mouse anti-rabbit IgG FITC (Santa Cruz Biotechnology: sc-2359)	1:800
PXDN	PXDN mouse monoclonal antibody (Santa Cruz Biotechnology: sc-293408)	1:200	Goat anti-mouse kappa-FITC (Southern Biotech: 1050-02)	1:500

2.4.3 Microscope viewing and image analysis

Imaging was done on the Olympus BX63 Microscope with the cellSens imaging software (Shinjuku City, Tokyo, Japan). The 60X magnification was used and multichannel fluorescence was set up for DAPI and FITC with each having excitation and emission wavelengths of 364 nm/454 nm and 494 nm/525 nm respectively. DAPI was thus visualized as blue whilst FITC-stained target proteins had green fluorescence. Once images were captured, quantitative analysis of the fluorescence intensity was done using the Image J Fiji software. These values were used to calculate the correlated total cell fluorescence (CTCF) and this was done in Microsoft Excel (365).

2.5 ChIP assay

The ChIP assay was performed to determine whether EGR1 binds to the *PXDN* promoter. Using the results obtained from objectives 1 and 2 we selected the 6-hour TGF-β1 treatment time point to use as EGR1 is highly expressed and colocalized to the nucleus. In ChIP, nuclear proteins are first crosslinked to the chromatin, and this is subsequently sheared the target protein-bound fragments are immunoprecipitated and the DNA is analysed. For our study, we performed PCR directed at the two EBSs located in the *PXDN* promoter.

2.5.1 Identification of EBSs

Bioinformatics analyses were done on the *PXDN* promoter to find putative EBSs located within it. Ensembl was used to obtain the Human *PXDN* gene sequence (ENSG00000130508) and here we focused on the upstream promoter region. JASPAR (https://jaspar.genereg.net/analysis) was used to find putative EBSs at an 80% prediction threshold.

2.5.2 Primers design and testing

NCBI-Primer BLAST was used to design primers to amplify across the putative EBSs in the *PXDN* promoter. *COL1A2* was chosen as a positive control gene as it has been shown to be a target of EGR1 (Chen *et al.*, 2006). Primers were also designed for regions in both the *PXDN* and *COL1A2* promoters with no EBS, so they act as negative control sites (see mapping in Appendix C). The primers were ordered from Inqaba Biotechnical Industries (Pretoria, Gauteng, South Africa). The sequences of the primers are detailed in Table 2.4. The lyophilized primer pellets were resuspended in 10 mM Tris and 1 mM EDTA buffer and 10 µM dilutions were prepared and genomic DNA (gDNA) was extracted from HEK293 cells using the Quick-DNA™ Miniprep Kit (Zymo Research, Irvine, California, United States) to test that the primers worked and at the correct annealing temperature (Table 2.4). The KAPA Taq ReadyMix master mix (KAPA Biosystems, San Francisco, California, United States) was used for this and the reaction mixtures were prepared and incubated in a thermocycler as per the manufacturers' conditions (Table C2). A 1.5% agarose gel was prepared in 1X TAE and stained with ethidium bromide. The PCR products were loaded on the gel and electrophoresed alongside a 100 bp DNA ladder (New England Biolabs (NEB), Ipswich, Massachusetts, United States) in a Mini Sub-Cell® GT Horizontal electrophoresis tank (Bio-Rad) at 100 V for 45 minutes. Bands were visualized using the Bio-Rad Gel Doc XR system and Image Lab 6.0 software (Bio-Rad).

2.5.3 Chromatin crosslinking

The chromatin was crosslinked with 1% formaldehyde for 10 minutes at room temperature with shaking at 55 rpm. The crosslinking was quenched with 125 mM glycine for 5 minutes at room temperature. Cells were then washed three times with cold 1X PBS and then scraped in 1 ml 1X PBS. The cell suspension was transferred to clean 1.5 ml microfuge tubes and pelleted at 5000 rpm for 5 minutes at 4 ℃. The pellet was resuspended in 1X RIPA with 0.1 M PMSF and 10 mM leupeptin to lyse the cells whilst inhibiting the enzymatic degradation of the proteins crosslinked to the DNA.

2.5.4 Sonication

The chromatin was sheared by sonicating with the Q125 sonicator (QSonica, Newtown, Connecticut, United States). This was initially done for 15 minutes at a 60% amplitude, 15 seconds on and 30 seconds off with cooling on ice in between and the time was later changed to 10 minutes to obtain lengths ranging between 500-1000 bp. The lysate was pelleted at 10 000 rpm for 10 minutes at 4 ℃ and the samples were then resolved on a 1.5% agarose gel to determine the fragment sizes.

2.5.5 Immunoprecipitation

Sheared chromatin samples were mixed with the ChIP dilution buffer containing protease inhibitors (0.1 M PMSF and 10 mM leupeptin) in a 1:10 ratio. The EGR1-DNA chromatin complexes were immunoprecipitated with 1:50 of the EGR1 monoclonal antibody (Cell Signaling Technology , Danvers, Massachusetts, United States) overnight 4 ℃ with constant spinning on the RM-Multi 1 Rotator Mixer (Starlab). Protein A/G beads (Santa Cruz Biotechnology, Dallas, Texas, United States) were then added, and the samples were incubated for 4 hours at 4 ℃ with rotation. Following this samples were centrifuged at 5 000 rpm at 4 ℃ to pellet the beads. The beads were then washed three times with the low salt wash buffer and then once with a high salt wash buffer. Samples were centrifuged at 5 000 rpm at 4 ℃ in between washes. Tubes were then incubated on ice for 5 minutes and the supernatant was discarded.

2.5.6 Reversal of the chromatin crosslinks

The pellet was resuspended in 120 µl of prewarmed elution buffer with 2 µl of proteinase K and RNase A (NEB). The chromatin crosslinks were reversed by incubating the samples for 1 hour at 65 ℃ in a water bath to heat denature the proteins. The samples were then centrifuged at 5 000 rpm for 1 minute and the immunoprecipitated DNA in the supernatant was collected and purified with the DNA Clean & Concentrator (Zymo Research, Irvine, California, United States) following the manufacturer's instructions. The DNA was eluted in Tris-HCl (pH 7.8) and quantified with the NanoDrop One UV-Vis Microvolume Spectrophotometer (ThermoFisher Scientific) at 260 nm and 280 nm.

2.5.7 ChIP-PCR

PCR was done to amplify the purified immunoprecipitated DNA. The optimized primers and the KAPA Taq ReadyMix master mix (KAPA Biosystems) were used to prepare 25 µl reactions with the purified DNA fragment (Table C1). The volume of the reaction mixture

was later halved to 12.5 µl so that there was more input DNA that the DNA polymerase could bind to. Controls for the assay included a gDNA control to ensure that the primers were amplifying the DNA, an input control which contained DNA which was only sonicated and not subjected to immunoprecipitation, a NAC to ensure that the precleared DNA was bound to EGR1 proteins and lastly a no template control (NTC) to check for any nucleic acid contamination in the PCR reaction mixtures. The samples were incubated in a thermocycler and the manufacturer's cycling conditions were followed (Table C2). Amplicons were then analysed on a 1.5% agarose gel.

Table 2.2: ChIP-PCR primers.

Primer	**Primer sequences (5′-3′)**	**Amplicon size (bp)**	**Annealing temperature (℃)**
EBS1	Forward-GTCCAGTGTGAGCTGGAACA	500	48
	Reverse-AATCTTGCAGGAGAGACGACA		
EBS2	Forward-GAACGTTAAATAATTTCCTACGT	578	58
	Reverse-GGCGCAGAACAGCACGAGCG		
EBS-	Forward-TCTGAATCTGGCACCGTCACCCTG	476	60
	Reverse-AAAGCCCCTCATTCCTTTTGAGGA		
COL1A2^{EBS+}	Forward-CTACAGGGCACAGGTGAGG	422	60
	Reverse-AAAGCCCGGATCTGCCCTA		
COL1A2^{EBS-}	Forward-CCCTGCAAAGGTAATTCAGCAC	536	56
	Reverse-GCAGCTTCTGTAAATAAAAGGG		

2.6 Luciferase reporter assay

To confirm if the binding of a EGR1 to EBS1 results in the functional expression of the gene, the luciferase reporter assay was performed after the ChIP assay. We cloned the EBS1/PXDN promoter region into the pGL4.10 luciferase vector and transfected into HEK239 and be analysed the luciferase gene expression to determine if EGR1 can drive *PXDN* expression.

2.6.1 Oligonucleotides design

The insert DNA for cloning was made from oligonucleotides designed to contain the putative EBS sequences found in the *PXDN* promoter. This sequence is 9 bp and was extended to bilaterally neighbouring bases to create oligonucleotide sequences of about 35 bp and these would anneal to each other and form double-stranded DNA (dsDNA) sequences. The pGL4.10 vector contains various restriction sites in its backbone and NEBcutter (Version 2.0) (http://nc2.neb.com/NEBcutter2/) was used to find the restriction enzymes which do not cleave the *PXDN* promoter. From this KpnI and EcoRV were selected to achieve directional cloning. The KpnI recognition sequence was added to the 5′ end of the oligonucleotides and EcoRV on the 3′ end. The sequences are detailed in Table 2.5.

Table 2.3: Cloning oligonucleotides.

Oligonucleotide	**Sequence (5′-3′)**	**Length (bp)**
LUPXDN^{EBS1} sense	GGTACCTCTGGAGTGCGTGGACAGGACCCTGCAGATATC	39
LUPXDN^{EBS1} antisense	GATATCTGCAGGGTCCTGTCCACGCACTCCAGAGGTACC	39
LUPXDN^{EBS-} sense	GGTACCACCTTTCATTTTCCCAACTGTGCTGGATATC	37
LUPXDN^{EBS-} antisense	GATATCCAGCACAGTTGGGAAAATGAAAGGTGGTACC	37
LUCOL1A2 $^{EBS1+}$ sense	GGTACCTCTGCGCCCCCGCAGGCTCCGATATC	32
LUCOL1A2^{EBS+} antisense	GATATCGGAGCCTGCGGGGGCGCAGAGGTACC	32
LUCOL1A2^{EBS1} sense	GGTACCGTTAGTTCTGTAACGGTGATATTTCGATATC	37
LUCOL1A2^{EBS1-} antisense	GATATCGAAATATCACCGTTACAGAACTAACGGTACC	37

*The underlined sequence on the 5′-end indicates the KpnI restriction site 5’-GGTAC/C-3’ and on the 3′ end it is the EcoRV site 5’-GAT/ATC-3’.

2.6.2 Annealing the oligonucleotides

The lyophilized oligonucleotides were resuspended in the oligonucleotide annealing buffer to a 100 µM concentration. The sense and antisense sets were mixed in a 1:1 molar ratio and the mixtures were incubated in a thermocycler set at 95 ℃ for 2 minutes then the temperature was reduced to 25 ℃ for 45 minutes. The annealed dsDNA was then quantified with a Nanodrop spectrophotometer, diluted into a working concentration with nuclease-free water and stored at -20 ℃.

2.6.3 Cloning vector

The promoterless pGL4.10 [*luc2*] vector (Promega, Madison, Wisconsin, United States) was selected as the cloning plasmid as it has a multiple cloning site (MCS) in its backbone to allow for the insertion of genes, has ampicillin resistance (Amp^R), which allows for the selection of colonies harbouring it, and lastly because it contains the luciferase gene which would ultimately allow us to determine if EGR1 can drive expression from the *PXDN* promoter regions containing the putative binding sites for this transcription factor. The vector map along with the restriction enzyme sites we chose are illustrated in Appendix D.

2.6.4 Restriction enzyme digests

The annealed oligonucleotide inserts and the pGL4.10 vector were digested with KpnI and EcoRV (both from NEB). KpnI creates a sticky end ($\frac{\text{GGTA}\downarrow\text{CC}}{\text{CC}\uparrow\text{ATGG}}$) whereases EcoRV creates a blunt end ($\frac{\text{GAT}\downarrow\text{ATC}}{\text{CTA}\uparrow\text{TAG}}$). These dissimilar cleavage patterns are important as they facilitate the directional cloning of genes. The pGL4.10 is 4.2 kB and single digests were done on it as it is 4.2 kB and would be visible on gels, unlike the 35 bp inserts. This was done to verify the cutting efficiency of each restriction enzyme. Once the single digests had been assessed, double digests were done on both the vector and insert DNA following the manufacturer's instructions. Following the digestion, the vector DNA was analyzed on a 1.5% agarose gel alongside an uncut vector control to verify that the restriction digest was successful. The 1 kB DNA ladder (ThermoFisher Scientific) was used as the molecular weight marker. The linearized plasmid DNA samples were pooled and purified with a the Zymo Clean and Concentrator™-5 kit (Zymo Research) and the concentration was quantified with a Nanodrop spectrophotometer (ThermoFisher Scientific) and stored at -20 ℃.

2.6.5 Ligation

The restricted pGL4.10 vector and oligonucleotide inserts were ligated in a 1:3 molar ratio. 0 (ng) of the insert to use for 50 ng of the vector.

$$\text{Amount of insert (ng)} = \frac{vector\ (ng) x\ insert(kb)}{vector(kb)} \text{ x} \frac{molar\ amount\ insert}{molar\ amount\ vector}$$

The corresponding volumes were calculated for both the purified vector DNA and the restricted oligo inserts and these were then mixed with a T4 DNA ligase (NEB) and buffer and made up to a 20 µl reaction and incubated at 16 ℃ overnight. A no-ligase control was set up to check for vector re-circularization.

2.6.6 Preparation of chemically competent bacterial cells

JM109 *E. coli* glycerol stocks were thawed on ice and plated onto Luria-Bertani (LB) agar plates and cultured overnight at 37 ℃. A single colony was picked and inoculated into 5ml LB broth and cultured overnight at 37 ℃ with shaking at 200 rpm. The overnight broth culture was inoculated into 200 ml fresh LB and kept for about 2 hours at 37 ℃ until an OD_{600} of 0.4-0.6 was reached. A pellet was collected by centrifugation at 5 000 rpm, at 4 ℃ for 10 minutes. The supernatant was discarded, and the pellet was resuspended in cold 10 ml 0.1 M $MgCl_2$ and then incubated on ice for 30 minutes. The *E. Coli* was again pelleted by centrifugation at 4 000 rpm, at 4 ℃ for 10 minutes and the pellet was resuspended in cold 1 ml calcium chloride ($CaCl_2$) containing 15% glycerol. The bacterial suspension was aliquoted into 50 µl volumes and stored at -80 ℃.

2.6.7 Bacterial transformation

Competent *E. Coli* in 50 µl aliquots were thawed on ice and was mixed with 10 µl of the ligated mixture and kept on ice for 30 minutes. Cells were heat shocked at 42 ℃ for 2 minutes then 500 µl of sterile super optimal broth with catabolite repression (SOC) broth was added. The bacterial cultures were incubated at 37 ℃ for 1 hour with shaking at 200 rpm. Following this, 80 µl of the culture was spread onto LB agar plates supplemented with 100 µg/ml ampicillin and cultured overnight at 37 ℃. Control plates were set also set up, and a positive control of bacteria transformed with the pGL4.10 vector and this checked and if the transformation was successful, a negative control of competent cells transformed with the no ligase control to check for vector recirculation and to test if the ampicillin antibiotic was selective.

2.6.8 Colony PCR

Colonies from the overnight cultures were screened for containing the EBS inserts using colony PCR with pGL4.10 primers (Table 2.6) that amplify across the MCS. Without an insert the size of the amplicon is 243 bp and with the 35 bp inserts, this size increases to 264 bp. Multiple colonies were picked from each plate and dropped into 1.5 ml microcentrifuge tubes containing 50 µl LB broth and incubated at 37 ℃ for 1 hour with shaking at 180 rpm. Thereafter, 5 µl of the bacterial suspension mixture was used as the template DNA in the PCR reaction using KAPA Taq ReadyMix (KAPA Biosystems). The amplicons were analysed on a 5% agarose gel alongside the Ultra-low MassRuler DNA Ladder (ThermoFisher Scientific). A colony was also picked from the agar plate with pGL4.10 transformed cells to act as the negative control to contrast the band size increase and NTC was included to check for untargeted nucleic acid contamination in the PCR reaction mixture.

Table 2.4: pGL4.10 vector amplifying primers.

Primer	**Primer sequences (5′-3′)**	**Amplicon size (bp)**	**Annealing temperature (℃)**
pGL4.10 vector primers	Forward- CTAGCAAAATAGGCTGTCCC	243	60
	Reverse- TTCATGGCTTTGTGCAGCT		

2.6.9 Growing the transformed bacteria

Colonies containing the insert DNA were selected to be grown to make more of the recombinant vector. The 45 µ1 broth remaining after colony PCR was inoculated into a 15 ml Falcon tube with 5 ml LB broth with ampicillin and cultured overnight at 37 ℃ with shaking at 200 rpm. Two controls were set up for the overnight outgrowth, a positive control containing bacteria transformed with the pGL4.10 vector and a negative control with the no ligase control from the transformation step. The controls would verify if the ampicillin was selective and in addition, the first control would check if the growth media and conditions were optimal for the bacteria whilst the second control would check if the broth contained any contaminants. Following the overnight incubation, 1ml of the bacterial culture was cryopreserved in 250 µl of sterile glycerol and stored at -80 ℃ and the rest of the mixture was used to extract the recombinant vector using alkaline lysis.

2.6.10 Alkaline lysis

A pellet from the overnight LB cultures was collected by centrifugation at 12 000 rpm, at 4 ℃ for 1 minute then resuspended in 110 µl of solution I. Cells were lysed with 200 µl of solution II and the contents were mixed by inverting. A 120 µl of solution III was added and cells were again pelleted at 12 000 rpm, at 4 ℃ for 5 minutes. The vector DNA was precipitated with 200 µl isopropanol and incubated on ice for 30 minutes then pelleted at 13 000 rpm for 1 minute at 4 ℃. The pellet was washed with 700 µl of 70% ethanol and air dried for 15 minutes. The pellet was resuspended in 50 µl Tris-HCl (pH 7.8) and quantified with a NanoDrop Spectrophotometer and stored at -20 ℃.

2.6.11 Post-alkaline lysis PCR

PCR was performed on the purified plasmid DNA to further confirm the presence of an insert in the pGL4.10 vector. The same primers and conditions outlined in section 3.1.6 were used and amplicons were analysed on a 5% agarose gels. The remaining 20 µl PCR mixture from each sample was sent for sequencing with 10 µM of the pGL4.10 forward primer (Table 2.6).

2.6.12 Sanger sequencing

Sanger sequencing was used to confirm the presence and orientation of the EBS/PXDN inserts in the pGL4.10 luciferase vector. Samples were sequenced by Inqaba Biotechnical Industries (Pretoria, Gauteng, South Africa) using the ABI 3500XL Genetic Analyzer. The sequencing results were analysed using FinchTV (Version 1.4.0).

2.6.13 Transfection optimization

Before transfecting HEK293 cells with the different recombinant EBS/PXDN and EBS/COL1A2 vectors we first transfected them with the pcDNA3.1-*lacZ* vector (Addgene, Watertown, Massachusetts, United States) and performed the X-gal assay to ensure that the conditions used for the transfection were optimal. The *lacZ* gene codes for β-galactosidase and when expressed in cells, it hydrolyses X-gal into a blue pigmented precipitate and this stains cells blue (Burn, 2012). This therefore allows for the screening of cells that have been successfully transfected with the vector and this can be used to determine the transfection efficiency.

HEK293 cells were transfected with the pcDNA3.1-*lacZ* vector (Addgene, Watertown, Massachusetts, United States) using the TurboFect™ Transfection Reagent (ThermoFisher Scientific). Cells were seeded into 96-well plate and transfected 0.2, 0.4 and 0.6 µg of the vector into the cells and used transfection reagent volumes of 0.3 and 0.6 µl. We analysed the

transgene expression after 24 and 48 hours. Table 2.7 shows the various conditions that were set up. Vector-only controls were included (Samples 4 and 8) to check the efficiency of the transfection reagent and a negative control of cells-only to assess for background colour readings (Sample 9).

Table 2.5: Transfection optimization conditions

Sample	Transfection reagent (µl)	Vector amount (µg)
1	0.3	0.2
2		0.4
3		0.8
4		-
5	0.6	0.2
6		0.4
7		0.8
8		-
9	-	-

Cells were cultured as detailed in section 2.2.1 until confluent and transfected with the various mixtures listed above and one plate was incubated at 37 ℃ for 24 hours and the other for 48 hours. Following this, the cells were washed twice with 1X PBS and fixed with 3% formaldehyde then washed again. The cells were then treated with 20 mg/ml X-gal (VWR Prolabo chemicals, Lutterworth, Leicestershire, England) and incubated at 37 ℃ and thereafter observed under a light microscope.

2.7 Statistical analysis

Statistical analysis was done for the triplicate data obtained from western blot densitometric and the immunofluorescence microscopy CTCF readings (n=3). The data was reported as mean ± standard deviation (n=3 ± SD) and analysed in Microsoft Excel (Office 365). Student's t-tests were used to compare the differences between treated and untreated samples and * P <0.05, ** P <0.01 and *** P <0.001 were considered as statistically significant.

3. Results

3.1 EGR1 and PXDN are expressed in HEK293 cells

Our first objective was to determine if EGR1 and PXDN are expressed in HEK293 cells and whether their expression levels would change in response to TGF-β1, which is a master regulator for EMT and fibrosis. Cells were treated with 5 ng/ml TGF-β1 for 0, 6, 12 and 24 hours, then western blotting was performed for the quantification of EGR1 and PXDN expression and normalized to the β-actin loading control. EGR1 was detected in the untreated and the treated time points (Figure 3.1A). The expression slightly increased at 6 hours but densitometric analysis showed that this change was not significant in comparison to the untreated sample (Figure 3.1B). PXDN was also expressed in the cells however the bands were not well-defined due to the high background around them (Figure 3.1A). Unfortunately, despite multiple attempts to troubleshoot the protocol, there was little improvement in the background and as such this made quantification of PXDN via western blotting not possible. To compensate for this immunofluorescence microscopy was performed and fluorescence intensity from these images were quantified instead. Clear and equally sized bands were obtained for β-actin (Figure 3.1A).

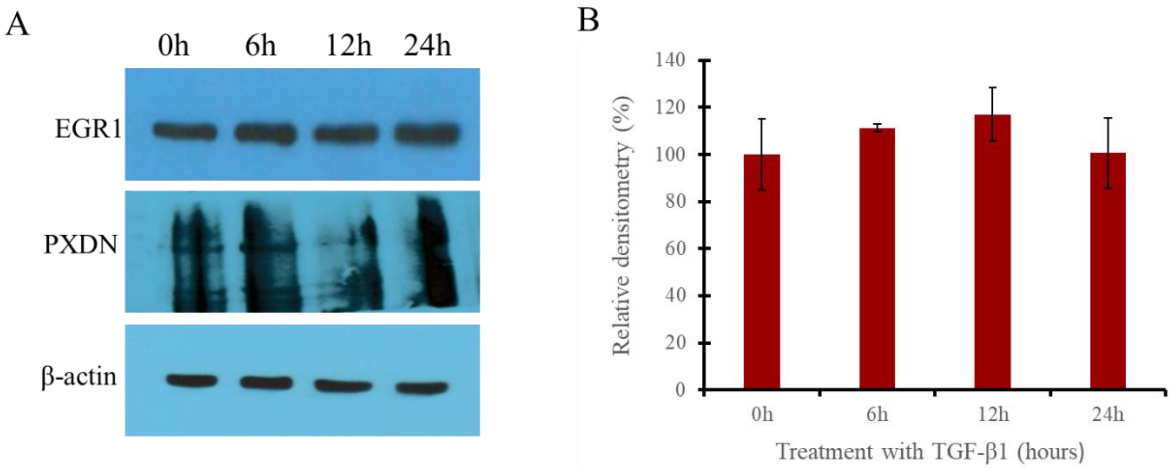

Figure 3.1: EGR1 and PXDN expression in HEK293 cells. HEK293 cells were treated with 5 ng/ml TGF-β1 for 6,12 and 24 hours and western blotting was done on the extracted protein. A) EGR1 (80 kDa) was detected in untreated and treated samples and appeared to have the similar levels of protein expression. PXDN (165 kDa) was also detected, however there was a lot of background around the bands. β-actin (45 kDa) was also probed for to ensure equal protein loading in the wells. B) EGR1 densitometry analyses show an increase in the expression at 6 hours and this decreased at 12 and 24 hours however this change was not statistically significant ($p > 0.05$) ($n = 3$, mean ± SD).

3.2 EGR1 localizes to the nucleus and PXDN to the ECM

To identify the cellular localization of EGR1 and PXDN before and after TGF-β1 treatment, immunofluorescence microscopy was performed with FITC-conjugated antibodies (green), and the nuclei were counterstained with DAPI (blue) (Figure 3.2 and 3.3). EGR1 fluorescence was seen in the nucleus of the untreated (0h) and treated cells with the brightest expression at 6 hours. Little fluorescence was seen in the controls as expected (Figure 3.2A). The CTCF analysis show a significant increase in EGR1 expression at 6 and 12 hours and the expression decreased at 24 hours (Figure 3.2B).

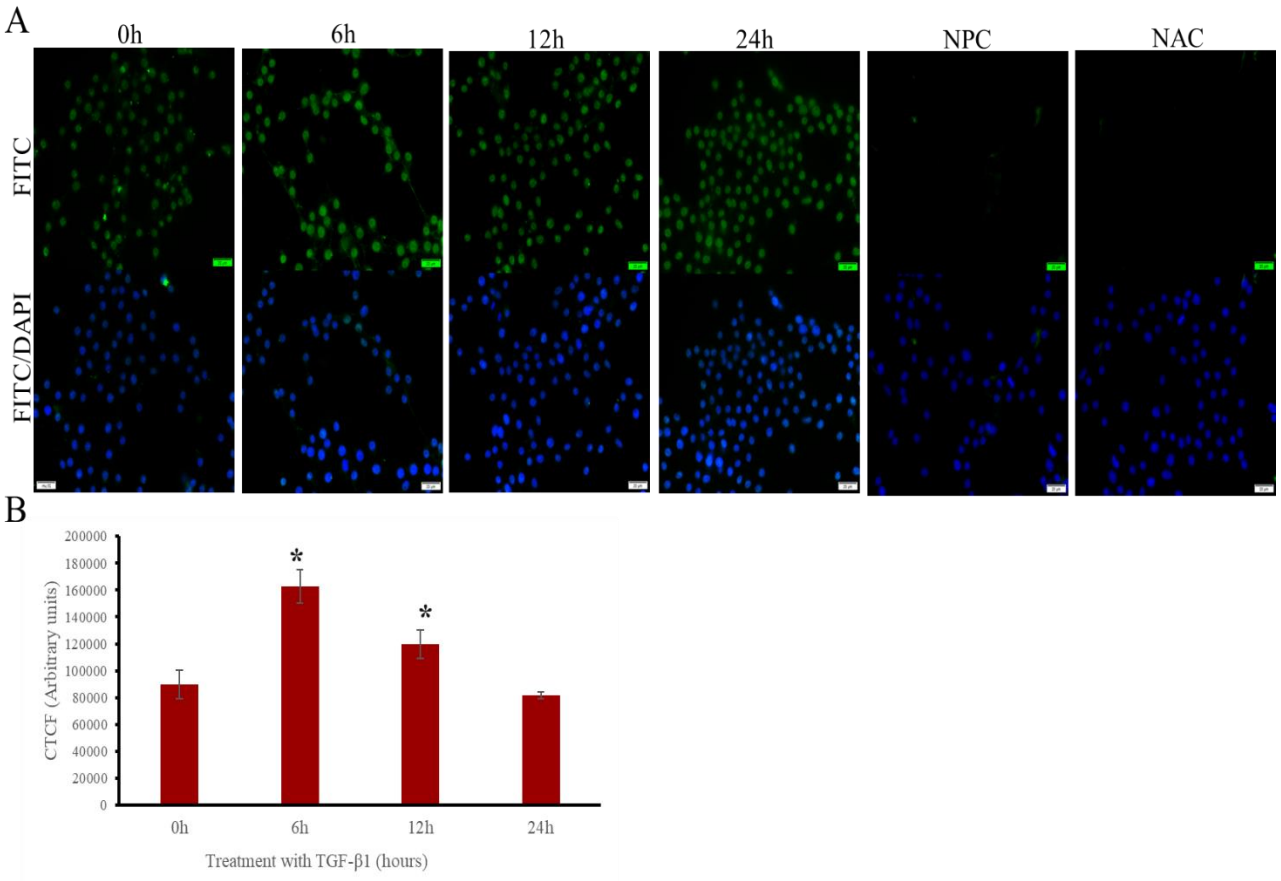

Figure 3.2: EGR1 expression and localization in HEK293 cells. Immunofluorescence microscopy was performed on HEK293 cells treated with 10 ng/ml TGF-β1 for 0, 6, 12 and 24 hours, and FITC-conjugated antibodies were used to detect the localization of EGR1. A) The protein was expressed in the nuclei and was present in both the untreated (0h) and treated samples (6,12 and 24h) (Magnification= 60X, scale bar= 20 µm). B) The correlated total cell fluorescence (CTCF) analyses show that the expression increased at 6 hours, then decreased at 12 and 48 hours. At 6 and 12 hours the expression was significant in comparison to the untreated samples (*$p < 0.05$).

PXDN fluorescence was seen in the untreated (0h) and in the treated samples. In the FITC panel, green fluorescence was seen inside the cells and this was not expected. In the merged panel however, the PXDN fluorescence can be seen extracellularly. In the untreated cells, the green colour is faint and it becomes brighter in the TGF-β1 treated cells. The brightest intensity of PXDN is seen at 12 and 24 hours around the cells. Some fluorescence was seen in the NPC and none was seen in the NAC (Figure 3.3A). The CTCF analysis show a linear increase in the expression levels of PXDN and this was change was significant at 12 and 24 hours.

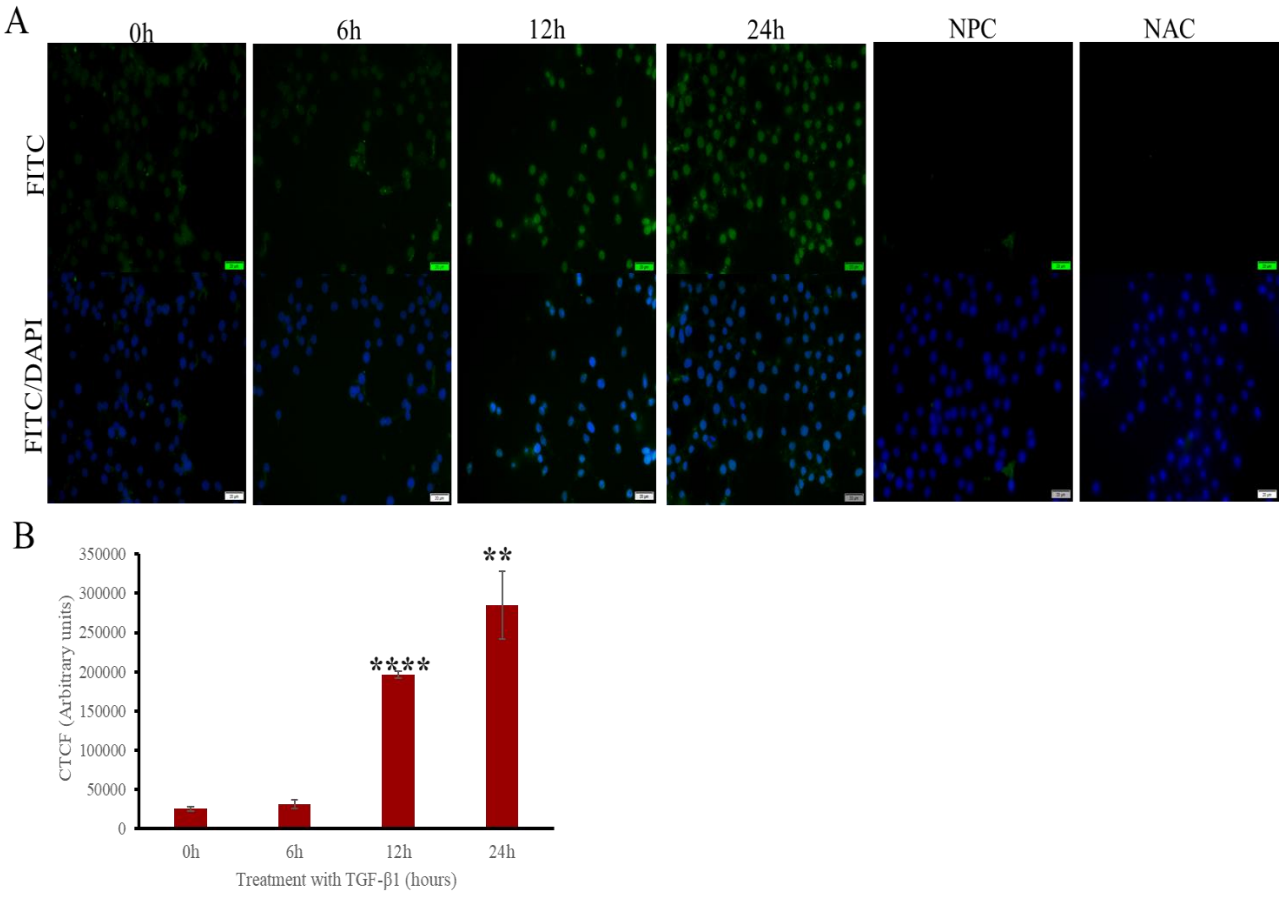

Figure 3.3: PXDN expression and localization in HEK293 cells. Immunofluorescence microscopy was performed on HEK293 cells treated with 10 ng/ml TGF-β1 and FITC-conjugated antibodies were used to detect the localization of PXDN. A) PXDN was predominantly expressed extracellularly, and some expression was seen in the nucleus. The expression was high in the 12 and 24 hour treated cells (Magnification= 60X, scale bar= 20 µm). B) The correlated total cell fluorescence (CTCF) increased significantly at 12 and 24 hours in comparison to the untreated cells (0h) (**p< 0.01 and ****p<0.0001).

3.3 EGR1 has two putative binding sites in the *PXDN* promoter

To determine whether the EGR1 transcription factor interacts with *PXDN* we first analysed the promoter using the JASPAR open-access software to find putative binding sites within the promoter sequence. The conserved GC-rich EGR1 consensus sequence was used to find these sites at an 80% relative threshold (Figure 3.4A). Two sites were found, EBS1 which was on the positive strand and located -1662/-1675 upstream of the transcription start site (TSS) and EBS2 on the negative stand at position -387/-400 (Figure 3.4B).

A

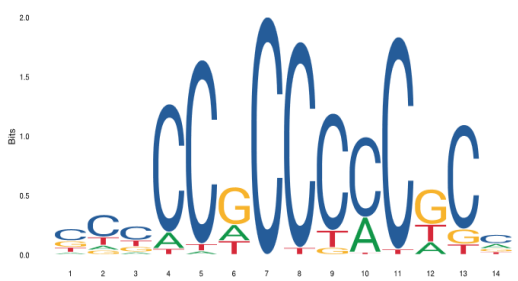

B

Matrix ID	Name	Score	Relative score	Sequence ID	Start	End	Strand	Predicted sequence
MA0162.3	EGR1	7.2943	0.817034312455	2	1662	1675	+	CACGCCCATGCTGT
MA0162.3	EGR1	6.0642	0.802370895787	2	387	400	-	CCTGTCCACGCACT

Figure 3.4: Putative EBSs in the *PXDN* promoter: A) The GC-rich EGR1 consensus sequence used by the JASPAR software to find putative EGR1 binding sites (EBSs) in target promoters. B) Two EBSs were identified in the *PXDN* promoter at an 80% relative score threshold and we named these EBS1 (second row of the table) and EBS2 (third row of the table). The start and end positions for each site is given for each site and EBS1 is found on positive strand and EBS2 is on the negative stand. The predicted EBSs have the characteristic EGR1 GC-rich bases.

3.4 EGR1 interacts with EBS1 in the *PXDN* promoter

Once we established that the *PXDN* promoter contained two possible sites for EGR1, we performed ChIP to determine whether there was protein-DNA interaction between them. Five primer sets were designed to amplify the immunoprecipitated and these were first tested on gDNA to verify if they could amplify the target EBSs. Bands were obtained for all primer sets and no band was seen in the NTC as expected (Figure 3.5A). The chromatin in HEK293 cells was crosslinked and sonicated into fragment sizes of 500-1000 bp, this is seen with the bright aggregated smears on the gel in Figure 3.5B. We then immunoprecipitated EGR1-bound fragments and performed PCR to selectively amplify the EBSs in the *PXDN* and *COL1A2* promoters.

COL1A2 is a known EGR1 target gene and as expected, we obtained bands for the EBSs in both the untreated and TGF-β1 treated samples. Bands were also seen in the input and gDNA controls showing that the primers were able to amplify the fragmented immunoprecipitated DNA and the intact gDNA. Bands were not seen in the NAC control and this shows that the antibody used to immunoprecipitated the EGR1-bound fragmented DNA was specific only to the EGR1 protein. Bands were also not obtained in the NTC, therefore, showing that the PCR reaction mixture that was prepared only had the target EGR1-immunoprecipitated DNA and no contaminants. The negative control region of COL1A2 only had amplification of the input and gDNA controls (Figure 3.5C). In the *PXDN* sites, bands were seen in the EBS1 untreated and treated samples and none were seen in EBS2 or the *PXDN* EBS negative control. This shows that in the absence and presence of TGF-β1, EGR1 interacts with EBS1 and not EBS2. Bands were obtained in all the input and gDNA sites for the *PXDN* promoter and none were obtained in the NAC and NTC (Figure 3.5D).

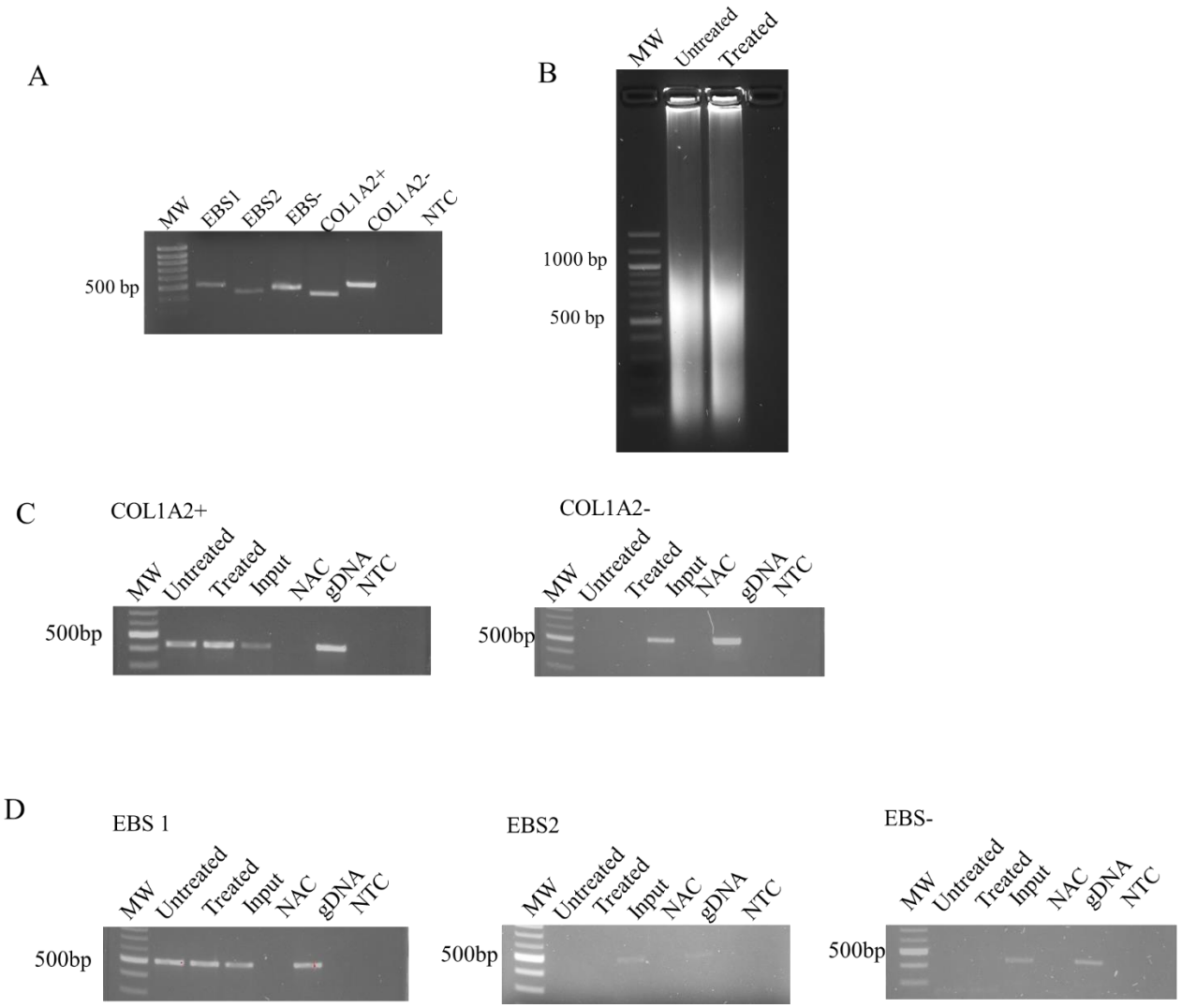

Figure 3.5: EGR1 interacts with EBS1 in the *PXDN* promoter. ChIP was performed to determine whether EGR1 binds to the *PXDN* promoter. A) Five primer sets were designed to amplify the immunoprecipitated DNA, EBS1 (500 bp), EBS2 (441 bp), EBS- (441bp), COL1A2+ (422 bp) and COL1A2- (536 bp) and all these amplified HEK293 gDNA. B) Untreated and 10 ng/ml TGF-β1 treated HEK293 cells were sonicated into the desired fragment lengths of 400-1000 bp. C) ChIP-PCR bands were obtained for the untreated and treated COL1A2+ therefore illustrating that EGR1 binds to its promoter and no bands were seen in the COL1A2- as it doesn't contain an EBS. D) In the *PXDN* promoter EGR1 only interacts with EBS1 in both the untreated and treated lanes but not with EBS2 or the EBS- control. As expected, amplicons were observed in all input and gDNA controls and not in the no antibody control (NAC) and no template controls (NTC) (n=1).

3.5 EBS1 was successfully cloned into the pGL4.10 luciferase vector

In the absence of the two ChIP biological replicates, we proceeded with the luciferase reporter assay as it would verify if EGR1 could drive *PXDN* expression by binding to EBS1. EBS1 was cloned into the pGL4.10[*luc2*] vector. The *COL1A2* EBS was also cloned into the pGL4.10 and here we expected EGR1 to downregulate the luciferase reporter gene expression as EGR1 was shown to activate its expression (Chen *et al.*, 2006). Sites withing both the PXDN and COL1A2 without any EBSs were also included to act as negative controls. The constructs were cleaved with the the KpnI and EcoRV restriction enzymes and ligated into pGL4.10 vectors. Sanger sequencing was done and it confirmed that all the inserts had the correct sequence and were ligated in a 5'- 3' direction (Figure 3.6).

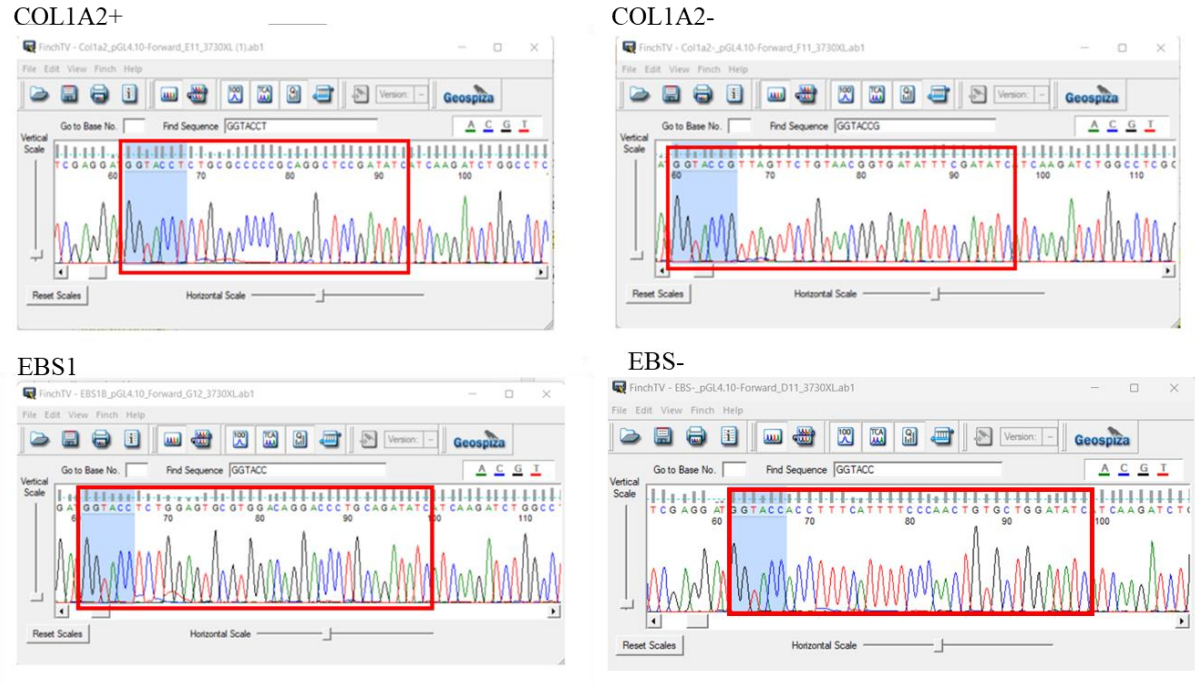

Figure 3.6: Sanger sequencing of the recombinant pGL4.10 vectors. The cloning of putative EGR1 binding sites in the PXDN promoter (EBS1 and EBS-) and those of a known EGR1 target gene (COL1A2+ and COL1A2-). The highlighted regions in the electropherograms show that the inserts were properly cloned into the pGL4.10 vector and had the correct sequence and orientation with flanking KpnI sites (GGTACC) on the 5′ end and the EcoRV sites (GATATC) on the 3′ end.

Once the inserts were cloned, we proceeded with the X-gal assay to optimize the transfection to ensure that the conditions were optimal to enable HEK293 cells to uptake the recombinant vectors. The *lacZ* vector, which when expressed in cells hydrolyses X-gal into a blue

precipitation that stains them. This allows for the differentiation of transfected and non-transfected cells. Various conditions were tested including altering the amount of the vector, the volume of the transfection reagent and the incubation period of the cells following transfection. In all conditions no blue cells were observed indicating that the transfection did not work. As such we could not perform the luciferase assay to determine if EGR1 can drive PXDN expression.

4. Discussion

PXDN is a novel member of the peroxidase-COX protein family of oxidoreductases, and it crosslinks collagen IV protomers in the ECM (Bhave *et al.,* 2012). *PXDN* has been implicated as one of the genes that are upregulated during the fibrotic process (Péterfi *et al.,* 2009; Liu *et al.,* 2019; Sojoodi *et al.,* 2022). Its increased expression causes matrix stiffening through excessively crosslinking collagen IV fibres in the BM and it also activates the proliferation and migration of fibroblasts (Péterfi, *et al.,* 2009; Bhave *et al.,* 2017; Liu *et al.,* 2019). As a novel protein, there is little that is known about the cellular functions of the protein and the mechanisms that dysregulate its expression in pathological states. Apart from Snai1 and Nrf2 (Sitole and Mavri-Damelin 2018; Hanmer and Mavri-Damelin, 2018), no other upstream transcriptional activators have been identified for PXDN and because the expression of proteins is primarily modulated at a transcriptional level, it is important to identify these. In this research, we considered EGR1 as a potential regulator of *PXDN*. EGR1 is a TF that regulates cell growth, proliferation, and apoptosis (Krones-Herzig *et al.,* 2005; Shimoyamada *et al.,* 2010; Wei *et al.,* 2017). It is also implicated in the fibrotic process and here it predominantly targets ECM proteins such as fibronectin, *COL1A2, MMP1* and *TIMP* (Liu *et al.,* 2000; Aicher *et al.,* 2003; Chen *et al.,* 2006; Yeo *et al.,* 2020). We therefore investigated the regulation of *PXDN* expression by EGR1 under TGF-β1 conditions which is a key mediator of fibroproliferation (Meng *et al.,* 2016).

Immunoblotting showed that EGR1 is expressed in HEK293 cells, and we observed bands at 80 kDa. Although Sukhatme *et al.* (1988) reported that EGR1 has 533 amino acids and a molecular weight of 57 kDa, other studies have detected the bands to be much higher and this is considered to be due to post-translational modifications. EGR1 was expressed in the untreated and TGF-β1 treated samples and this is in line with most studies but in different cells lines such as human dermal fibroblasts, MDA-MB-231 and HaCaT cells (Chen *et al.,* 2006; Gorbacheva *et al.,* 2021; Feng *et al.,* 2022). The expression levels of EGR1 increased in the treated samples at 6 and 12 hours then decreased to baseline levels at 24 hours. TGF-β1

has been shown to induce activation of EGR1 and we observed a similar pattern (Chen *et al.,* 2006; Passiatore *et al.,* 2011). The peak expression was observed at 6 and 12 hours but overall, the changes were not statistically significant in comparison to the untreated sample. This finding is in opposition to literature findings as exposure of cells to TGF-β1 concentrations between 2- 10 ng/ml significantly increases EGR1 expression levels (Chen *et al.,* 2006; Gorbacheva *et al.,* 2021; Feng *et al.,* 2022).

PXDN was also expressed in the HEK293 cells, however, we were unable to quantify the changes in its expression levels as the blots had a lot of background. In an attempt to remove the background, the protein loading amount, the primary and the secondary antibody concentrations were modified along with the Tween-20 concentration to reduce the background on the blots (see Table 2.1). From these adjustments, we got clearer blots as compared to the almost black ones that we had been previously getting but they were still not clear enough to perform densitometry. As a last attempt we did protein immunoprecipitation before blotting, however, the background persisted. The most plausible explanation for the background is that the PXDN antibody that we used probably does not function well when the target antigen is denatured as there is a lot of non-specific binding. Given all these attempts we had to stop PXDN blotting. It is worth mentioning that based on our literature review, we expected to see increased PXDN expression in the treated samples similar to the results obtained by Péterfi *et al.* (2009) in human dermal fibroblasts treated with 5 ng/ml TGF-β1 for 24, 48 and 72 hours and we hypothesized to see a peak at 24 hours.

Immunofluorescence microscopy showed that EGR1 was expressed in nuclei and it was detected in the untreated and treated samples. Duclot and Kabbaj. (2017) report that the phosphorylation of EGR1 is low in the absence of is stimulants and once these are present, all the EGR1 proteins in the cells are then activated and this would explain the increase we observed post-treatment. The CTCF analysis showed a significant change at 6 hours and 12 hours, with a drop to untreated levels at 24 hours. This paired with other literature findings thus leads us to conclude that EGR1 expression is significantly changed by TGF-β1 at the earlier time points (Chen *et al.,* 2006; Bhattacharyya *et al.,* 2009). These findings also confirm that once EGR1 is activated, it translocates to the nucleus and transactives genes and once it has finished, its expression is reduced. This is either by its inhibitors NAB1/2 or itself via negative feedback or proteasome-mediated degradation (Kumbrink *et al.,* 2005; Manente *et al.,* 2011).

PXDN on the other hand was observed extracellularly however we also saw the expression in the nucleus and this was not expected. The extracellular localization of the protein however affirms that PXDN is an ECM protein and this fits in with its structure as it has an N-terminal secretion signal peptide (Soudi *et al*., 2012). Once PXDN is synthesized it is then transported to the matrix and here it catalyses the formation of sulfilimine bonds in collagen IV and this stabilizes the BM (Bhave *et al.,* 2012). To correct for the nuclear expression of PXDN, for the CTCF analysis only the fluorescence outside the nuclei was measured and here we saw an increase in expression at 12 and 24 hours with the highest expression in the latter time point. This change was statistically significant indicating that PXDN is upregulated by TGF-β1 signalling. This finding agrees with that observed by Péterfi *et al.* (2009) when treating human pulmonary fibroblasts with TGF-β1. PXDN is expressed in a range of cells such as fibroblasts, endothelial and epithelial cells (Péterfi *et al.,* 2009; Lázár *et al.,* 2015) and our western blot and immunofluorescence show that it is also expressed in HEK293 cells.

We then performed bioinformatics analysis on the *PXDN* promoter to find putative EBSs in its sequence and we found two sites, EBS1 and EBS2. These sites had the characteristic GC-rich sequence of EGR1 target genes and EBS1 was located further upstream from the TSS whilst EBS2 was much closer to the TSS. The ChIP-PCR results for the first replicate showed that there was an interaction between EGR1 and EBS1. This was a surprising finding because EBS2 was closer to the TSS than EBS1 and EGR1 has been reported to preferentially bind to proximal promoters and regions closer to the TSS as transcription can be initiated faster at those regions (Koldamova *et al.,* 2014). Unfortunately, we could only validate this binding in one biological replicate. Thereafter we got no bands for either EBS sites or in the *COL1A2* positive control. The lack of bands in our PXDN promoter sites could have been interpreted as negative results which show that EGR1 does not bind to the *PXDN* promoter, however, the lack of the binding in the positive control points to problems in the assay as the *COL1A2* promoter has been validated to be an EGR1 target gene (Chen *et al.,* 2006). Again, in our samples, bands were always obtained in the input and gDNA controls, which respectively validate the presence of the target sites after sonication and that the primers can amplify DNA. We then concluded that we were not recovering enough DNA during immunoprecipitation and the purification step and thus no amplicons were seen for the EBS in both the *COL1A2* and *PXDN* promoters. The DNA concentration recovered from ChIP is inherently low as only the sites the antibody binds to will be immunoprecipitated, so to optimize the PCR step we halved the PCR reaction mixture but we were still unable to get

amplicons for both promoter regions. For future work, the antibody concentration can be increased, ChIP-sequencing can be done instead of ChIP-PCR to analyse if EGR1 binds to the EBSs in the PXDN promoter or alternatively, another primary antibody which targets a different epitope of the EGR1 protein can be used. It is worth mentioning that the #4154 anti-EGR1 antibody has been validated for ChIP by the manufacture to show that EGR1 binds to the *PCM1* gene, and the antibody was also used to show that EGR1 bound to and regulated the *CCL2* and *UL135* genes (Buehler *et al*., 2019; Yan *et al*., 2021).

The ChIP assay is accompanied by the luciferase reporter assay, which confirms whether the binding of a TF leads to any functional gene regulation. In the absence of the two ChIP biological replicates, we proceeded with this assay to verify if the binding we obtained in EBS1 would drive *PXDN* expression. We successfully cloned the EBS1 site into the pGL4.10 vector along with the *COL1A2* promoter constructs. Following this, the transfection was optimized using the *lacZ* vector. The *lacZ* gene encodes β-galactosidase, which turns transfected cells blue by hydrolysing X-gal, a type of β-galactosides (Burn, 2012). In our different transfection conditions however, none of the cells turned blue. We expected to see varying degrees of blue cells and that would be representative of the transfection efficiency. The most plausible explanation for this is that the transfection reagent did not work as varying amounts of the vector and the transfection reagent volumes were tested and therefore some transfection should have happened. The transfection reagent is responsible for permeabilizing the membrane of cells and if this is not done properly or at all, the vector cannot enter the cells and thus any transgene expression cannot be analysed. Better optimization of the conditions is therefore needed including using a different transfection reagent as HEK293 cells are highly transfectable (Ooi *et al.,* 2016). If the transfection efficiency was optimal, the luciferase assay would have been done and if EGR1 bound to and positively regulated *PXDN*, there would be an increase in the RLU readings in the transfected cells compared to the untransfected controls and if the regulation was negative the readings would be lower. If there was no regulation at all the readings would be comparable to the control.

5. Conclusion

We have shown that PXDN is a TGF-β1-responsive gene and may be regulated by EGR1. One of the limitations of this study was that an optimal TGF-β1 treatment concentration was not done at the beginning as the initial concentration we used did not give a response similar to that reported in the literature for both of the target proteins. The ChIP assay results were also not reproducible and because luciferase assay could not be done, we cannot definitively say if EGR1 indeed binds to and regulates *PXDN*. Another limitation of the study was the use of HEK293 cells instead of fibroblasts which are a better model of fibrosis. Because the bioinformatics analysis and the preliminary ChIP result suggest a relationship between EGR1 and PXDN, future work should include redoing ChIP and instead of doing ChIP-PCR on the recovered immunoprecipitated DNA do ChIP-qPCR which is more sensitive. This should then be followed by the luciferase reporter assay to verify if EGR1 can drive *PXDN* expression or not. Should EGR1 regulate *PXDN* expression, novel roles would be established for it in cell growth, differentiation, and apoptosis. PXDN can therefore be used as a prognostic and therapeutic marker for diseases where these cellular processes are dysregulated such as fibrosis.

6. References

Abdulkadir, S.A., Carbone, J.M., Naughton, C.K., Humphrey, P.A., Catalona, W.J. and Milbrandt, J., 2001. Frequent and early loss of the EGR1 corepressor NAB2 in human prostate carcinoma. *Human pathology*, *32*(9), pp.935-939.

Aicher, W.K., Alexander, D., Haas, C., Kuchen, S., Pagenstecher, A., Gay, S., Peter, H.H. and Eibel, H., 2003. Transcription factor early growth response 1 activity up-regulates expression of tissue inhibitor of metalloproteinases 1 in human synovial fibroblasts. *Arthritis & Rheumatism*, *48*(2), pp.348-359.

Alexander, D., Judex, M., Meyringer, R., Weis-Klemm, M., Gay, S., Müller-Ladner, U. and Aicher, W.K., 2002. Transcription factor Egr-1 activates collagen expression in immortalized fibroblasts or fibrosarcoma cells. *Biological chemistry*, *383*(12), 1845–1853.

Ali, R.M.M. and Ghonimy, M.B.I., 2021. Post-COVID-19 pneumonia lung fibrosis: a worrisome sequela in surviving patients. *Egyptian Journal of Radiology and Nuclear Medicine*, *52*, pp.1-8.

Añazco, C., López-Jiménez, A.J., Rafi, M., Vega-Montoto, L., Zhang, M.Z., Hudson, B.G. and Vanacore, R.M., 2016. Lysyl oxidase-like-2 cross-links collagen IV of glomerular basement membrane. *Journal of Biological Chemistry*, *291*(50), pp.25999-26012.

Armstrong, A.W. and Golan, D.E., 2011. Pharmacology of hemostasis and thrombosis. *Principles of Pharmacology: The Pathophysiologic Basis of Drug Therapy. 3rd ed. Philadelphia: Lippincott Williams & Wilkins*, pp.372-400.

Arpino, V., Brock, M. and Gill, S.E., 2015. The role of TIMPs in regulation of extracellular matrix proteolysis. *Matrix biology*, *44*, pp.247-254.

Bahrami, S. and Drabløs, F., 2016. Gene regulation in the immediate-early response process. *Advances in biological regulation*, 62, pp.37-49.

Bai, Y.P., Hu, C.P., Yuan, Q., Peng, J., Shi, R.Z., Yang, T.L., Cao, Z.H., Li, Y.J., Cheng, G. and Zhang, G.G., 2011. Role of VPO1, a newly identified haem-containing peroxidase, in ox-LDL induced endothelial cell apoptosis. *Free Radical Biology and Medicine*, *51*(8), pp.1492-1500.

Barton, D.E., Foellmer, B.E., Du, J., Tamm, J., Derynck, R. and Francke, U., 1988. Chromosomal mapping of genes for transforming growth factors beta 2 and beta 3 in man and mouse: dispersion of TGF-beta gene family. *Oncogene research*, *3*(4), pp.323-331.

Bathish, B., Paumann-Page, M., Paton, L.N., Kettle, A.J. and Winterbourn, C.C., 2020. Peroxidasin mediates bromination of tyrosine residues in the extracellular matrix. *Journal of Biological Chemistry*, *295*(36), pp.12697-12705.

Beckmann, A.M. and Wilce, P.A., 1997. Egr transcription factors in the nervous system. *Neurochemistry international*, *31*(4), pp.477-510.

Ben Amar, M. and Wu, M., 2014. Re-epithelialization: advancing epithelium frontier during wound healing. *Journal of The Royal Society Interface*, *11*(93), p.20131038.

Benyon, R.C. and Arthur, M.J., 2001. Extracellular matrix degradation and the role of hepatic stellate cells. In *Seminars in liver disease*, *21*(3), 373–384.

Bhattacharyya, S., Chen, S.J., Wu, M., Warner-Blankenship, M., Ning, H., Lakos, G., Mori, Y., Chang, E., Nihijima, C., Takehara, K. and Feghali-Bostwick, C., 2008. Smad-independent transforming growth factor-β regulation of early growth response-1 and sustained expression in fibrosis: Implications for scleroderma. *The American journal of pathology*, *173*(4), pp.1085-1099.

Bhattacharyya, S., Wei, J., Melichian, D.S., Milbrandt, J., Takehara, K. and Varga, J., 2009. The transcriptional cofactor Nab2 is induced by TGF-β and suppresses fibroblast activation: physiological roles and impaired expression in scleroderma. *PLoS One*, *4*(10), p.e7620.

Bhattacharyya, S., Wu, M., Fang, F., Tourtellotte, W., Feghali-Bostwick, C. and Varga, J., 2011. Early growth response transcription factors: key mediators of fibrosis and novel targets for anti-fibrotic therapy. *Matrix Biology*, *30*(4), pp.235-242.

Bhave, G., Colon, S. and Ferrell, N., 2017. The sulfilimine cross-link of collagen IV contributes to kidney tubular basement membrane stiffness. *American Journal of Physiology-Renal Physiology*, *313*(3), pp.F596-F602.

Bhave, G., Cummings, C.F., Vanacore, R.M., Kumagai-Cresse, C., Ero-Tolliver, I.A., Rafi, M., Kang, J.S., Pedchenko, V., Fessler, L.I., Fessler, J.H. and Hudson, B.G., 2012. Peroxidasin forms sulfilimine chemical bonds using hypohalous acids in tissue genesis. *Nature chemical biology*, *8*(9), pp.784-790.

Borchiellini, C., Coulon, J. and Le Parco, Y., 1996. The function of type IV collagen during Drosophila muscle development. *Mechanisms of development*, *58*(1-2), pp.179-191.

Borthwick, L.A., Wynn, T.A. and Fisher, A.J., 2013. Cytokine mediated tissue fibrosis. *Biochimica et biophysica acta (BBA)-molecular basis of disease*, *1832*(7), pp.1049-1060.

Bradford, M.M., 1976. A rapid and sensitive method for the quantitation of microgram quantities of protein utilizing the principle of protein-dye binding. *Analytical biochemistry*, *72*(1-2), pp.248-254.

Braga, T.T., Agudelo, J.S.H. and Camara, N.O.S., 2015. Macrophages during the fibrotic process: M2 as friend and foe. *Frontiers in immunology*, *6*, p.602.Kalluri, R., Gattone 2nd, V.H., Noelken, M.E. and Hudson, B.G., 1994. The alpha 3 chain of type IV collagen induces autoimmune Goodpasture syndrome. *Proceedings of the National Academy of Sciences*, *91*(13), pp.6201-6205.

Bramhall, S., Noack, N., Wu, M. and Loewenberg, J.R., 1969. A simple colorimetric method for determination of protein. *Analytical biochemistry*, *31*, pp.146-148.

Briem, E., Budkova, Z., Sigurdardottir, A.K., Hilmarsdottir, B., Kricker, J., Timp, W., Magnusson, M.K., Traustadottir, G.A. and Gudjonsson, T., 2019. MiR-203a is differentially expressed during branching morphogenesis and EMT in breast progenitor cells and is a repressor of peroxidasin. *Mechanisms of development*, *155*, pp.34-47.

Brown, C.A., Toth, A.P. and Magnussen, B., 2010. Clinical benefits of intra-articular anakinra for arthrofibrosis. *Orthopedics*, *33*(12).

Brown, C., Toth, A. and Magnussen, R., 2011. Clinical benefits of intra-articular anakinra for persistent knee effusion. *The journal of knee surgery*, *24*(01), pp.061-066.

Brown, K.L., Cummings, C.F., Vanacore, R.M. and Hudson, B.G., 2017. Building collagen IV smart scaffolds on the outside of cells. *Protein Science*, *26*(11), pp.2151-2161.

Brunt, E.M., 2004. Nonalcoholic steatohepatitis. *Seminars in liver disease* (Vol. 24, No. 01, pp. 3-20).

Buehler, J., Carpenter, E., Zeltzer, S., Igarashi, S., Rak, M., Mikell, I., Nelson, J.A. and Goodrum, F., 2019. Host signaling and EGR1 transcriptional control of human cytomegalovirus replication and latency. *PLoS pathogens*, *15*(11), p.e1008037.

Burn, S.F., 2012. Detection of β-galactosidase activity: X-gal staining. *Kidney Development: Methods and Protocols*, pp.241-250.

Cai, L., Xiong, X., Kong X. and Xie, J., 2017. The role of the lysl oxidases in tissue repair and remodelling: a concise review. *Tissue engineering and regenerative medicine*, 141(1), pp.15-30.

Caley, M.P., Martins, V.L. and O'Toole, E.A., 2015. Metalloproteinases and wound healing. *Advances in wound care*, *4*(4), pp.225-234.

Cao, X., Mahendran, R., Guy, G.R. and Tan, Y.H., 1992. Protein phosphatase inhibitors induce the sustained expression of the Egr-1 gene and the hyperphosphorylation of its gene product. *Journal of Biological Chemistry*, *267*(18), pp.12991-12997.

Cao, X.M., Koski, R.A., Gashler, A., McKiernan, M., Morris, C.F., Gaffney, R., Hay, R.V. and Sukhatme, V.P., 1990. Identification and characterization of the Egr-1 gene product, a DNA-binding zinc finger protein induced by differentiation and growth signals. *Molecular and cellular biology*, 10(5), pp.1931-1939.

Chen, G., Chen, H., Wang, C., Peng, Y., Sun, L., Liu, H. and Liu, F., 2012. Rapamycin ameliorates kidney fibrosis by inhibiting the activation of mTOR signaling in interstitial macrophages and myofibroblasts. *PloS one*, *7*(3), p.e33626.

Chen, J., Liu, M.Y., Parish, C.R., Chong, B.H. and Khachigian, L., 2011. Nuclear import of early growth response-1 involves importin-7 and the novel nuclear localization signal serine-proline-serine. *The international journal of biochemistry & cell biology*, *43*(6), pp.905-912.

Chen, S.J., Ning, H., Ishida, W., Sodin-Semrl, S., Takagawa, S., Mori, Y. and Varga, J., 2006. The early-immediate gene EGR-1 is induced by transforming growth factor-β and mediates stimulation of collagen gene expression. *Journal of Biological Chemistry*, *281*(30), pp.21183-21197.

Cheng, G., Li, H., Cao, Z., Qiu, X., McCormick, S., Thannickal, V.J. and Nauseef, W.M., 2011. Vascular peroxidase-1 is rapidly secreted, circulates in plasma, and supports dityrosine cross-linking reactions. *Free Radical Biology and Medicine*, *51*(7), pp.1445-1453.

Cheng, G., Salerno, J.C., Cao, Z., Pagano, P.J. and Lambeth, J.D., 2008. Identification and characterization of VPO1, a new animal haem-containing peroxidase. *Free Radical Biology and Medicine*, *45*(12), pp.1682-1694.

Cheng, J.C., Chang, H.M. and Leung, P.C.K., 2013. Egr-1 mediates epidermal growth factor-induced downregulation of E-cadherin expression via Slug in human ovarian cancer cells. *Oncogene*, *32*(8), pp.1041-1049.

Cho, M.H., 2010. Renal fibrosis. *Korean journal of pediatrics*, *53*(7), p.735.

Choi, A., Lao, R., Ling-Fung Tang, P., Wan, E., Mayer, W., Bardakjian, T., Shaw, G.M., Kwok, P.Y., Schneider, A. and Slavotinek, A., 2015. Novel mutations in PXDN cause microphthalmia and anterior segment dysgenesis. *European Journal of Human Genetics*, *23*(3), pp.337-341.

Christy, B. and Nathans, D., 1989. DNA binding site of the growth factor-inducible protein Zif268. *Proceedings of the National Academy of Sciences*, *86*(22), pp.8737-8741.

Close, R., Toro, S., Martial, J.A. and Muller, M., 2002. Expression of the zinc finger Egr1 gene during zebrafish embryonic development. *Mechanisms of development*, *118*(1-2), pp.269-272.

Colon, S. and Bhave, G., 2016. Proprotein convertase processing enhances peroxidasin activity to reinforce collagen IV. *Journal of Biological Chemistry*, *291*(46), pp.24009-24016.

Colon, S., Luan, H., Liu, Y., Meyer, C., Gewin, L. and Bhave, G., 2019. Peroxidasin and eosinophil peroxidase, but not myeloperoxidase, contribute to renal fibrosis in the murine unilateral ureteral obstruction model. *American Journal of Physiology-Renal Physiology*, 316(2), pp.F360-F371.

Conte, E., Gili, E., Fagone, E., Fruciano, M., Iemmolo, M. and Vancheri, C., 2014. Effect of pirfenidone on proliferation, TGF-β-induced myofibroblast differentiation and fibrogenic activity of primary human lung fibroblasts. *European Journal of Pharmaceutical Sciences*, *58*, pp.13-19.

Cucoranu, I., Clempus, R., Dikalova, A., Phelan, P.J., Ariyan, S., Dikalov, S. and Sorescu, D., 2005. NAD (P) H oxidase 4 mediates transforming growth factor-β1–induced differentiation of cardiac fibroblasts into myofibroblasts. *Circulation research*, *97*(9), pp.900-907.

Cui, S., Lv, X., Li, W., Li, Z., Liu, H., Gao, Y. and Huang, G., 2018. Folic acid modulates VPO1 DNA methylation levels and alleviates oxidative stress-induced apoptosis in vivo and in vitro. Redox biology, 19, pp.81-91.

Darby, I.A., Zakuan, N., Billet, F. and Desmoulière, A., 2016. The myofibroblast, a key cell in normal and pathological tissue repair. *Cellular and Molecular Life Sciences*, *73*(6), pp.1145-1157.

Davies, M.J., Hawkins, C.L., Pattison, D.I. and Rees, M.D., 2008. Mammalian haem peroxidases: from molecular mechanisms to health implications. *Antioxidants & redox signalling*, 10(7), pp.1199-1234.

de Bruyn, J.R., Becker, M.A., Steenkamer, J., Wildenberg, M.E., Meijer, S.L., Buskens, C.J., Bemelman, W.A., Löwenberg, M., Ponsioen, C.Y., van den Brink, G.R. and D'Haens, G.R., 2018. Intestinal fibrosis is associated with lack of response to Infliximab therapy in Crohn's disease. *PloS one*, *13*(1), p.e0190999.

Demidova-Rice, T.N., Hamblin, M.R. and Herman, I.M., 2012. Acute and impaired wound healing: pathophysiology and current methods for drug delivery, part 1: normal and chronic wounds: biology, causes, and approaches to care. *Advances in skin & wound care*, *25*(7), p.304.

Di, Y., Chen, D., Yu, W. and Yan, L., 2019. Bladder cancer stage-associated hub genes revealed by WGCNA co-expression network analysis. *Hereditas*, *156*(1), pp.1-11.

Dougan, J., Hawsawi, O., Burton, L.J., Edwards, G., Jones, K., Zou, J., Nagappan, P., Wang, G., Zhang, Q., Danaher, A. and Bowen, N., 2019. Proteomics-Metabolomics Combined Approach Identifies Peroxidasin as a Protector against Metabolic and Oxidative Stress in Prostate Cancer. *International Journal of Molecular Sciences*, 20(12), p.3046.

Drakopanagiotakis, F., Xifteri, A., Polychronopoulos, V. and Bouros, D., 2008. Apoptosis in lung injury and fibrosis. *European Respiratory Journal*, *32*(6), pp.1631-1638.

Dubois, C.M., Blanchette, F., Laprise, M.H., Leduc, R., Grondin, F. and Seidah, N.G., 2001. Evidence that furin is an authentic transforming growth factor-β1-converting enzyme. *The American journal of pathology*, *158*(1), pp.305-316.

Feng, X., Feng, W., Ji, Y., Jin, T., Li, J. and Guo, J., 2022. Transforming growth factor-β1 negatively regulates SOCS7 via EGR1 during wound healing. *Cell Communication and Signaling*, *20*(1), pp.1-12.

Fidler, A.l., Vanacore, R.M., Chetyrikin, S.V., Pedchenko, V.K., Bhave, G., Yin, V.P., Stothers, C.L Rose, K.L., McDonald, W.H., Clark, T.A and Borza, D.B., 2014. A unique covalent bond in the basement membrane is a primordial innovation for tissue evolution. *Proceedings of the National Academy of Sciences, 111(1),* pp.331-336.

Fowell, A.J., Collins, J.E., Duncombe, D.R., Pickering, J.A., Rosenberg, W.M. and Benyon, R.C., 2011. Silencing tissue inhibitors of metalloproteinases (TIMPs) with short interfering RNA reveals a role for TIMP-1 in hepatic stellate cell proliferation. *Biochemical and biophysical research communications*, *407*(2), pp.277-282.

Fujii, D., Brissenden, J.E., Derynck, R. and Francke, U., 1986. Transforming growth factor β gene maps to human chromosome 19 long arm and to mouse chromosome 7. *Somatic cell and molecular genetics*, *12*(3), pp.281-288.

Georges, P.C., Hui, J.J., Gombos, Z., McCormick, M.E., Wang, A.Y., Uemura, M., Mick, R., Janmey, P.A., Furth, E.E. and Wells, R.G., 2007. Increased stiffness of the rat liver precedes matrix deposition: implications for fibrosis. *American Journal of Physiology-Gastrointestinal and Liver Physiology*, *293*(6), pp.G1147-G1154.

Go, C.K., Gross, S., Hooper, R. and Soboloff, J., 2019. EGR-mediated control of STIM expression and function. *Cell Calcium*, *77*, pp.58-67.

Gorbacheva, A.M., Uvarova, A.N., Ustiugova, A.S., Bhattacharyya, A., Korneev, K.V., Kuprash, D.V. and Mitkin, N.A., 2021. EGR1 and RXRA transcription factors link TGF-β pathway and CCL2 expression in triple negative breast cancer cells. *Scientific Reports*, *11*(1), p.14120.

Gotenstein, J.R., Swale, R.E., Fukuda, T., Wu, Z., Giurumescu, C.A., Goncharov, A., Jin, Y. and Chisholm, A.D., 2010. The C. elegans peroxidasin PXN-2 is essential for embryonic morphogenesis and inhibits adult axon regeneration. *Development*, 137(21), pp.3603-3613.

Grieb, G., Steffens, G., Pallua, N., Bernhagen, J. and Bucala, R., 2011. Circulating fibrocytes—biology and mechanisms in wound healing and scar formation. *International review of cell and molecular biology*, *291*, pp.1-19.

Grotegut, S., von Schweinitz, D., Christofori, G. and Lehembre, F., 2006. Hepatocyte growth factor induces cell scattering through MAPK/Egr-1-mediated upregulation of Snail. *The EMBO journal*, *25*(15), pp.3534-3545.

Guerin, D.J., Kha, C.X. and Tseng, K.A.S., 2021. From cell death to regeneration: rebuilding after injury. *Frontiers in Cell and Developmental Biology*, *9*, p.655048.

Guha, M., O'Connell, M.A., Pawlinski, R., Hollis, A., McGovern, P., Yan, S.F., Stern, D. and Mackman, N., 2001. Lipopolysaccharide activation of the MEK-ERK1/2 pathway in human monocytic cells mediates tissue factor and tumor necrosis factor α expression by inducing Elk-1 phosphorylation and Egr-1 expression. *Blood, The Journal of the American Society of Hematology*, *98*(5), pp.1429-1439.

Guo, B., Tian, X.C., Li, D.D., Yang, Z.Q., Cao, H., Zhang, Q.L., Liu, J.X. and Yue, Z.P., 2014. Expression, regulation and function of Egr1 during implantation and decidualization in mice. *Cell cycle*, *13*(16), pp.2626-2640.

Hanmer, K.L. and Mavri-Damelin, D., 2018. Peroxidasin is a novel target of the redox-sensitive transcription factor Nrf2. *Gene*, 674, pp.104-114.

Havis, E. and Duprez, D., 2020. EGR1 transcription factor is a multifaceted regulator of matrix production in tendons and other connective tissues. *International journal of molecular sciences*, *21*(5), p.1664.

Heyens, L.J., Busschots, D., Koek, G.H., Robaeys, G. and Francque, S., 2021. Liver fibrosis in non-alcoholic fatty liver disease: from liver biopsy to non-invasive biomarkers in diagnosis and treatment. *Frontiers in medicine*, *8*, p.615978.

Hinz, B. and Lagares, D., 2020. Evasion of apoptosis by myofibroblasts: a hallmark of fibrotic diseases. *Nature Reviews Rheumatology*, *16*(1), pp.11-31.

Ho, C.Y., López, B., Coelho-Filho, O.R., Lakdawala, N.K., Cirino, A.L., Jarolim, P., Kwong, R., Gonzalez, A., Colan, S.D., Seidman, J.G. and Diez, J., 2010. Myocardial fibrosis as an early manifestation of hypertrophic cardiomyopathy. *New England Journal of Medicine*, *363*(6), pp.552-563.

Horikoshi, N., Cong, J., Kley, N. and Shenk, T., 1999. Isolation of differentially expressed cDNAs from p53-dependent apoptotic cells: activation of the human homologue of the Drosophila peroxidasin gene. *Biochemical and Biophysical Research Communications*, 261(3), pp. 864-869.

Huang, F. and Chen, Y.G., 2012. Regulation of TGF-β receptor activity. *Cell & bioscience*, *2*, pp.1-10.

Huang, R.P., Fan, Y., deBelle, I., Ni, Z., Matheny, W. and Adamson, E.D., 1998. Egr-1 inhibits apoptosis during the UV response: correlation of cell survival with Egr-1 phosphorylation. *Cell Death & Differentiation*, *5*(1), pp.96-106.

Itoh, K., Chiba, T., Takahashi, S., Ishii, T., Igarashi, K., Katoh, Y., Oyake, T., Hayashi, N., Satoh, K., Hatayama, I. and Yamamoto, M., 1997. An Nrf2/small Maf heterodimer mediates the induction of phase II detoxifying enzyme genes through antioxidant response elements. *Biochemical and biophysical research communications*, 236(2), pp.313-322.

Jayachandran, A., Königshoff, M., Yu, H., Rupniewska, E., Hecker, M., Klepetko, W., Seeger, W. and Eickelberg, O., 2009. SNAI transcription factors mediate epithelial–mesenchymal transition in lung fibrosis. *Thorax*, *64*(12), pp.1053-1061.

Jayadev, R. and Sherwood, D.R., 2017. Basement membranes. *Current Biology*, *27*(6), pp.R207-R211.

Jiang, J., Wang, K., Chen, Y., Chen, H., Nice, E.C. and Huang, C., 2017. Redox regulation in tumor cell epithelial–mesenchymal transition: Molecular basis and therapeutic strategy. *Signal Transduction and Targeted Therapy*, *2*(1), pp.1-12.

Kaissling, B., LeHir, M. and Kriz, W., 2013. Renal epithelial injury and fibrosis. *Biochimica et Biophysica Acta (BBA)-Molecular Basis of Disease*, *1832*(7), pp.931-939.

Kalluri, R. and Weinberg, R.A., 2009. The basics of epithelial-mesenchymal transition. *The Journal of clinical investigation*, *119*(6), pp.1420-1428.

Kalluri, R., Gattone 2nd, V.H., Noelken, M.E. and Hudson, B.G., 1994. The alpha 3 chain of type IV collagen induces autoimmune Goodpasture syndrome. *Proceedings of the National Academy of Sciences*, *91*(13), pp.6201-6205.

Kendall, R.T. and Feghali-Bostwick, C.A., 2014. Fibroblasts in fibrosis: novel roles and mediators. *Frontiers in pharmacology*, *5*, p.123.

Keshet, Y. and Seger, R., 2010. The MAP kinase signaling cascades: a system of hundreds of components regulates a diverse array of physiological functions. *MAP kinase signaling protocols*, pp.3-38.

Khachigian, L.M., Anderson, K.R., Halnon, N.J., Gimbrone, M.A., Resnick, N. and Collins, T., 1997. Egr-1 is activated in endothelial cells exposed to fluid shear stress and interacts with a novel shear-stress-response element in the PDGF A-chain promoter. *Arteriosclerosis, thrombosis, and vascular biology*, 17(10), pp.2280-2286.

Khan, K., Rudkin, A., Parry, D.A., Burdon, K.P., McKibbin, M., Logan, C.V., Abdelhamed, Z.I., Muecke, J.S., Fernandez-Fuetes, N., Laurie, K.J. and Shries, M., 2011. Homozygous mutations in PXDN cause congenital cataract, corneal opacity, and developmental glaucoma. *The American Journal of Human Genetics*, 89(3), pp. 464-473.

Khoshnoodi J., Pedchenko, V. and Hudson, B.G., 2008. Mammalian collagen IV. *Microscopy research and technique*, 71(5), pp.357-370.

Kim, H.K., Ham, K.A., Lee, S.W., Choi, H.S., Kim, H.S., Kim, H.K., Shin, H.S., Seo, K.Y., Cho, Y., Nam, K.T. and Kim, I.B., 2019. Biallelic deletion of pxdn in mice leads to anophthalmia and severe eye malformation. *International Journal of Molecular Sciences*, *20*(24), p.6144.

Klingberg, F., Hinz, B. and White, E.S., 2013. The myofibroblast matrix: implications for tissue repair and fibrosis. *The Journal of pathology*, *229*(2), pp.298-309.

Kobelska-Dubiel, N., Klincewicz, B. and Cichy, W., 2014. Liver disease in cystic fibrosis. *Gastroenterology Review/Przegląd Gastroenterologiczny*, *9*(3), pp.136-141.

Koldamova, R., Schug, J., Lefterova, M., Cronican, A.A., Fitz, N.F., Davenport, F.A., Carter, A., Castranio, E.L. and Lefterov, I., 2014. Genome-wide approaches reveal EGR1-controlled regulatory networks associated with neurodegeneration. *Neurobiology of disease*, 63, pp.107-114.

Krieg, T., Abraham, D. and Lafyatis, R., 2007. Fibrosis in connective tissue disease: the role of the myofibroblast and fibroblast-epithelial cell interactions. *Arthritis research & therapy*, *9*(2), pp.1-7.

Krones-Herzig, A., Adamson, E. and Mercola, D., 2003. Early growth response 1 protein, an upstream gatekeeper of the p53 tumor suppressor, controls replicative senescence. *Proceedings of the National Academy of Sciences*, *100*(6), pp.3233-3238.

Krones-Herzig, A., Mittal, S., Yule, K., Liang, H., English, C., Urcis, R., Soni, T., Adamson, E.D. and Mercola, D., 2005. Early growth response 1 acts as a tumor suppressor in vivo and in vitro via regulation of p53. *Cancer research*, *65*(12), pp.5133-5143.

Kubiczkova, L., Sedlarikova, L., Hajek, R. and Sevcikova, S., 2012. TGF-β–an excellent servant but a bad master. *Journal of translational medicine*, *10*(1), pp.1-24.

Kumbrink, J., Gerlinger, M. and Johnson, J.P., 2005. Egr-1 induces the expression of its corepressor nab2 by activation of the nab2 promoter thereby establishing a negative feedback loop. *Journal of Biological Chemistry*, *280*(52), pp.42785-42793.

Kurihara-Shimomura, M., Sasahira, T., Shimomura, H. and Kirita, T., 2020. Peroxidan plays a tumor-promoting role in oral squamous cell carcinoma. *International Journal of Molecular Sciences*, *21*(15), p.5416.

Kuusniemi, A.M., Lapatto, R., Holmberg, C., Karikoski, R., Rapola, J. and Jalanko, H., 2005. Kidneys with heavy proteinuria show fibrosis, inflammation, and oxidative stress, but no tubular phenotypic change. *Kidney international*, *68*(1), pp.121-132.

Lagares, D., Santos, A., Grasberger, P.E., Liu, F., Probst, C.K., Rahimi, R.A., Sakai, N., Kuehl, T., Ryan, J., Bhola, P. and Montero, J., 2017. Targeted apoptosis of myofibroblasts with the BH3 mimetic ABT-263 reverses established fibrosis. *Science Translational Medicine*, *9*(420), p.eaal3765.

Lamouille, S., Xu, J. and Derynck, R., 2014. Molecular mechanisms of epithelial–mesenchymal transition. *Nature reviews Molecular cell biology*, *15*(3), pp.178-196.

Lázár E., Péterfi, Z., Sirokmány, G., Kovács, H.A., Klement, E., Medzihradszky, K.F., and Geiszt, M., 2015. Structure-function analysis of peroxidasin provides insight into the mechanism of collagen IV crosslinking. *Free Radical Biology and Medicine*, 83, pp.273-282.

LeBleu, V.S., MacDonald, B. and Kalluri, R., 2007. Structure and function of basement membranes. *Experimental Biology and medicine*, 232(9), pp1121-1129.

Lee, S.B. and Kalluri, R., 2010. Mechanistic connection between inflammation and fibrosis. *Kidney International*, *78*, pp.S22-S26.

Lee, S.W., Kim, H.K., Naidansuren, P., Ham, K.A., Choi, H.S., Ahn, H.Y., Kim, M., Kang, D.H., Kang, S.W. and Joe, Y.A., 2020. Peroxidasin is essential for endothelial cell survival and growth signaling by sulfilimine crosslink-dependent matrix assembly. *The FASEB Journal*, *34*(8), pp.10228-10241.

Lemaire, P., Revelant, O., Bravo R., and Charnay, P., 1988. Two mouse genes encoding potential transcription factors with identical DNA-binding domains are activated by growth factors in cultured cells. *Proceedings of the National Academy of Sciences*, *85*(13), pp.4691-4695.

Li, B., Power, M.R. and Lin, T.J., 2006. De novo synthesis of early growth response factor-1 is required for the full responsiveness of mast cells to produce TNF and IL-13 by IgE and antigen stimulation. *Blood*, *107*(7), pp.2814-2820.

Li, C.L., Yang, D., Cao, X., Wang, F., Hong, D.Y., Wang, J., Shen, X.C. and Chen, Y., 2017. Fibronectin induces epithelial-mesenchymal transition in human breast cancer MCF-7 cells via activation of calpain. *Oncology letters*, *13*(5), pp.3889-3895.

Li, H., Cao, Z., Moore, D.R., Jackson, P.L., Barnes, S., Lambeth, J.D., Thannickal, V.J. and Cheng, G., 2012. Microbicidal activity of vascular peroxidase 1 in human plasma via generation of hypochlorous acid. *Infection and immunity*, *80*(7), pp.2528-2537.

Li, J., Zhang, Y.P. and Kirsner, R.S., 2003. Angiogenesis in wound repair: angiogenic growth factors and the extracellular matrix. *Microscopy research and technique*, *60*(1), pp.107-114.

Li, J.F., Duan, H.F., Wu, C.T., Zhang, D.J., Deng, Y., Yin, H.L., Han, B., Gong, H.C., Wang, H.W. and Wang, Y.L., 2013. HGF accelerates wound healing by promoting the dedifferentiation of epidermal cells through-integrin/ILK pathway. *BioMed research international*, *2013*.

Lim, C.P., Jain, N. and Cao, X., 1998. Stress-induced immediate-early gene, egr-1, involves activation of p38/JNK1. *Oncogene*, *16*(22), pp.2915-2926.

Liu, C., Yao, J., Mercola, D. and Adamson, E., 2000. The transcription factor EGR-1 directly transactivates the fibronectin gene and enhances attachment of human glioblastoma cell line U251. *Journal of Biological Chemistry*, *275*(27), pp.20315-20323.

Liu, C.Y., Lin, H.H., Tang, M.J. and Wang, Y.K., 2015. Vimentin contributes to epithelial-mesenchymal transition cancer cell mechanics by mediating cytoskeletal organization and focal adhesion maturation. *Oncotarget*, *6*(18), p.15966.

Liu, Z., Xu, Q., Yang, Q., Cao, J., Wu, C., Peng, H., Zhang, X., Chen, J., Cheng, G., Wu, Y. and Shi, R., 2019. Vascular peroxidase 1 is a novel regulator of cardiac fibrosis after myocardial infarction. *Redox Biology*, *22*, p.101151.

Loh, C.Y., Chai, J.Y., Tang, T.F., Wong, W.F., Sethi, G., Shanmugam, M.K., Chong, P.P. and Looi, C.Y., 2019. The E-cadherin and N-cadherin switch in epithelial-to-mesenchymal transition: signaling, therapeutic implications, and challenges. *Cells*, *8*(10), p.1118.

Løtvedt, P., Fallahshahroudi, A., Bektic, L., Altimiras, J. and Jensen, P., 2017. Chicken domestication changes expression of stress-related genes in brain, pituitary and adrenals. *Neurobiology of stress*, *7*, pp.113-121.

Lu, M., Qin, Q., Yao, J., Sun, L. and Qin, X., 2019. Induction of LOX by TGF-β1/Smad/AP-1 signaling aggravates rat myocardial fibrosis and heart failure. *IUBMB life*, *71*(11), pp.1729-1739.

Ma, C.P., Guo, Z.M., Zhang, F.L. and Su, J.Y., 2020. Molecular identification, expression and function analysis of peroxidasin in *Chilo suppressalis*. *Insect science*, *27*(6), pp.1173-1185.

Manente, A.G., Pinton, G., Tavian, D., Lopez-Rodas, G., Brunelli, E. and Moro, L., 2011. Coordinated sumoylation and ubiquitination modulate EGF induced EGR1 expression and stability. *PloS one*, *6*(10), p.e25676.

Marconi, G.D., Fonticoli, L., Rajan, T.S., Pierdomenico, S.D., Trubiani, O., Pizzicannella, J. and Diomede, F., 2021. Epithelial-Mesenchymal Transition (EMT): the type-2 EMT in wound healing, tissue regeneration and organ fibrosis. *Cells*, *10*(7), p.1587.

McCall, A.S., Bhave, G., Pedchenko, V., Hess, J., Free, M., Little, D.J., Baker, T.P., Pendergraft, W.F., Falk, R.J., Olson, S.W. and Hudson, B.G., 2018. Inhibitory anti-peroxidasin antibodies in pulmonary-renal syndromes. *Journal of the American Society of Nephrology*, *29*(11), pp.2619-2625.

McCall, A.S., Cummings, C.F., Bhave, G., Vanacore, R., Page-McCaw, A. and Hudson, B.G., 2014. Bromine is an essential trace element for assembly of collagen IV scaffolds in tissue development and architecture. *Cell*, *157*(6), pp.1380-1392.

Medici, D., Hay, E.D. and Olsen, B.R., 2008. Snail and Slug promote epithelial-mesenchymal transition through β-catenin–T-cell factor-4-dependent expression of transforming growth factor-β3. Molecular biology of the cell, 19(11), pp.4875-4887.

Meng, X.M., Nikolic-Paterson, D.J. and Lan, H.Y., 2016. TGF-β: the master regulator of fibrosis. *Nature Reviews Nephrology*, *12*(6), pp.325-338.

Milbrandt, J., 1987. A nerve growth factor-induced gene encodes a possible transcriptional regulatory factor. *Science*, *238*(4828), pp.797-799.

Molnar, G., Crozat, A. and Pardee, A.B., 1994. The immediate-early gene Egr-1 regulates the activity of the thymidine kinase promoter at the G0-to-G1 transition of the cell cycle. *Molecular and cellular biology*, *14*(8), pp.5242-5248.

Moore, L.D., Le, T. and Fan, G., 2013. DNA methylation and its basic function. *Neuropsychopharmacology*, *38*(1), pp.23-38.

Morrissey, M.A. and Sherwood, D.R., 2015. An active role for basement membrane assembly and modification in tissue sculpting. *Journal of cell science*, *128*(9), pp.1661-1668.

Nakamura, Y. and Suda, T., 2015. Idiopathic pulmonary fibrosis: diagnosis and clinical manifestations. *Clinical Medicine Insights: Circulatory, Respiratory and Pulmonary Medicine*, *9*, pp.CCRPM-S39897.

Nakerakanti, S. and Trojanowska, M., 2012. Suppl 1: the role of TGF-β receptors in fibrosis. *The open rheumatology journal*, *6*, p.156.

Namba, D.R., Ma, G., Samad, I., Ding, D., Pandian, V., Powell, J.D., Horton, M.R. and Hillel, A.T., 2015. Rapamycin inhibits human laryngotracheal stenosis–derived fibroblast proliferation, metabolism, and function in vitro. *Otolaryngology--Head and Neck Surgery*, *152*(5), pp.881-888.

Nelson, R.E., Fessler, L.I., Takagi, Y., Blumberg, B., Keene, D.R., Olson, P.F., Parker, C.G. and Fessler, J.H., 1994. Peroxidasin: a novel enzyme-matrix protein of *Drosophila* development. *The EMBO Journal*, 13(15), pp.3438-3447

Nieto, M.A., 2002. The snail superfamily of zinc-finger transcription factors. *Nature reviews Molecular cell biology*, *3*(3), pp.155-166.

Nisticò, P., Bissell, M.J. and Radisky, D.C., 2012. Epithelial-mesenchymal transition: general principles and pathological relevance with special emphasis on the role of matrix metalloproteinases. *Cold Spring Harbor perspectives in biology*, *4*(2), p.a011908.

O'Donovan, K.J., Tourtellotte, W.G., Millbrandt, J. and Baraban, J.M., 1999. The EGR family of transcription-regulatory factors: progress at the interface of molecular and systems neuroscience. *Trends in neurosciences*, *22*(4), pp.167-173.

Ooi, A., Wong, A., Esau, L., Lemtiri-Chlieh, F. and Gehring, C., 2016. A guide to transient expression of membrane proteins in HEK-293 cells for functional characterization. *Frontiers in physiology*, *7*, p.300.

Pakyari, M., Farrokhi, A., Maharlooei, M.K. and Ghahary, A., 2013. Critical role of transforming growth factor beta in different phases of wound healing. *Advances in wound care*, *2*(5), pp.215-224.

Palta, S., Saroa, R. and Palta, A., 2014. Overview of the coagulation system. *Indian journal of anaesthesia*, *58*(5), p.515.

Pan, J., Li, D., Xu, Y., Zhang, J., Wang, Y., Chen, M., Lin, S., Huang, L., Chung, E.J., Citrin, D.E. and Wang, Y., 2017. Inhibition of Bcl-2/xl with ABT-263 selectively kills senescent type II pneumocytes and reverses persistent pulmonary fibrosis induced by ionizing radiation in mice. *International Journal of Radiation Oncology* Biology* Physics*, *99*(2), pp.353-361.

Panjwani, A.H., Deoskar, R.B., SM, J.F. and Rajan, K.E., 2003. Goodpasture's Syndrome. *Medical Journal Armed Forces India*, *59*(1), pp.77-79.

Papageorgiou, A.P. and Heymans, S., 2014. Peroxidasin-like protein: expanding the horizons of matrix biology. *Cardiovascular research*, *101*(3), pp.342-343.

Passiatore, G., Gentilella, A., Rom, S., Pacifici, M., Bergonzini, V. and Peruzzi, F., 2011. Induction of Id-1 by FGF-2 involves activity of EGR-1 and sensitizes neuroblastoma cells to cell death. *Journal of cellular physiology*, *226*(7), pp.1763-1770.

Paumann-Page, M., Katz, R.S., Bellei, M., Schwartz, I., Edenhofer, E., Sevcnikar, B., Soudi, M., Hofbauer, S., Battistuzzi, G., Furtmüller, P.G. and Obinger, C., 2017. Pre-steady-state kinetics reveal the substrate specificity and mechanism of halide oxidation of truncated human peroxidasin 1. *Journal of Biological Chemistry*, *292*(11), pp.4583-4592.

Paumann-Page, M., Kienzl, N.F., Motwani, J., Bathish, B., Paton, L.N., Magon, N.J., Sevcnikar, B., Furtmüller, P.G., Traxlmayr, M.W., Obinger, C. and Eccles, M.R., 2021. Peroxidasin protein expression and enzymatic activity in metastatic melanoma cell lines are associated with invasive potential. *Redox Biology*, *46*, p.102090.

Paumann-Page, M., Tscheliessnig, R., Sevcnikar, B., Katz, R.S., Schwartz, I., Hofbauer, S., Pfanzagl, V., Furtmüller, P.G. and Obinger,C., 2020. Monomeric and homotrimeric solutions structures of truncated human peroxidasin 1 variants. *Biochemica et Biophysica Acta (BBA)-Proteins and Proteomics, 1868*(1), p.140249.

Pavletich, N.P. and Pabo, C.O., 1991. Zinc finger-DNA recognition: crystal structure of a Zif268-DNA complex at 2.1 Å. *Science*, *252*(5007), pp.809-817.

Pećina-Šlaus, N., 2003. Tumor suppressor gene E-cadherin and its role in normal and malignant cells. *Cancer cell international*, *3*(1), pp.1-7.

Péterfi, Z. and Geiszt, M., 2014. Peroxidasins: novel players in tissue genesis. *Trends in biochemical sciences*, *39*(7), pp.305-307.

Péterfi, Z., Donkó, A., Orient, A., Sum, A., Prókai, A., Molnár, B., Veréb, Z., Rajnavölgyi, E., Kovács, K.J., Müller, V. and Szabó, A.J., 2009. Peroxidasin is secreted and incorporated into the extracellular matrix of myofibroblasts and fibrotic kidney. *The American journal of pathology*, 175(2), pp.725-735.

Péterfi, Z., Tóth, Z.E., Kovács, H.A., Lázár, E., Sum, A., Donkó, Á., Sirokmány, G., Shah, A.M. and Geiszt, M., 2014. Peroxidasin-like protein: a novel peroxidase homologue in the human heart. *Cardiovascular research*, *101*(3), pp.393-399.

Poggioli, G., Laureti, S., Campieri, M., Pierangeli, F., Gionchetti, P., Ugolini, F., Gentilini, L., Bazzi, P., Rizzello, F. and Coscia, M., 2007. Infliximab in the treatment of Crohn's disease. *Therapeutics and clinical risk management*, *3*(2), pp.301-308.

Poniatowski, Ł.A., Wojdasiewicz, P., Gasik, R. and Szukiewicz, D., 2015. Transforming growth factor Beta family: insight into the role of growth factors in regulation of fracture healing biology and potential clinical applications. *Mediators of inflammation*, *2015*.

Puche, J.E., Saiman, Y. and Friedman, S.L., 2013. Hepatic stellate cells and liver fibrosis. *Compr Physiol*, *3*(4), pp.1473-1492.

Ramos-Lewis, W. and Page-McCaw, A., 2019. Basement membrane mechanics shape development: Lessons from the fly. *Matrix Biology*, *75*, pp.72-81.

Reis, L.M. and Semina, E.V., 2011. Genetics of anterior segment dysgenesis disorders. *Current opinion in ophthalmology*, *22*(5), p.314.

Richter, K., Konzack, A., Pihlajaniemi, T., Heljasvaara, R. and Kietzmann, T., 2015. Redox-fibrosis: Impact of TGFβ1 on ROS generators, mediators and functional consequences. *Redox biology*, *6*, pp.344-352.

Rockel, J.S., Bernier, S.M. and Leask, A., 2009. Egr-1 inhibits the expression of extracellular matrix genes in chondrocytes by TNFα-induced MEK/ERK signalling. *Arthritis research & therapy*, *11*(1), pp.1-14.

Rouzer, C.A. and Marnett, L.J., 2009. Cyclooxygenases: structural and functional insights. *Journal of lipid research*, 50, pp.S29-S34.

Ruf, J. and Carayon, P., 2006. Structural and functional aspects of thyroid peroxidase. *Archives of biochemistry and biophysics*, *445*(2), pp.269-277.

Samarakoon, R., Higgins, S.P., Higgins, C.E. and Higgins, P.J., 2008. TGF-β1-induced plasminogen activator inhibitor-1 expression in vascular smooth muscle cells requires pp60c-src/EGFRY845 and Rho/ROCK signaling. *Journal of molecular and cellular cardiology*, *44*(3), pp.527-538.

Sayasith, K., Brown, K.A., Lussier, J.G., Doré, M. and Sirois, J., 2006. Characterization of bovine early growth response factor-1 and its gonadotropin-dependent regulation in ovarian follicles prior to ovulation. *Journal of molecular endocrinology*, *37*(2), pp.239-250.

Schieber, M. and Chandel, N.S., 2014. ROS function in redox signaling and oxidative stress. *Current biology*, *24*(10), pp.R453-R462.

Schjoldager, K.T., Narimatsu, Y., Joshi, H.J. and Clausen, H., 2020. Global view of human protein glycosylation pathways and functions. *Nature reviews Molecular cell biology*, *21*(12), pp.729-749.

Schwachtgen, J.L., Houston, P., Campbell, C., Sukhatme, V. and Braddock, M., 1998. Fluid shear stress activation of egr-1 transcription in cultured human endothelial and epithelial cells is mediated via the extracellular signal-related kinase 1/2 mitogen-activated protein kinase pathway. *The Journal of clinical investigation*, *101*(11), pp.2540-2549.

Shen, J., Xing, W., Gong, F., Wang, W., Yan, Y., Zhang, Y., Xie, C. and Fu, S., 2019. MiR-150-5p retards the progression of myocardial fibrosis by targeting EGR1. *Cell Cycle*, *18*(12), pp.1335-1348.

Shi, R., Cao, Z., Li, H., Graw, J., Zhang, G., Thannickal, V.J. and Cheng, G., 2018. Peroxidasin contributes to lung host defense by direct binding and killing of gram-negative bacteria. *PLoS Pathogens*, *14*(5), p.e1007026.

Shi, R., Hu, C., Yuan, Q., Yang, T., Peng, J., Li, Y., Bai, Y., Cao, Z., Cheng, G. and Zhang, G., 2011. Involvement of vascular peroxidase 1 in angiotensin II-induced vascular smooth muscle cell proliferation. *Cardiovascular research*, *91*(1), pp.27-36.

Shi, W., Ding, W., Zhao, Z., Wang, R., Wang, F., Tang, Y., Zhu, J., Su, C., Zhao, X. and Liu, L., 2022. Peroxidase is a novel potential marker in glioblastoma through bioinformatics method and experimental validation. *Frontiers in Genetics*, *13*.

Shimoyamada, H., Yazawa, T., Sato, H., Okudela, K., Ishii, J., Sakaeda, M., Kashiwagi, K., Suzuki, T., Mitsui, H., Woo, T. and Tajiri, M., 2010. Early growth response-1 induces and enhances vascular endothelial growth factor-An expression in lung cancer cells. *The American journal of pathology*, 177(1), pp.70-83.

Shin, D. and Minn, K.W., 2004. The effect of myofibroblast on contracture of hypertrophic scar. *Plastic and reconstructive surgery*, *113*(2), pp.633-640.

Shin, S.Y., Kim, J.H., Baker, A., Lim, Y. and Lee, Y.H., 2010. Transcription Factor Egr-1 Is Essential for Maximal Matrix Metalloproteinase-9 Transcription by Tumor Necrosis Factor αEgr-1 Regulation of MMP-9 Transcription. *Molecular Cancer Research*, *8*(4), pp.507-519.

Shinde, A.V., Humeres, C. and Frangogiannis, N.G., 2017. The role of α-smooth muscle actin in fibroblast-mediated matrix contraction and remodeling. *Biochimica et Biophysica Acta (BBA)-Molecular Basis of Disease*, *1863*(1), pp.298-309.

Sirokmány, G. and Geiszt, M., 2019. The relationship of NADPH oxidases and haem peroxidases: fallin'in and out. *Frontiers in Immunology*, *10*, p.394.

Sirokmány, G., Kovács, H.A., Lázár, E., Kónya, K., Donkó, Á., Enyedi, B., Grasberger, H. and Geiszt, M., 2018. Peroxidasin-mediated crosslinking of collagen IV is independent of NADPH oxidases. *Redox Biology*, *16*, pp.314-321.

Sitole, B.N. and Mavri-Damelin, D., 2018. Peroxidasin is regulated by the epithelial-mesenchymal transition master transcription factor Snai1. *Gene*, *646*, pp.195-202.

Sojoodi, M., Erstad, D.J., Barrett, S.C., Salloum, S., Zhu, S., Qian, T., Colon, S., Gale, E.M., Jordan, V.C., Wang, Y. and Li, S., 2022. Peroxidasin deficiency re-programs macrophages toward pro-fibrolysis function and promotes collagen resolution in liver. *Cellular and Molecular Gastroenterology and Hepatology*, *13*(5), pp.1483-1509.

Soudi, M., Paumann-Page, M., Delporte, C., Pirker, K.F., Bellei, M., Edenhofer, E., Stadlmayr, G., Battistuzzi, G., Boudjeltia, K.Z., Furtmüller, P.G. and Van Antwerpen, P., 2015. Multidomain human peroxidasin 1 is a highly glycosylated and stable homotrimeric high spin ferric peroxidase. *Journal of Biological Chemistry*, *290*(17), pp.10876-10890.

Soudi, M., Zamocky, M., Jakopitsch, C., Furtmüller, P.G. and Obinger, C., 2012. Molecular evolution, structure, and function of peroxidasins. *Chemistry & biodiversity*, *9*(9), pp.1776-1793.

Sperandio, S., Fortin, J., Sasik, R., Robitaille, L., Corbeil, J. and de Belle, I., 2009. The transcription factor Egr1 regulates the HIF-1α gene during hypoxia. *Molecular Carcinogenesis*, *48*(1), pp.38-44.

Sukhatme, V.P., Cao, X., Chang, L.C., Tsai-Morris, C.H., Stamenkovich, D., Ferreira, P.C., Cohen, D.R., Edwards, S.A., Shows, T.B., Curran, T. and Le Beau, M.M., 1988. A zinc finger-encoding gene coregulated with c-fos during growth and differentiation, and after cellular depolarization. *Cell*, *53*(1), pp.37-43.

Tatsukawa, H. and Hitomi, K., 2021. Role of transglutaminase 2 in cell death, survival, and fibrosis. *Cells*, *10*(7), p.1842.

Tauber, S., Jais, A., Jeitler, M., Haider, S., Husa, J., Lindroos, J., Knöfler, M., Mayerhofer, M., Pehamberger, H., Wagner, O. and Bilban, M., 2010. Transcriptome analysis of human cancer reveals a functional role of haem oxygenase-1 in tumor cell adhesion. *Molecular cancer*, *9*, pp.1-16.

Ten Dijke, P., van Kessel, A.G. and Le Beau, J.F.M., 1988. Transforming growth factor typeß3 maps to human chromosome 14, region q23-q24. *Molecular characterization of transforming growth factor-03*, *3*, p.83.

Thannickal, V.J., Henke, C.A., Horowitz, J.C., Noble, P.W., Roman, J., Sime, P.J., Zhou, Y., Wells, R.G., White, E.S. and Tschumperlin, D.J., 2014. Matrix biology of idiopathic pulmonary fibrosis: a workshop report of the national heart, lung, and blood institute. *The American Journal of Pathology*, *184*(6), pp.1643-1651.

Thomas, H.M., Cowin, A.J. and Mills, S.J., 2017. The importance of pericytes in healing: wounds and other pathologies. *International journal of molecular sciences*, *18*(6), p.1129.

Tindall, A.J., Pownall, M.E., Morris, I.D. and Isaacs, H.V., 2005. Xenopus tropicalis peroxidasin gene is expressed within the developing neural tube and pronephric kidney. *Developmental Dynamics: an official publication of the American Association of Anatomists*, 232(2), pp.377-384.

Tracy, L.E., Minasian, R.A. and Caterson, E.J., 2016. Extracellular matrix and dermal fibroblast function in the healing wound. *Advances in wound care*, *5*(3), pp.119-136.

Tremblay, J.J. and Drouin, J., 1999. Egr-1 is a downstream effector of GnRH and synergizes by direct interaction with Ptx1 and SF-1 to enhance luteinizing hormone β gene transcription. *Molecular and Cellular Biology*, *19*(4), pp.2567-2576.

Varki, A., 2017. Biological roles of glycans. *Glycobiology*, *27*(1), pp.3-49.

Walton, K.L., Makanji, Y., Chen, J., Wilce, M.C., Chan, K.L., Robertson, D.M. and Harrison, C.A., 2010. Two distinct regions of latency-associated peptide coordinate stability of the latent transforming growth factor-β1 complex. *Journal of Biological Chemistry*, *285*(22), pp.17029-17037.

Wang, Y., Liu, J., Ying, X., Lin, P.C. and Zhou, B.P., 2016. Twist-mediated epithelial-mesenchymal transition promotes breast tumor cell invasion via inhibition of hippo pathway. Scientific reports, 6(1), p.24606.

Wang, Y., Qin, C., Zhao, B., Li, Z., Li, T., Yang, X., Zhao, Y. and Wang, W., 2023. EGR1 induces EMT in pancreatic cancer via a P300/SNAI2 pathway. *Journal of Translational Medicine*, *21*(1), p.201.

Wei, L.L., Wu, X.J., Gong, C.C. and Pei, D.S., 2017. Egr-1 suppresses breast cancer cells proliferation by arresting cell cycle progression via down-regulating Cyclin Ds. *International Journal of Clinical and Experimental Pathology*, *10*(10), p.10212.

Weiler, S.R., Taylor, S.M. and Deans, R.J., 1994. Assignment of a human melanoma associated gene MG50 (D2S448) to chromosome 2p25. 3 by fluorescence in situ hybridization. *Genomics*, *22*(1).

Werner, S., Krieg, T. and Smola, H., 2007. Keratinocyte–fibroblast interactions in wound healing. *Journal of investigative dermatology*, *127*(5), pp.998-1008.

Willis, B.C. and Borok, Z., 2007. TGF-β-induced EMT: mechanisms and implications for fibrotic lung disease. *American Journal of Physiology-Lung Cellular and Molecular Physiology*, *293*(3), pp. L525-L534.

Wollin, L., Wex, E., Pautsch, A., Schnapp, G., Hostettler, K.E., Stowasser, S. and Kolb, M., 2015. Mode of action of nintedanib in the treatment of idiopathic pulmonary fibrosis. *European Respiratory Journal*, *45*(5), pp.1434-1445.

Wu, M., Melichian, D.S., De La Garza, M., Gruner, K., Bhattacharyya, S., Barr, L., Nair, A., Shahrara, S., Sporn, P.H., Mustoe, T.A. and Tourtellotte, W.G., 2009. Essential roles for early growth response transcription factor Egr-1 in tissue fibrosis and wound healing. *The American journal of pathology*, *175*(3), pp.1041-1055.

Wynn, T., 2008. Cellular and molecular mechanisms of fibrosis. *The Journal of Pathology: A Journal of the Pathological Society of Great Britain and Ireland*, *214*(2), pp.199-210.

Xiao, D., Chinnappan, D., Pestell, R., Albanese, C. and Weber, H.C., 2005. Bombesin regulates cyclin D1 expression through the early growth response protein Egr-1 in prostate cancer cells. *Cancer research*, *65*(21), pp.9934-9942.

Xu, J., Lamouille, S. and Derynck, R., 2009. TGF-β-induced epithelial to mesenchymal transition. *Cell research*, *19*(2), pp.156-172.

Yamamoto, T., Matsushima, S., Okabe, K., Ikeda, S., Ishikita, A., Enzan, N., Sada, M., Tsutsui, Y., Miyake, R. and Tsutsui, H., 2020. Cyclin dependent kinase 1 (CDK1) positively regulates cardiac hypertrophy and fibrosis via TGF-beta pathway. *European Heart Journal*, *41*(Supplement_2), pp.ehaa946-3743.

Yan, J., Gao, Y., Lin, S., Li, Y., Shi, L. and Kan, Q., 2021. EGR1-CCL2 feedback loop maintains epithelial-mesenchymal transition of cisplatin-resistant gastric cancer cells and promotes tumor angiogenesis. *Digestive diseases and sciences*, pp.1-12.

Yan, X., Sabrautzki, S., Horsch, M., Fuchs, H., Gailus-Durner, V., Beckers, J., Hrabě de Angelis, M. and Graw, J., 2014. Peroxidasin is essential for eye development in the mouse. *Human molecular genetics*, *23*(21), pp.5597-5614.

Yang, S.Z. and Abdulkadir, S.A., 2003. Early growth response gene 1 modulates androgen receptor signaling in prostate carcinoma cells. *Journal of Biological Chemistry*, *278*(41), pp.39906-39911.

Yang, Y., Cao, Z., Tian, L., Garvey, W.T. and Cheng, G., 2013. VPO1 mediates ApoE oxidation and impairs the clearance of plasma lipids. *PloS one*, 8(2).

Yang, Y., Shi, R., Cao, Z., Zhang, G. and Cheng, G., 2016. VPO1 mediates oxidation of LDL and formation of foam cells. *Oncotarget*, 7(24), p.35500.

Yeo, H., Lee, J.Y., Kim, J., Ahn, S.S., Jeong, J.Y., Choi, J.H., Lee, Y.H. and Shin, S.Y., 2020. Transcription factor EGR-1 transactivates the MMP1 gene promoter in response to TNFα in HaCaT keratinocytes. *BMB reports*, *53*(6), p.323.

Young, C.D., Zimmerman, L.J., Hoshino, D., Formisano, L., Hanker, A.B., Gatza, M.L., Morrison, M.M., Moore, P.D., Whitwell, C.A., Dave, B. and Stricker, T., 2015. Activating PIK3CA mutations induce an epidermal growth factor receptor (EGFR)/extracellular signal-regulated kinase (ERK) paracrine signaling axis in basal-like breast cancer. *Molecular & cellular proteomics*, *14*(7), pp.1959-1976.

Zámocký, M. and Obinger, C., 2010. Molecular phylogeny of haem peroxidases. In *Biocatalysis based on haem peroxidases* (pp. 7-35). Springer, Berlin, Heidelberg.

Zámocký, M., Furtmüller, P.G. and Obinger, C., 2010. Evolution of structure and function of Class I peroxidases. *Archives of Biochemistry and Biophysics*, *500*(1), pp.45-57.

Zandarashvili, L., Vuzman, D., Esadze, A., Takayama, Y., Sahu, D., Levy, Y. and Iwahara, J., 2012. Asymmetrical roles of zinc fingers in dynamic DNA-scanning process by the inducible transcription factor Egr-1. *Proceedings of the National Academy of Sciences*, *109*(26), pp. E1724-E1732.

Zederbauer, M., Furtmüller, P.G., Brogioni, S., Jakopitsch, C., Smulevich, G. and Obinger, C., 2007. Heme to protein linkages in mammalian peroxidases: impact on spectroscopic, redox and catalytic properties. *Natural product reports*, *24*(3), pp.571-584.

Zhang, J., Zhang, Y., Sun, T., Guo, F., Huang, S., Chandalia, M., Abate, N., Fan, D., Xin, H.B., Chen, Y.E. and Fu, M., 2013. Dietary obesity-induced Egr-1 in adipocytes facilitates energy storage via suppression of FOXC2. *Scientific reports*, *3*(1), pp.1-10.

Zhang, Y., Alexander, P.B. and Wang, X.F., 2017. TGF-β family signaling in the control of cell proliferation and survival. *Cold Spring Harbor perspectives in biology*, *9*(4), p.a022145.

Zhang, Y.E., 2017. Non-Smad signaling pathways of the TGF-β family. *Cold Spring Harbor perspectives in biology*, *9*(2), p.a022129.

Zhang, Y.S., He, L., Liu, B., Li, N.S., Luo, X.J., Hu, C.P., Ma, Q.L., Zhang, G.G., Li, Y.J. and Peng, J., 2012. A novel pathway of NADPH oxidase/vascular peroxidase 1 in mediating oxidative injury following ischemia–reperfusion. *Basic Research in Cardiology*, *107*, pp.1-19.

Zheng, Y.Z. and Liang, L., 2018. High expression of PXDN is associated with poor prognosis and promotes proliferation, invasion as well as migration in ovarian cancer. *Annals of diagnostic pathology*, *34*, pp.161-165.

Zhou, X., Sun, Q., Xu, C., Zhou, Z., Chen, X., Zhu, X., Huang, Z., Wang, W. and Shi, Y., 2022. A systematic pan-cancer analysis of PXDN as a potential target for clinical diagnosis and treatment. *Frontiers in Oncology*, *12*.

Zi, Z., Chapnick, D.A. and Liu, X., 2012. Dynamics of TGF-β/Smad signaling. *FEBS letters*, 586(14), pp.1921-1928.

7. Appendices

Appendix A

Table A1: Recipes of chemical reagents and storage conditions

Reagent	Recipe
Glycerol freezing media	Dulbecco's Modified Eagle Medium/Nutrient Mixture F-12 (DMEM/F-12) containing 10% fetal bovine serum (FBS) 1% penicillin-streptomycin 20% FBS 15% glycerol -Filter sterilize and store at 4 ℃
Trypan blue	0.2% Trypan blue made to volume with 1X PBS -Filter sterilize and store at 4 ℃
Coomassie blue	3 mM Coomassie brilliant blue G250 50% Methanol 10% Glacial acetic acid -Store at RT, in the dark
Destain	10% Acetic acid 10% Methanol -Store at RT
Elution buffer	66% Methanol 1% of 25% Ammonia -Store at RT
4X Protein loading buffer	240 mM Tris-HCl, pH 6.8 8% Sodium dodecyl sulfate (SDS) 40% Glycerol 0.04% Bromophenol blue 5% β-mercaptoethanol -Store at -20 ℃
SDS-PAGE running buffer	25 mM Tris-HCl, pH 8.8 192 mM Glycine 0.1% SDS
Transfer buffer	25 mM Tris-HCl pH 8.3 192 mM Glycine 20% Methanol -Store at 4 ℃
1X TBST	20 mM Tris-HCl, pH 7.6 137 mM NaCl 0.1% Tween® 20 -Store at 4 ℃
Developer	6.4 M Metol

	0.6 M Sodium sulfite 80 mM Hydroquinone 0.45 M Sodium carbonate 34 mM Potassium bromide -Store at RT, in the dark
Fixer	0.8 M Sodium thiosulfate 0.2 M Sodium metabisulfite -Store at RT, in the dark
ChIP dilution buffer	1% Triton X-100 2 mM EDTA, pH 8.0 20 mM Tris-HCl, pH 8.0 150 mM NaCl -Store at 4 ℃
ChIP low salt wash buffer	0.1% SDS 1% Triton X-100 2 mM EDTA, pH 8.0 20 mM Tris-HCl, pH 8.0 150 mM NaCl -Store at 4 ℃
ChIP high salt wash buffer	0.1% SDS 1% Triton X-100 2 mM EDTA, pH 8.0 20 mM Tris-HCl, pH 8.0 500 mM NaCl -Store at 4 ℃
ChIP elution buffer	1% SDS 100 mM $NaHCO_3$
Oligonucleotide annealing buffer	10 mM Tris-HCl, pH 8.0 50 mM NaCl 1 mM EDTA -Store at RT
Solution I	25 mM Tris-HCl, pH 8.0 10 mM EDTA -Store at 4 ℃
Solution II	2% SDS 0.4 M NaOH
Solution III	5 mM Potassium acetate, pH 5.5 - Store at 4 ℃
1X PBS	137 mM NaCl 2.7 mM KCl 8.1 mM $Na_2HPO_4 \cdot 12H_2O$ 1.8 mM KH_2PO_4, pH 7

	-Store at 4℃
1X TAE	40 M Tris-HCl, pH 8.0 0.11% Glacial acetic acid 1 mM EDTA -Store at RT
1X RIPA	50 mM Tris-HCl, pH 8.0 150 mM NaCl 0.1% SDS 1% Triton X-100 0.5% Sodium deoxycholate -Store at 4 ℃

Appendix B

Table B1: Catalogue numbers of purchased reagents.

Category	Reagent	Manufacturer	Catalogue number
Cell culture reagents	DMEM/Hams F12	Gibco™	11320033
	FBS	Gibco™	10493106
	Penicillin-streptomycin	Gibco™	15140122
	1X PBS	Gibco™	10010015
	Trypsin-EDTA	Gibco™	25200072
Antibodies	EGR1 rabbit monoclonal antibody	Cell Signaling Technology	#4154
	PXDN mouse monoclonal antibody	Santa Cruz Biotechnology	sc-293408
	β-actin rabbit monoclonal antibody	Cell Signaling Technology	#4967
	Goat anti-rabbit IgG HRP	Cell Signaling Technology	#7074
	Horse anti-mouse IgG HRP	Cell Signaling Technology	#7076
	Mouse anti-rabbit IgG FITC	Santa Cruz Biotechnology	sc-2359
	Goat anti-mouse kappa-FITC	Southern Biotech	1050-02
Western blotting reagents	WesternBright® ECL Chemiluminescent HRP Substrate	Advansta	K-12045-C20
	WesternBright ® Nitrocellulose Transfer Membrane	Advansta	L-08009-001
ChIP reagents	Protein A/G beads	Santa Cruz Biotechnology	sc-2003
PCR master mix	KAPA Taq ReadyMix	Sigma-Merk	KK1024

Cloning reagents	KpnI	NEB	R0142S
	EcoRV	NEB	R0195S
	T4 DNA ligase	NEB	M0202
	pGL4.10 [*luc2*]	Promega	E6651
	pcDNA3-Egr1	Addgene	#11729
Transfection reagents	TurboFect™ Transfection Reagent	ThermoFisher Scientific	R0532

Appendix C

Table C1: KAPA Taq ReadyMix PCR reaction mixture components.

Component	**25 µl reaction**
PCR grade water	5.5 µl
2X KAPA Taq ReadyMix	12.5 µ1
10 µM Forward primer	1 µ1
10 µM Reverse primer	1 µl
Template DNA	5 µ1

Table C2: KAPA Taq ReadyMix PCR cycling conditions.

Phase	**Temperature (°C)**	**Time**	**Cycles**
Initial denaturation	95	3 min	1
Denaturation	95	30 sec	35
Annealing	Tm-5	30 sec	
Extension	72	1 min/kb	
Final extension	72	1 min/kb	1
Hold	4	∞	1

Appendix D

Mapping of the *PXDN* promoter with putative EGR1 binding sites (EBSs) and the corresponding amplifying primers

>2 dna:chromosome chromosome:GRCh38:2:1631887:1744515:-1

GCAGGAGAGATGGCAATCTTGCAGGAGAGACGACAACAGGAGGGTGTGGAGAGGATCC
AGGAGGAGTGATGGCATCTGCATCTGGACCCACTGGTGTGTGTGCACAGGATCCTGCGG
GGTGATGGCTGAACCCACTGGCGTGTGTGCACAGGATCCTGCGGGGTGATGGCTGAACT
CACTGGAGTGTGTGCACAGGATCCTGCAGGGGTGATGGCACCCGGAGTCTAATCTGAAC
CCACTGGAGTGTGTGCACAGGATCCCGCAGGGGCGATGGCACCCGGAGTCTGAAATGAA
TCCTCTGGAGTGCGTGGACAGGACCCTGCAGGGGTGATGGCATCGGAATCTGAACTAAACCCACT
CGAATGTGTGCGCAGGATCCCGCAGGGGCGATGGCACCCGGAGTCTAATCTGAACCCACTGGAGA
GTGTGCGCAGGATCCCGCAGGGGCGATGGCATATGGAGTTTCAGCTGGACCTACTCGAGTGTGTG
GATAGAATCTTGCAGGAGAGACGACATGTAGAATGTAAACTGGACTGAGTGGAGTGTATGGAGAG
AATCCTGCAGGTGAGATGGCGTGTGCAGTGGGAAGCGGACCCACTGGAATCTTTGGGTGGGACCC
AAACTCAACCACTGCTATGTGTAGACAGGATCTTTGAGGAGAGATGGCATCTGCAGTGTGAACCG
AACCCACTGGAGTGTATGGATAGCATCTTGCAGGAGTGATGACATCTGCAGTGTGATCTGGACTGC
CTCGAGTGTGTGGGTAGGATCCTGCAAGAGTGATGGCATGTGGAGTGAGCACTGCATCCACAGGA
CTGTGTGGACAGCAGCCTTCAGCAGTGATGATGTCTGCTGTGTGAAGTGGAGCACTGTAGTGTGTG
GGTAGGGTCCTGCAGGAGAGATGGCAACTGGAGTGTGAACTGCACCCACTTGAGTGAGAGGTTGG
GATGCTGCAGGTGGATGGCATTTGGAGTGTGAACTGGACCCACTTGAGTGTATGGGTAGGGTCCTG
CAGGAGAGATGGCAACTGGAGTGTGAACTGGACCCACTGTTGTGCCTGGAGAGGATCCTGCAGAA
GACAAGGCATCTGCAGTGTAAACTGGGCCACTGGGGTGTGTAGCTAGAATCATGCTGGAGTAACG
GCTTCTGGACTGTGAGCTGGCCCCATTAAAGTGTGTGTATAGGATCCTGCAAAAGTGATAGCCTCT
GGAGTGTGAATGGGACCCACTGAGGTGTGTGGATAGGATACTGCAGGGGTGATGGTGTCTGCAGT
GTGAGCTGCAGCCCTGGGGCATGTGGATAGGACTCTGCAAAGAGACAGCATCTGTGGTGTGAATG
GCACCGGTGGAATGTGTAGAGAGGATCCTGCAAAAGTGATGTCCTCTAGAGTGTGAACTGGACCC
ACTGGAGGGTGTGGACATCGTCCTGCAGGAGAGATGGCATCTAGAGTGTGAATGGCACCTCCGGA
GTGTGTGGATAGGAGCCCGCAGGAGAGAGCACATGTAGAGCGTGAACTGGACCCACTGAAATGTG
TGGACAGGATTCTGCAGAAGATACGGCATCCGGAGTGTGAAATGCACCACTAGTGTGTGTGCATA
GAATCCTGCATAAGTTTTGGCATCTACAGTGTGAACTGGAGTCACTGGAATGTGTGAATAGGATCT
TGCAGGAGAGATGTCTGCAGTGTGAGCTGGACCCACTTCTGTGTGTGGATAGTATCCTGCAGGAGA
GATGTTGTCTGCAGTGTGAGCTGGGCCCACCGGAGTGTGTGAATAGGATCCTGCAGGAGAAATGG
AATCCGGAGTGTGAGCTGCATCCGCTGTAGAGGGTGGATAAAATCCTGCAGGAAAGATGGCATCT
GGAATGTCAGCGGGAGCCACCGACCTCTGAGGATGCACCCCGCAGGTGTGATGCGGGGCCAGTTC
CAAGGCTGGGTTAGGTTTTACCCTGGCTTCTGTGTTGTACTCTCATTCTCTTCCTCTTTCTTCTAATA
CCTGCTCTGGGAGGCATCAGGCCATGTCCAGTGTGCAGGCCATGGAGACCCACACGGCAAGGAAC
TGGAACCCCCTGCCAGCAGCCTCGGGGGTCCAGTCCTTAGATGGTGCCCTGTGGTCAGCAATGCAC
CTGTGACCTCCGGGCTATGTCTCGTGGTAGTTGCTTTTGTGTTTTAACATAGCAACAGGAAACTAG
CCTATTACCCACCAATCCCATTCCAGGCTGCTTTCAAACGCAGCTCAGGCTAGAACACCAGCACGG
GGACACAGCTGAGACTTGGGGTTTGCGACGGGAACACGCCCATGCTGTGCCTCTGAATCTGGCAC
CGTCACCCTGTGGCCTGGGTTCAGCAACTTGGCCTCACCTTCCTTGTCTGTGAAATTCAGACTGGGT
CCTTGTGAGATGATTGGAGAGAATGTATGAACTATGTGAGAACGCCACCTTTGTGCGTATCTCACG
CAGTGTCTTCCCTCCTTTCCAAAGTCTTCTGCTGTCTCTAGACACACCCGACGTGGGGGGGGGGGG
TTCCCTGGGTCTCCTCCTAGGTCTGTCCCAGGAGGGCACGCACTGAAGGCCGCGAGAATCCCGGGG
GCTGCATTGCGCCGCGCCAAGGACTCCACACAGGACCTTTCATTTTCCCAACTGTGCTGAGCCAGG
CGGCCGGCAGAGAGCAGGTGGCTGACAGGCCCCGGGGAGCCGGACCGCCTGGGTCTAATCTTCCC
GCAGACTCCCTTGCTGTGCGCTTTGGGGCTTGGGCCTCAGTTTCCTCAAAAGGAATGAGGGGCTTT
TTTGGAACGTTAAATAATTTCCTACGTGGTTGCGGGTAGGGAGAAGGAGAAAGAGAGGAGCGCGC
CTGCGCGCCTGGAATCGTGCCCGGATCAGAGCAAGCGCTCTAAAAGTGTTACAAACATTAAGGCG
CCAACTAAAAAACCCGTAGTGAGCGCAGGCAGAAACCACGGGTAAGAGAAGTGGAGAAGCTTCG
CGTAGGCCCCAGGGTCCCGAGCCCCGAGTCTCGAGCGCAGAATCAGGGGTGCCAATGCTCTCCTC
CGCGCCCCCGAGCGCTCGCCTTGGCCATGCGGGCCGCCCCACCGGGATGAGGGCGCTCAGGCCGG
ACGCTGGGGCCCCGGGTTCTCGCCCCGCCCCGCCCTCGGGGATTCAGAGGGGCCGGGAGGAGCCT
CGCGCATGTGCACAGCTGGCGCCCCCCGCCCCCCGCGCACAGCTGGGACGTGGGCCGCGGCCGGG
CGGGCGCAGTCGGGAGCCGGCCGTGGTGGCTCCGTGCGTCCGAGCGTCCGTCCGCGCCGTCGGCC

ATGGCCAAGCGCTCCAGGGGCCCCGGGCGCCGCTGCCTGTTGGCGCTCGTGCTGTTCTGCGCCTGG
GGGACGCTGGCCGTGGTGGCCCAGAAGCCGGGCGCAGGGTGTCCGAGCC

Key:

EBS1

EBS2

EBS1 primers

EBS2 primers

EBS- primers

Transcription start site (TSS)

Appendix E

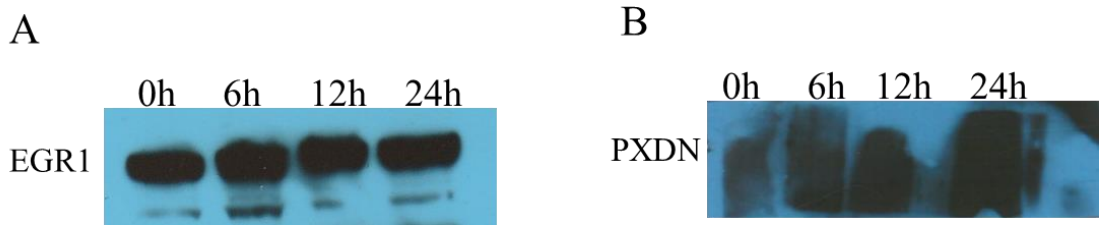

Figure 1E: Western blot optimization. A) EGR1 blots with 40 µg loaded protein and the standard recommended 1:1000 primary antibody dilution. The protein loading amount was then changed to 20 µg to reduce the thickness of the bands B) PXDN blots obtained from 100 µg protein and a 1:1000 primary antibody dilution and a 1:2000 HRP-conjugated secondary antibody. To reduce the background, the protein loading amount was changed to 80 µg, the primary antibody dilution to 1:2000 primary and the secondary antibody dilution of 1:1500.

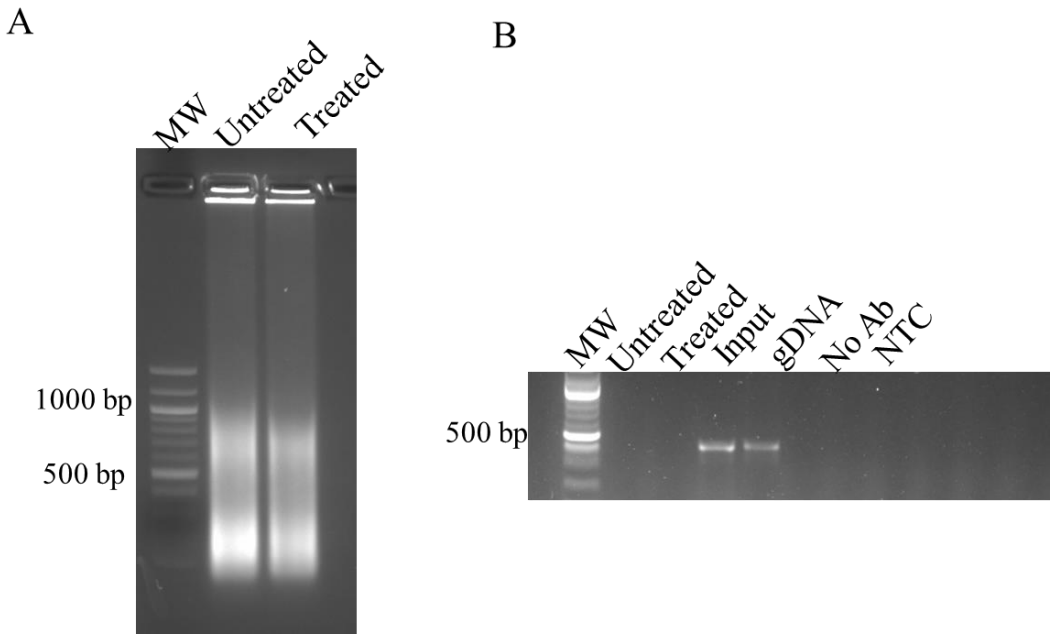

Figure 2E: ChIP assay optimization. A) The sonication of fragments was done for 15 minutes, 60% amplitude, 15 sec on and 15 sec off. A majority of the fragments were below 500 bp with others between 500-1000 bp. The sonication time was then changed to 10 minutes so that the DNA fragments aggregated more between 500-1000 bp. ChIP-PCR for the COL1A2+ site (422 bp) shows bands for only the input and gDNA controls. The EGR1-immunoprecipitated samples in the TGF-β1 untreated and treated had no bands and this was unexpected as this is a known EGR1 target gene.

A

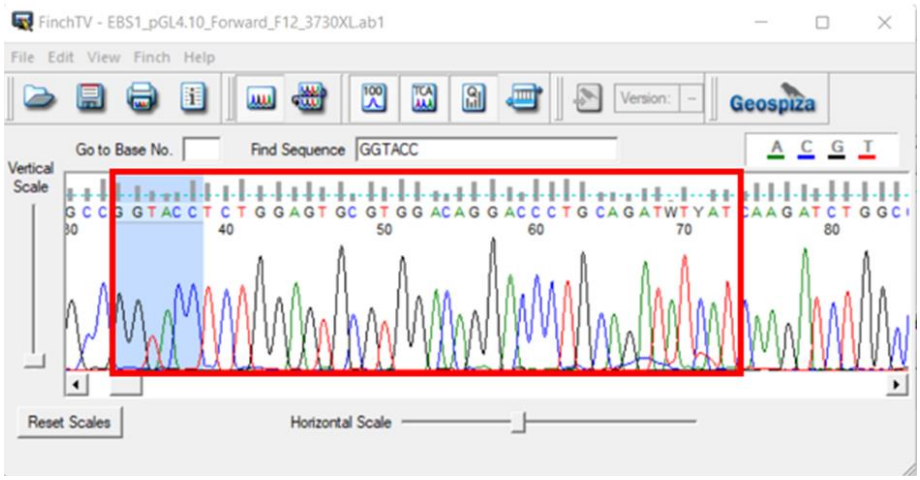

B

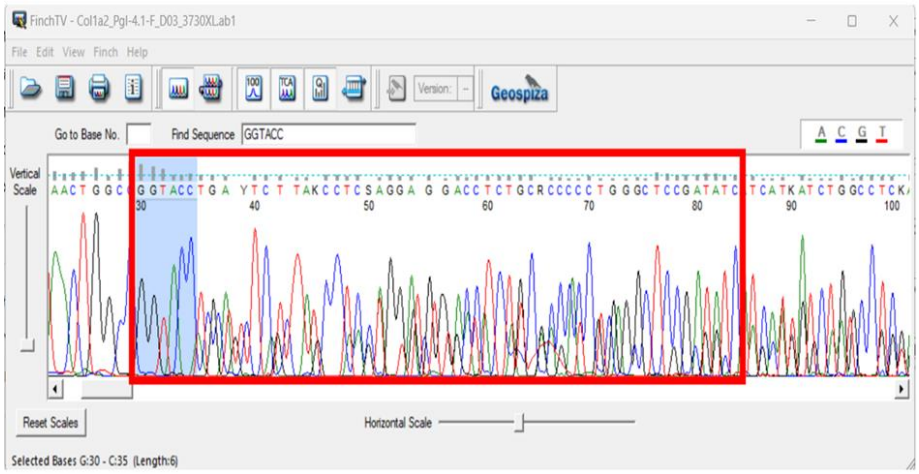

Figure 3E: Sanger sequencing showing sequences of cloned inserts. Inserts of EGR1 binding sites (EBSs) in the *PXDN* and *COL1A2* promoters were cloned into the pGL4.10 vector and are shown in red with the KpnI restriction site (GGTACC) on the 5′ end and the EcoRV site (GATATC) on the 3′ end. The sequences shown in both electropherograms were not the same as the designed constructs and the cloning was therefore repeated. A) The EBS1 insert had an incorrect W base in the EcoRV site. B) The COL1A2+ insert is longer than the designed length of the insert.

Appendix F

Table F1: EGR1 densitometry analysis

Sample	EGR1 signal	EGR1 relative densitometry	β-actin signal	β-actin relative densitometry	EGR1 to β-actin normalization	
0h	67893	100.00	134898	100.00	100.00	
6h	66429	97.84	136405	101.12	96.76	
12h	48189	70.98	125773	93.24	76.13	
24h	32075	47.24	134867	99.98	47.25	
0h	51217	100.00	121543	100.00	100.00	
6h	45729	89.28	132472	108.99	81.92	
12h	53032	103.54	133241	109.62	94.45	
24h	49949	97.52	127775	105.13	92.77	
0h	27022	100.00	89968	100.00	100.00	
6h	46802	173.20	92429	102.74	168.59	
12h	42641	157.80	92172	102.45	154.03	
24h	51608	190.99	101785	113.13	168.81	
Sample	**Rep 1**	**Rep 2**	**Rep 3**	**Average**	**Stdev**	**p-value**
0h	100.00	100.00	100.00	100.00	15.0161	-
6h	93.83	85.62	166.09	115.18	1.6648	0.63773
12h	69.74	101.74	155.06	108.85	11.3086	0.966109
24h	44.54	91.93	180.04	105.50	14.9460	0.780392

* Rep- Replicate

*Stdev- Standard deviation

Table F2: EGR1 CTCF analysis

Sample	CTCF1	CTCF2	CTCF3	AVERAGE	STDEV	P-VALUE
0h	97728.96	77543.9	93801.94	89691.6	10701.88	-
6h	158344.5	176594.9	152752.1	162563.8	12468.87	0.030821
12h	131196.2	116664.2	110855.9	119572.1	10477.31	0.045712
24h	83404.4	79004.96	82391.27	81600.21	2303.929	0.237172
NPC	43480.23	31329.23	22949.11	32586.19	10323.11	0.004529
NAC	623.22	699.94	672.42	665.1933	38.86719	0.002593

* CTCF- Correlated total cell fluorescence

*Stdev- Standard deviation

Table F3: PXDN CTCF analysis

Sample	CTCF1	CTCF2	CTCF3	AVERAGE	STDEV	P-VALUE
0h	22817.29	24678.73	28478.30	25324.77	2885.27	-
6h	25667.57	31460.57	36793.49	31307.21	5564.55	0.066686
12h	191926.32	196566.47	200282.94	196258.58	4186.81	2.37E-05
24h	242256.58	284468.64	328643.62	285122.95	43197.23	0.058681
NPC	3396.72	4417.33	4307.18	4040.41	560.17	0.007622
NAC	355.13	345.94	233.66	311.58	67.63	0.008385

* CTCF- Correlated total cell fluorescence

*Stdev- Standard deviation